Abiotic and biotic controls on soil organo-mineral stability

Sam Walrond

Master of Environmental Geology (Hons)

Lancaster Environment Centre

Lancaster University

Submitted for the degree of Doctor of Philosophy

June 2025

Abiotic and biotic controls on soil organo-mineral stability

Sam Walrond MSci (Hons)

Submitted for the degree of Doctor of Philosophy, December 2024. Revisions submitted June 2025.

Abstract

Reversing the trend of decreasing soil carbon stocks is important to help mitigate current environmental challenges. Improving knowledge on the mechanisms that control the stabilisation and persistence of soil organic carbon will provide a foundation to tackle the issue. This includes the mechanisms controlling the stability of organo-mineral associations, considered to be the most persistent pool of soil carbon. Uncertainties remain in how the composition of carbon involved in mineral associations can control the persistence of this soil organic carbon pool. Carboxylic acid richness of organic carbon (OC) are important indicators for OC stability in ocean sediments, however, it remains to be seen whether this is replicated for organo-minerals in terrestrial soil settings.

Experiments were designed to investigate if OC carboxyl richness controls organo-mineral stability by using synthesised model organo-minerals. These model organo-minerals consist of simple homogenous carboxylic acids of varying carboxyl richness to more complex heterogeneous microbial necromass OC associated to ferrihydrite. Organo-mineral OC stability was tested by measuring the change in solid organo-mineral OC from before to after destabilisation treatments. These treatments were NaOH and NaOCl chemical washes that induce desorption and oxidation of OC, and redox fluctuations that enable the reductive dissolution of ferrihydrite. This accompanied a soil mesocosm incubation experiment containing ^{13}C labelled necromass organo-minerals from different microbial types.

Results indicate that carboxyl rich OC has greater stability in organo-mineral associations, compared to carboxyl poor OC. Findings also indicate that heterogeneous necromass OC follows this trend, where fungal necromass organo-minerals has greater organo-mineral stability compared to other microbial necromass organo-minerals. These results imply that carboxyl rich OC can enhance the persistence of the mineral associated pool of soil organic carbon.

Declaration

I declare that this thesis is my own work and has not been submitted for a degree elsewhere. Contributions from supervisors and collaborators are properly acknowledged.

Sam Walrond

Lancaster University, December 2024

Statement of authorship

This thesis has been submitted in the standard thesis format.

COVID-19 mitigation statement

Hereby is a statement highlighting the impact of the COVID-19 pandemic on my PhD.

My PhD began in October 2020 during the COVID-19 pandemic meaning that I had significant disruption during my first 15 months of my PhD. This time-period included multiple nationwide and regional lockdowns, which impacted my ability to attend the university and conduct laboratory experiments. During this time-period the laboratory and office regulations at UKCEH and Lancaster University limited the capacity of person in each room to 1 or 2 people. Although this enabled me to slowly progress with my experimental work in the lab, it was difficult to adjust to a new lab and receive the required support in the lab for my development during this time. In-person supervision was also limited.

The anaerobic chamber that was a key piece of equipment required for my first experiment (chapter 2), had repeated issues during the summer of 2021 from which I spent up to 6 months trying to resolve issues before relocating the experiment to the Cohen geochemistry lab at Leeds University. This meant experiment 1 wasn't completed until spring 2022. Ideally, this relocation of the experiment would have occurred sooner, but covid restrictions on the Leeds University labs stayed in place much later than many other institutions, meaning that this wasn't possible.

Due to the emphasis of laboratory experiments in my PhD, the COVID-19 pandemic inhibited progress at the start of my PhD and subsequently delayed its completion.

Acknowledgements

Thank you to my supervisors, Jeanette Whitaker, Caroline Peacock, Nick Ostle for their support. They showed lots of patience with me whilst I slowly did my best, giving me the opportunity to learn, develop and participate in scientific research. Thank you to NERC and Envision DTP who funded the PhD and to UK Centre for Ecology and Hydrology (UKCEH) and Lancaster University for hosting me.

Thank you to all the colleagues and associates within the plant-soil interactions group at UKCEH during my time, whom I have learned an awful lot from and helped me become competent in the lab. I was always inspired by their science and now have some great friends for life. Thank you to the Locked-up team who enabled me to conduct my research alongside their project.

Thank you to Tim Goodall at UKCEH Wallingford for providing the soil microbial cultures for chapter 4, teaching me how to use a microbiology lab and for helping me use FTIR spectroscopy at Wallingford.

Thank you to Andrew Hobson for hosting me at the Cohen Geochemistry laboratory at Leeds University, whilst I used the anoxic glovebox for chapter 2.

Thank you to my family and to all my friends, in Lancaster and elsewhere, for always being supportive and creating memories to cherish. Thank you to volleyball, tennis, climbing, hiking and cycling for giving me an outlet and welcoming me into lovely communities.

Contents

List of Tables and Figures

1. General introduction

Anthropogenic activity such as the burning of fossil fuels and land use change since the industrial revolution has led to a sharp rise in CO_2 emissions and ultimately increased the concentration of CO_2 in the atmosphere from 280ppm to 423ppm by November 2024 (IPCC, 2018, 2023; NOAA, 2024). This elevation in atmospheric CO_2 along with other greenhouse gasses has led to climate change induced by global warming, which is adversely affecting both natural and anthropogenic systems around the planet (IPCC, 2023). The Intergovernmental Panel on Climate Change (IPCC) aims to limit global warming within 1.5-2°C above the pre-industrial temperatures by the end of the century, which is predicted to limit the most adverse impacts of climate change (IPCC, 2018). This requires a mitigation pathway that will reach net zero CO_2 emissions which includes reducing emissions and developing CO_2 removal (CDR) technologies (Fuss *et al.*, 2018; IPCC, 2018; Minx *et al.*, 2018; Nemet *et al.*, 2018; Fawzy *et al.*, 2020) that remove CO_2 from the atmosphere and store the carbon in a long-term carbon pool. CDR technologies include engineering solutions as well as nature-based solutions such as removals through forestry, agriculture, and other land-use changes (Fuss *et al.*, 2018; IPCC, 2018; Fawzy *et al.*, 2020). These nature-based solutions include storing carbon within soils (Fuss *et al.*, 2018; Georgiou *et al.*, 2022).

Soils are the largest global terrestrial store of carbon (Schmidt *et al.*, 2011; Georgiou *et al.*, 2022), which has been decreasing due to the impacts of land use change, land use intensification, and climate change (Duarte-Guardia *et al.*, 2020). Therefore, soils can have a significant impact on the ability for the IPCC to achieve its goal of limiting warming to 1.5°C, both by being a CO_2 source and by providing a large terrestrial store of carbon (Schmidt *et al.*, 2011; Luo *et al.*, 2017; Fuss *et al.*, 2018). Reversing this trend of soil being a net emitter of CO_2 to becoming net positive carbon store is important to achieve the IPPC's goal.

The 4 per mille initiative, is a plan that aims to increase soil organic carbon (SOC) content by 0.4% per year by promoting soil carbon sequestration (Minasny *et al.*, 2017), provides a target for

utilising the soil carbon store within nature-based CDR technologies. Soil carbon has the potential to sequester up to 5 $GtCO_2yr^{-1}$ by some estimates, exceeding other nature-based CDR technologies (Fuss *et al.*, 2018). Some land management practices such as no-tillage agriculture and cover cropping appear to increase SOC stocks within agricultural lands (Chenu *et al.*, 2019; Sykes *et al.*, 2020), however, there are uncertainties concerning the longevity of soil inputs being retained within the soil (Schmidt *et al.*, 2011; Fuss *et al.*, 2018; Fawzy *et al.*, 2020). This knowledge gap needs to be resolved to increase the confidence of soils being an effective long-term carbon pool to be utilised for the mitigation of climate change (Fuss *et al.*, 2018; Dynarski, Bossio and Scow, 2020).

Soil is a dynamic system, where carbon is continuously introduced and then turned back over into CO_2 by soil microbes (section 1.1) (Dynarski, Bossio and Scow, 2020). Therefore, either an increase in SOC input or a decrease in the rate of SOC turnover can lead to increased carbon stocks within soil. SOC turnover can be slowed by interacting with soil minerals (Cotrufo *et al.*, 2013; Lehmann and Kleber, 2015) forming mineral associated organic matter (MAOM) (section 1.3), where the SOC is less available to be utilised by soil microbes (Lavallee, Soong and Cotrufo, 2020; Georgiou *et al.*, 2022). This MAOM pool is not permanent as SOC can be stabilised into and destabilised from associations with soil minerals (Kleber *et al.*, 2021). The mechanisms controlling the destabilisation determine the persistence of MAOM (Bailey, Pries and Lajtha, 2019), which can be up to 1000 years (Cotrufo and Lavallee, 2022), a timescale applicable for long-term carbon storage to for the mitigation of climate change. This thesis investigates how the composition of SOC in associations with minerals control its vulnerability to destabilisation.

1.1. Soil carbon dynamics

Carbon enters soil primarily from plants inputs, including dead above ground plant biomass and rhizodeposits (Jackson *et al.*, 2017) to form SOC. The current consensus is that SOC forms a continuum of progressively decomposing organic carbon (OC) compounds (Cotrufo *et al.*, 2013; Lehmann and Kleber, 2015) that is driven by soil microbes (Schimel and Schaeffer, 2012), which will

eventually return into the atmosphere as respired CO_2 (Fig. 1). SOC enters soil as large, complex, non-assimilable OC with a high carbon-nitrogen (CN) ratio such as lignin (Klotzbücher *et al.*, 2011; Lehmann and Kleber, 2015). Previously, thought to the most stable SOC due to its chemical recalcitrance (Bosatta and Ågren, 1999; Lehmann and Kleber, 2015), these large SOC compounds are readily decomposed by soil microbes if the right conditions are met (Grandy and Neff, 2008; Marschner *et al.*, 2008; Klotzbücher *et al.*, 2011; Lehmann and Kleber, 2015; Lehmann *et al.*, 2020). Microbes obtain energy by progressively degrading these large SOC molecules into smaller, more labile SOC (Gunina and Kuzyakov, 2022) releasing CO_2 through respiration. The depolymerisation and oxidation of large SOC molecules enable for the SOC to be more dynamic within the soil system (Kleber *et al.*, 2015). A greater abundance of reactive chemical functional groups, such as carboxyl and amine group, enables this SOC to be more soluble, engage in more chemical interactions, be easily assimilated into microbial biomass as well as be respired into CO_2 (Kleber *et al.*, 2015; Lehmann and Kleber, 2015; Roth *et al.*, 2019). This turnover of SOC can be interrupted by physical protection within aggregates (Six, Elliott and Paustian, 2000; Lehmann, Kinyangi and Solomon, 2007), or by chemical protection where labile SOC associates with minerals forming organo-mineral complexes (Jastrow, Amonette and Bailey, 2007; Kögel-Knabner *et al.*, 2008; Lehmann and Kleber, 2015; Waring *et al.*, 2020). SOC within the MAOM pool has a much slower (10-1000 years) compared to the unprotected SOC within the particulate organic matter (POM) pool (1-50 years) (Cotrufo and Lavallee, 2022).

Differences in the chemical composition of SOC will influence how the SOC interacts within the soil environment (Lehmann and Kleber, 2015; Luo *et al.*, 2017; Roth *et al.*, 2019; Lehmann *et al.*, 2020), thus is important to consider when investigating soil carbon dynamics. Chemical functional groups, functional group complexity, aromaticity and size of molecule are all important factors that impact how the SOC will behave within the soil environment (Lehmann and Kleber, 2015; Kleber *et al.*, 2021). These characteristics influence its potential to form dissolved organic carbon (DOC), its lability and susceptibility to microbial degradation, and its interactions with soil minerals, which are critical in the formation of MAOM (Lehmann and Kleber, 2015; Kleber *et al.*, 2021).

The carboxylic acid functional group could be the most important chemical characteristic in the formation of MAOM investigated further throughout this thesis (see chapter 2 and 4). These carboxylic acid functional groups can be introduced into SOC directly through organic acid root exudates such as oxalic acid (Keiluweit *et al.*, 2015). Alternatively carboxylic acid functional groups can be introduced into SOC as the result of microbial degradation of larger SOC molecules into smaller more labile SOC molecules (Grandy and Neff, 2008; Schmidt *et al.*, 2011; Lehmann and Kleber, 2015). Here, the oxidative degradation by microbial enzymes can cleave larger molecules and breakdown aromatic rings such as in lignin can form smaller aliphatic chains terminated by carboxylic acid groups (Chen and and Kirk, 1983; Kögel-Knabner, 2002; Janusz *et al.*, 2017). The introduction of these carboxylic acid functional groups make the molecules more labile, soluble and chemically reactive, thus playing an important role in the interactions of the SOC within the soil environment (Lehmann and Kleber, 2015; Luo *et al.*, 2017; Roth *et al.*, 2019; Lehmann *et al.*, 2020).

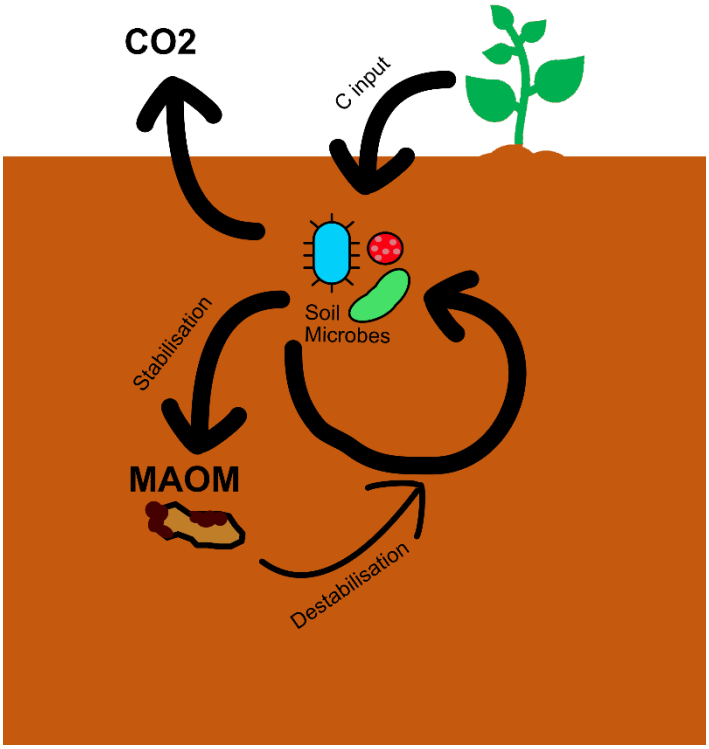

Figure 1 – Inforgraphic of the movement of carbon within soils. Soil OC enters the soil from plant biomass which gets transformed, recycled and respired by soil microbes. Soil OC can be stabilised on minerals which reduces its bioavailability until the OC becomes destabilised. Mineral associated OC has greater persistence within soil

1.2. Necromass SOC

Microbial necromass, consisting of dead microbial cells, components and extracellular components (Buckeridge, Creamer and Whitaker, 2022; Camenzind *et al.*, 2023), dominate SOC pool by contributing up to 80% of SOC (Simpson *et al.*, 2007; Liang, Schimel and Jastrow, 2017; Liang *et al.*, 2019; Buckeridge, Creamer and Whitaker, 2022; Deng and Liang, 2022; Whalen *et al.*, 2022). Necromass is formed through the soil microbial pump (Buckeridge, Mason, *et al.*, 2020; Liang, 2020; Zhu *et al.*, 2020), where labile SOC is transformed through anabolic pathways and retained as microbial biomass and necromass. Necromass is constantly recycled as a substrate for new microbial biomass growth, unless it becomes chemically protected in organo-mineral complexes (Buckeridge, La

Rosa, *et al.*, 2020). Microbial necromass dominates the MAOM pool (Kopittke *et al.*, 2018, 2020; Klink *et al.*, 2022; Xuan *et al.*, 2024).

Microbial cell walls contribute greatly to microbial necromass, as well as contributing to variation in the chemical composition of necromass, making it important to consider when investigating how necromass SOC interacts within the soil environment. In particular, necromass composition varies between gram positive bacteria (Gr^+), gram negative bacteria (Gr^-) and fungi (Vollmer, Blanot and De Pedro, 2008; Garcia-Rubio *et al.*, 2020). Each of these microbial types contain a phospholipid bilayer, however, fungal cell walls are primarily composed of chitin (Garcia-Rubio et al., 2020), whereas Gr^+ bacteria feature thick peptidoglycan layers, and Gr^- bacteria possess a second outer phospholipid bilayer along with a thinner peptidoglycan layer (Vollmer, Blanot, & De Pedro, 2008).

The chemical structure of chitin contains repeating units of N-acetylglucosamine monomers linked by β(1→4) glycosidic bonds (Gooday, 1990). Peptidoglycan is structured as alternating units of N-acetylglucoseamine and N-acetylmuramic acid with peptide chains attached (Vollmer, Blanot and De Pedro, 2008). The N-acetylmuramic acid found in the peptidoglycan of both Gr^+ and Gr^- bacterial cell walls contain a carboxylic acid functional group, whereas the N-acetylglucosamine found in Fungi does not inherently contain these carboxyl functional groups that enhance the reactivity of the SOC in the soil environment (Gooday, 1990; Lehmann and Kleber, 2015). However, as the necromass enters the soil environment (see section 1.1), microbially mediated oxidative degradation can introduce new carboxylic acid functional groups to both N-acetylglucosamine and N-acetylmuramic acid units (Chen and and Kirk, 1983; Gooday, 1990; Jiang *et al.*, 2022) making these necromass components more labile, soluble and dynamic within the soil environment (Lehmann and Kleber, 2015; Luo *et al.*, 2017; Roth *et al.*, 2019; Lehmann *et al.*, 2020).

1.3. Soil minerals

Soil is a weathering interface where the biosphere, lithosphere, atmosphere and hydrosphere form dynamic interactions (Totsche *et al.*, 2010). Therefore, soils contain minerals that have formed

from the bedrock beneath the soil, which providing a surface that can interact with SOC and chemically protect the SOC within MAOM (Kögel-Knabner *et al.*, 2008; Kleber *et al.*, 2015, 2021). Important to the formation of MAOM are secondary minerals that have formed from the weathering of primary minerals within the bedrock (Huang and Schnitzer, 1986; Lehmann and Kleber, 2015). These minerals tend to have a surface charge and reactive functional groups on the mineral surface that can aid chemical interactions with SOC (Kleber, Sollins and Sutton, 2007; Kleber *et al.*, 2015, 2021). Two important minerals in the MAOM fraction are clays and metal oxides, where clays can contribute up to 60% of content of soils (Ito and Wagai, 2017) and metal oxides can contribute up to 72% of MAOM stocks (Kramer and Chadwick, 2018; Jia *et al.*, 2024).

Clays are aluminosilicates, interlayered tetrahedral silica sheets and octahedral aluminium oxide sheets, that have formed from the weathering of silicate primary minerals such as feldspar (Huang and Schnitzer, 1986; Bergaya, Theng and Lagaly, 2006; Murray, 2006; Kleber *et al.*, 2021). There are 3 distinct classes of clays that depend upon the arrangement of layering of the tetrahedral silica and octahedral aluminium oxide sheets. These are kaolinites which are 1:1 clays, illites which are 2:1 non-swelling clays, and smectites which are 2:1 swelling clays (where 1:1 is an arrangement of 1 tetrahedral sheet to 1 octahedral sheet, and 2:1 clays have an arrangement of 2 tetrahedral sheets to 1 octahedral sheet). The structural differences between these 3 classes of clays affect the clay properties that can enhance or inhibit the clays ability to interact with SOC, such as surface area and surface charge (Singh *et al.*, 2018; Kleber *et al.*, 2021). Clays will predominantly interact with SOC through cation bridging (Singh *et al.*, 2018; Kleber *et al.*, 2021), which is enabled through the negative surface charge caused by isomorphic substitution (Singh *et al.*, 2018). The exposed edges of the octahedral aluminium oxide sheets which will contain some surface hydroxyl groups in the aluminium octahedral sheets enable SOC interaction through ligand-exchange and inner-sphere complexation (Singh *et al.*, 2018). Smectite 2:1 swelling clays such as montmorillonite have the greatest capacity for SOC interactions in clay minerals (Saidy *et al.*, 2013; Singh *et al.*, 2018), due to an expanding interlayer space. This expanding interlayer space can expand up to 4.8nm (Guo *et al.*, 2020) able to accommodate

OC molecules to interact within the interlayer space thus significantly increasing the surface area and capacity for organo-mineral interactions to occur.

Metal oxides also form as the product of the weathering of silicates (Cornell and Schwertmann, 2003). Metal ions such as Fe^{3+} and Al^{3+} are solubilised during the weathering process, which can hydrolyse and precipitate as metal oxide minerals (Stumm and Morgan, 1995; Cornell and Schwertmann, 2003; Stefánsson, 2007). Metal oxides can precipitate out of soil solution as amorphous metal oxide minerals such as amorphous aluminium oxide and ferrihydrite, which lack mineral structure but have an extremely high surface area (Cornell and Schwertmann, 2003; Hiemstra, 2013). The amorphous crystalline structure of these metal oxides are not thermodynamically stable (Das, Hendry and Essilfie-Dughan, 2011; Zhao *et al.*, 2022), meaning that over time the mineral structure rearranges to form more crystalline metal oxides with a lower surface area such as geothite and gibbsite. The restructuring of the minerals crystallinity can be sped up by temperature (Zhao *et al.*, 2022) or mineral dissolution and reprecipitation cycles (ThomasArrigo *et al.*, 2018; Zhou *et al.*, 2018; ThomasArrigo, Kaegi and Kretzschmar, 2019). The metal oxide surfaces are abundant with hydroxyl groups, which can interact with SOC through ligand exchange forming inner-sphere complexes (Kleber, Sollins and Sutton, 2007; Hiemstra, 2013; Newcomb *et al.*, 2017; Gao *et al.*, 2018; Kleber *et al.*, 2021), making metal oxides contribute significantly to the MAOM pool. However, unlike clays, metal oxide minerals are vulnerable to being solubilised in acidic pH conditions (Stumm and Morgan, 1995; Li *et al.*, 2021) and can be reductively dissolved in reducing conditions due to the redox reactivity of metals such as Fe (Chen *et al.*, 2020; Inagaki *et al.*, 2020; Possinger, Bailey, *et al.*, 2020).

1.4. Soil organo-minerals

Organo-mineral complexes form when SOC chemically interacts with soil minerals, combining to form the MAOM pool where SOC have a longer persistence within soils (Cotrufo and Lavallee, 2022). SOC within organo-mineral complexes is less bioavailable to microbes (Lavallee, Soong and Cotrufo, 2020; Georgiou *et al.*, 2022). Organo-minerals complexes have a layered structure (Kleber, Sollins and

Sutton, 2007; Possinger, Zachman, *et al.*, 2020; Kleber *et al.*, 2021) consisting of direct chemical interactions between SOC molecules and the surface of the mineral (direct organo-mineral interactions) and chemical interactions between two or more SOC molecules not directly involving the mineral surface (organo-organic interaction). The composition of the SOC molecules and the mineral surface controls the type of organo-mineral and organo-organic interactions in the organo-mineral complex (Kleber, Sollins and Sutton, 2007; Kleber *et al.*, 2021).

SOC with a high abundance of reactive functional groups such as carboxyl groups, phosphate groups, amine groups and hydroxyl groups, dominate direct organo-mineral interactions (Kleber, Sollins and Sutton, 2007; Kleber *et al.*, 2021). These OC functional groups so can interact with hydroxyl groups on the mineral surfaces of metal oxides and the exposed edges of octahedral aluminium oxide sheets in clays (Kleber, Sollins and Sutton, 2007; Hiemstra, 2013; Newcomb *et al.*, 2017; Gao *et al.*, 2018; Singh *et al.*, 2018; Kleber *et al.*, 2021) to form inner-sphere complexes via ligand exchange. Furthermore, SOC can form direct organo-mineral interactions through cation bridging to negatively charged clay mineral surfaces, as these OC functional groups are often in their deprotonated form in soil conditions (Tülp *et al.*, 2009; Singh *et al.*, 2018; Guo *et al.*, 2020; Kleber *et al.*, 2021). Cation bridging also plays a role in organo-organic interactions along with van der Walls and hydrophobic interactions that do not require reactive OC functional groups (Kleber *et al.*, 2021). Microbial necromass OC and other simple labile OC such as some root exudates are important in the formation of organo-mineral complexes (Keiluweit *et al.*, 2015; Buckeridge, La Rosa, *et al.*, 2020; Buckeridge, Creamer and Whitaker, 2022) as they can be abundant in reactive OC functional groups that enable direct organo-mineral and organo-organic interactions.

1.5. Organo-mineral destabilisation

These organo-mineral and organo-organic interactions within the organo-mineral complexes are not permanent but are dynamic interfaces where SOC can become associated (stabilised) or dissociated (destabilised) from the organo-mineral complex (Bailey, Pries and Lajtha, 2019; Buckeridge,

Creamer and Whitaker, 2022). There are multiple mechanisms that destabilise organo-mineral OC, such as through reductive dissolution of metal oxides (Possinger, Bailey, *et al.*, 2020) and desorption by plant root or microbial exudates (Keiluweit *et al.*, 2015), yet the clear understanding of destabilisation processes within soils is unresolved (Bailey, Pries and Lajtha, 2019).

Biotic destabilisation of organo-minerals transpires due to the soil microbial community and plant root exudates (Keiluweit *et al.*, 2015; Li *et al.*, 2021). Microbes and plants can release exudates that are strong organic ligands such as oxalic acid which can directly desorb OC organo-mineral OC or dissolve metal oxide minerals by reducing the pH (Keiluweit *et al.*, 2015; Li *et al.*, 2021). Biotic destabilisation of organo-mineral OC can also occur through extracellular enzymes released by the soil microbial community. Here, extracellular enzymes can work to hydrolyse and cleave part of the mineral bound OC (T. Wang *et al.*, 2020; Li *et al.*, 2021) or displace weakly bound OC (Mikutta *et al.*, 2019). Biotic destabilisation works to enable soil microbes to access organo-mineral OC, accessing nutrients such as N that can limiting in the wider soil environment (Jilling *et al.*, 2018). Soil priming induced by high CN root exudates such as glucose, primes soil microbes to increase extra-cellular enzyme production to mine N to fuel microbial biomass growth and destabilising organo-mineral OC in the process (Keiluweit *et al.*, 2015; Li *et al.*, 2021).

Soil organo-mineral destabilisation can also occur due to the reductive dissolution of metal oxides such as ferrihydrite (Inagaki *et al.*, 2020; Possinger, Bailey, *et al.*, 2020). Anaerobic conditions can occur within water saturated soil where the rate of oxygen transport into soil pores is less than the rate at which aerobic microbial communities consume the oxygen through respiration (Manzoni *et al.*, 2012). Here, microbes use alternative pathways for respiration that do not use oxygen as the terminal electron acceptor, such as nitrates, sulphates, metal oxides and carbon dioxide (Lecomte *et al.*, 2018). Some of these microbial communities specialise in the reduction of metal oxides such as ferrihydrite to assist with anaerobic respiration (Lipson *et al.*, 2010). This can bring about the microbial mediated reductive dissolution of Fe-oxides including ferrihydrite organo-minerals. Here, microbes such as

Geobacter spp. use Fe(III) within Fe-oxides as an electron acceptor to oxidise OC for respiration (Kato, Hashimoto and Watanabe, 2013; Merino *et al.*, 2021). This reduces Fe(III) to the highly soluble Fe(ii), thus solubilising and destabilising the Fe-oxide mineral and the associated OC.

The vulnerability of organo-mineral OC to destabilisation (organo-mineral stability) depends upon the mechanism of destabilisation the organo-mineral is exposed to, and the strength of the chemical interactions within the organo-mineral complex (Bailey, Pries and Lajtha, 2019). Therefore, many experiments use chemical washes of increasing destabilisation such as sodium hydroxide (NaOH), sodium hypochlorite (NaOCl) and sodium pyrophosphate to quantify fractions of organo-mineral OC of increasing stability (Lopez-Sangil and Rovira, 2013; Heckman, Lawrence and Harden, 2018; Curti *et al.*, 2021). Here, OC associated directly to the mineral surface by an inner-sphere complex will requires a significant energy to overcome the covalent bond and destabilise the interaction, whereas OC associated to the organo-mineral complex via van der Waals interactions will require much less energy to dissociate (Kleber, Sollins and Sutton, 2007; Feng *et al.*, 2014; Newcomb *et al.*, 2017; Kleber *et al.*, 2021). The stability of the organo-mineral will affect the residence time of organo-mineral OC.

1.6. Thesis aims and objectives

The stabilisation of SOC into organo-minerals has been well researched, however, the mechanisms controlling organo-mineral destabilisation is less resolved (Bailey, Pries and Lajtha, 2019; Buckeridge, Creamer and Whitaker, 2022). Advancements in the understanding of organo-mineral stability under pressures of different destabilisation mechanisms could assist in the development of soil management practices to maximise the capacity and persistence of the MAOM soil carbon pool (Wiesmeier *et al.*, 2019; Lehmann *et al.*, 2020; Parada *et al.*, 2024). This would aid towards the 4 per mille initiative using soil as a nature based CDR (IPCC, 2018).

The composition of SOC involved in organo-mineral complexes are important controls on organo-mineral stability by influencing the type and strength of interaction between the OC molecule

and mineral surface(Kleber, Sollins and Sutton, 2007; Kleber *et al.*, 2015, 2021). In particular, carboxylic acid OC appear to represent more stable organo-mineral OC (Mikutta *et al.*, 2007; Possinger, Zachman, *et al.*, 2020), interacting with mineral surfaces through inner-sphere complexation (Kleber, Sollins and Sutton, 2007; Newcomb *et al.*, 2017; Kleber *et al.*, 2021). The number of carboxyl functional groups in OC (carboxyl-richness) influences the stability of organo-minerals in previous experiments (ThomasArrigo, Kaegi and Kretzschmar, 2019; Curti *et al.*, 2021; Zhao *et al.*, 2022).

There has been use of synthesised organo-mineral complexes for research investigating organo-mineral stability in an ocean sediment context, at the Cohen geochemisty laboratory, University of Leeds. In this thesis, similar synthesised organo-mineral complexes were used to investigate organo-mineral stability in a soil relevant context. The thesis is composed of three experimental chapters addressing the following research questions:

Chapter 2: Does carboxyl-richness control organo-mineral stability in reducing conditions?

It is unknown whether the carboxyl-richness of a Fe-oxide organo-mineral impacts its vulnerability to destabilisation by reductive dissolution similarly to carboxyl-rich organo-minerals being more stable when destabilised by chemical wash (Curti *et al.*, 2021; Zhao *et al.*, 2022). This chapter explores the vulnerability to reductive dissolution of ferrihydrite organo-minerals of increasing carboxyl-richness by incubating the organo-minerals in an anoxic chamber and inducing reductive dissolution through the addition of Fe(II).

Chapter 3: Does carboxyl-richness control organo-mineral stability under the different destabilisation forces imposed by aerobic, anaerobic and oscillating soil conditions?

This chapter follows directly on from Chapter 2 testing whether the carboxyl-richness controls organo-mineral stability under biotic and physiochemical destabilisation mechanisms experienced in natural soils. Therefore, an soil incubation was set up where the same synthesised Fe-oxide organo-minerals of increasing carboxyl-richness used in Chapter 2 were mixed into soil and incubated under

aerobic, anaerobic and oscillation conditions. The organo-minerals were enriched in ^{13}C so that $^{13}CO_2$ gas samples of the soil headspace could be measured to quantify organo-mineral OC destabilisation.

Chapter 4: Are there differences in organo-mineral stability when they are composed of necromass from different microbial groups?

This chapter investigates differences in the stability synthesised necromass organo-minerals. Necromass is a larger, more complex and heterogenous OC, compared to the simple homogenous carboxyl-OC used in Chapters 2 and 3. The necromass OC used in this experiment is similar to OC that will be involved in organo-mineral complexes in real soils, where necromass dominates the MAOM pool (Kopittke *et al.*, 2018, 2020; Klink *et al.*, 2022; Xuan *et al.*, 2024). The stability of organo-mineral OC was tested using NaOH and NaOCl chemical washes.

2. Does carboxyl richness control organo-mineral stability in abiotic reducing conditions?

2.1. Introduction

Soils contribute the greatest global terrestrial carbon store (Schmidt *et al.*, 2011; Georgiou *et al.*, 2022). However, currently around the world soil organic carbon (SOC) stocks are decreasing due to the impacts of land use change, land use intensification, and climate change (Duarte-Guardia *et al.*, 2020). Mitigation of decreasing global SOC stocks must be driven by improved understanding of the mechanisms that control the persistence and vulnerability of SOC (Schmidt *et al.*, 2011; Liang, Schimel and Jastrow, 2017).

Carbon enters the soil through plants, as litter and rhizodeposits, to form SOC and will eventually be mineralised by soil microorganisms and returned to the atmosphere as CO_2 (Waring *et al.*, 2020). During its time in soil, SOC is processed biotically and abiotically and may enter different soil fractions, such as mineral associated organic matter (MAOM) and particulate organic matter (POM), that greatly impact the persistence of the SOC (Lehmann and Kleber, 2015; Roth *et al.*, 2019). MAOM forms when SOC interacts chemically and physically with soil minerals such as clays and metal oxides, forming organo-minerals. Here, the availability of SOC to soil microbes is reduced, inhibiting SOC mineralisation by soil microbes, thus increasing the persistence of the SOC (Kleber *et al.*, 2015; Lehmann and Kleber, 2015; Keiluweit *et al.*, 2022). The MAOM SOC pool has a much slower turnover (10-1000 years) compared to the particulate organic matter pool (POM) of SOC (1-50 years) (Cotrufo and Lavallee, 2022).

There is an apparent upper limit for soil minerals to store SOC as MAOM, at which MAOM is at saturation (Hassink, 1997; Cotrufo *et al.*, 2019). Most soils are under-saturated in MAOM (Georgiou *et al.*, 2022), so increasing MAOM towards saturation could help improve SOC persistence and mitigate decreasing global SOC stocks (Wiesmeier *et al.*, 2019; Georgiou *et al.*, 2022). Mechanisms of

MAOM stabilisation into organo-minerals is well researched, however, the mechanisms of organo-minerals destabilisation is much less resolved (Bailey, Pries and Lajtha, 2019; Buckeridge, Creamer and Whitaker, 2022). Conducting research on the controls of organo-mineral stability, which is organo-minerals vulnerability to destabilisation, can enhance our understanding of how MAOM persistence can be maximised (Bailey, Pries and Lajtha, 2019).

Iron (Fe) oxide soil minerals such as goethite and ferrihydrite have the greatest ability to associate to SOC due to the high density of reactive surface functional groups (hydroxyl groups (-OH)) and high specific surface area (Schwertmann and Cornell, 2008; Kleber *et al.*, 2021). Research has investigated the role of Fe oxides in soils for stabilising SOC and whether Fe-oxide content in soils is a predictor for stable SOC stocks (Rasmussen *et al.*, 2018). Despite the properties of Fe oxide minerals that enable high amounts of SOC stabilisation, the stability and persistence of the mineral phase is uncertain due to Fe oxides being redox reactive (Wagai and Mayer, 2007; Winkler *et al.*, 2018; Chen *et al.*, 2020). Fe can readily transfer electrons between its reduced Fe(II) form, which is very soluble, and its oxidised Fe(III) form, which is more often found in stable mineral phases (Reddy *et al.*, 2015; ThomasArrigo *et al.*, 2018). Anaerobic microsites found in soils that are caused by microbes consuming oxygen in water saturated pores, can lead to conditions where Fe(III) in Fe oxide minerals are reduced to soluble Fe(II) (Chen *et al.*, 2020; Possinger, Bailey, *et al.*, 2020). Previous work has shown that destabilisation and mineralisation of MAOM does occur in soils of higher water saturation and reducing conditions (Chen *et al.*, 2020; Possinger, Bailey, *et al.*, 2020). This can reduce the contribution and importance of Fe-oxide minerals in the MAOM fraction of soils in some environments (Inagaki *et al.*, 2020).

Redox conditions in soils are often heterogeneous, where variations in soil moisture and soil pore structure and microbial activity can lead to aerobic and anaerobic soil conditions that vary in locality and through time (Keiluweit *et al.*, 2017). In soils with water saturated conditions, brought about by weather or geography, oxygen transport from the atmosphere into the pore spaces within

soils is inhibited (Keiluweit *et al.*, 2017). Consequently, the onset of anaerobic conditions will occur once aerobic microbial communities within the soil use up oxygen during respiration (Manzoni *et al.*, 2012). Onwards, microbial communities that specialise in anaerobic conditions will use alternative pathways for respiration that do not use oxygen as the terminal electron acceptor, for example Fe(III) in Fe-oxides (Lipson *et al.*, 2010). This leads to an increase in aqueous Fe(II) in the soil pore water, enabling abiotic reductive dissolution of Fe-oxide minerals explored in the previous paragraph. Dissolution-re-precipitation cycles resulting from electron transfer between Fe(III) and Fe(II) can cause mineral transformation of ferrihydrite (amorphous Fe oxide mineral) towards more crystalline and well-ordered Fe oxide minerals such as Lepidocrocite and Goethite (Pedersen *et al.*, 2005; ThomasArrigo *et al.*, 2018). Previous studies have shown that in organo-minerals, OC chemistry can impact the extent of mineral transformation that can take place (ThomasArrigo *et al.*, 2018; ThomasArrigo, Kaegi and Kretzschmar, 2019). Although transformation of Fe-oxide minerals in MAOM has been investigated, the fate of the SOC involved has not been investigated (ThomasArrigo *et al.*, 2018; ThomasArrigo, Kaegi and Kretzschmar, 2019; Zhao *et al.*, 2022).

Carboxylic acid functional groups on OC are important in forming associations with iron oxide minerals (Kleber, Sollins and Sutton, 2007; Coward, Ohno and Sparks, 2019; Possinger, Zachman, *et al.*, 2020) and are common in SOC (Coward, Ohno and Sparks, 2019). Ligand exchange of carboxyl groups on SOC and hydroxyl groups on the surfaces of iron oxide minerals forming inner-sphere complexes (Kleber, Sollins and Sutton, 2007; Newcomb *et al.*, 2017; Kleber *et al.*, 2021), directly associating the SOC to the mineral surface with a strong covalent bond (Newcomb *et al.*, 2017). Previous experiments have investigated the behaviour and stability of organo-minerals in accordance to the number of carboxyl functional groups (carboxyl-richness) in the OC (ThomasArrigo, Kaegi and Kretzschmar, 2019; Curti *et al.*, 2021; Zhao *et al.*, 2022).

There remains a knowledge gap on whether carboxyl-richness controls organo-mineral stability in reducing conditions. To investigate this, model soil organo-minerals composed of

ferrihydrite and either mono-, di-, or tri-carboxylic acid (increasing in carboxyl-richness) were synthesised and incubated under reducing conditions. The fate of the carboxylic acid OC was traced through temporal measurements of Fe-oxide mineral transformation and OC retention in the mineral fraction, to test the hypothesis. The hypothesis is that **carboxyl-poor organo-minerals are more vulnerable to destabilisation by reductive dissolution compared to carboxyl-rich organo-minerals**, as carboxyl-poor organo-minerals have been shown to permit greater mineral transformation in reducing conditions compared to carboxyl-rich organo-minerals (ThomasArrigo, Kaegi and Kretzschmar, 2019). This indicates that greater reductive dissolution has occurred which could signify that a greater amount of OC has become liberated from the Fe-mineral.

2.2. Methods

2.2.1. Synthesis of model organo-mineral

Model organo-minerals composed of ferrihydrite and three carboxylic acids of increasing carboxyl-richness, were synthesised following methods developed by Schwertmann and Cornell (2008) and Zhao *et al.* (2022) (Fig. 2a). A reaction (Equation 1) between ferric nitrate ($Fe(NO_3)_3.9H_2O$), potassium hydroxide (KOH) and the chosen organic carbon (OrgC) at pH 7 forms a ferrihydrite organomineral composite ($Fe_5(OH)_8.4H_2O$ – OrgC) and potassium nitrate waste product (KNO_3) (Schwertmann and Cornell, 2008). Hexanoic acid (Fig. 2a), Adipic acid (Fig. 2b) and Tricarballylic acid (Fig. 2c), which are mono-, di- and tri-carboxylic acid respectively, were selected as the OC to co-

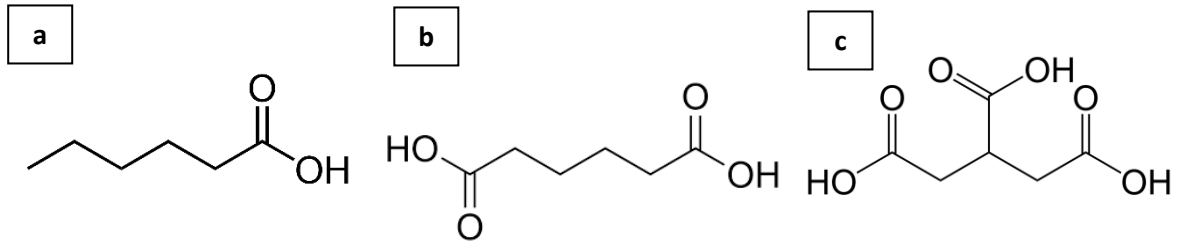

Figure 2 – OC used in synthesised organo-minerals; Hexanoic acid (a), Adipic acid (b) and Tricarballylic acid (c)

precipitate with ferrihydrite. These were chosen as each consist of five carbon atoms per molecule which enables a 1:1 relationship of carbon between the different OC types, will facilitate interpretation of organo-mineral carbon measurements.

To form the three organo-mineral composites, 1M KOH solution was added dropwise to a 250ml solution made of 20g of $Fe(NO_3)_3.9H_2O$, the selected organic carbon, and milliQ H_2O. This was constantly mixed and 1M KOH was added until the solution reached pH7±0.5. Here, ferrihydrite co-precipitated out of solution with the organic carbon, forming the organo-mineral. The protocol needed to be carefully followed, as a different mineralogy of Fe-oxide would precipitate out of solution above pH7. For example, at pH9 geothite would be synthesised (Schwertmann and Cornell, 2008). Several batches of each organo-mineral co-precipitate were synthesised in order to make enough organo-mineral for the incubation.

$$(Equation\ 1)\ Fe(NO_3)_3.9H_2O + KOH\ + OrgC\ \rightarrow\ Fe_5(OH)_8.4H_2O - OrgC + KNO_3$$

Then KNO_3 impurities were removed from the precipitated organo-mineral by replacing the organo-mineral bearing solution with milliQ water multiple times until the solution reached an electrical conductivity (EC) of less than 100µs, careful keep as much ferrihydrite organo-mineral from being washed away. This washing process could cause the pH of the solution to drop due to partial dissolution of Fe(III) (Schwertmann and Cornell, 2008) and liberation of some OC. If the solution drops below pH5, the ferrihydrite organo-mineral particles electrostatically repel each other and are unable to settle out of suspension (Morel and Herring, 1993). This phenomenon was enhanced as the carboxyl-richness of the organo-mineral increased, as the liberated OC reduced the pH further with a greater quantity of carboxylic acid functional groups. Drops of 0.1M NaOH is added to the solution to bring the solution back up to pH7, enabling the organo-mineral to settle out of suspension.

This organo-mineral containing solution was then divided into 50ml centrifuge tubes to be centrifuged at 27500xg for 20 minutes. This separated the solid organo-mineral pellet from the supernatant which was disposed of. Pilot tests were used to refine the protocol to synthesise ferrihydrite organo-minerals of 8wt%C (see section 2.2.5).

2.2.2. Experimental set-up

An abiotic incubation was set-up to test the hypothesis of carboxyl-poor organo-minerals being less stable than carboxyl-rich organo-minerals in reducing conditions. This required the organo-minerals synthesised (section 2.2.1) to be exposed to a Fe(II) reductant in an anoxic chamber for long enough for sufficient reductive dissolution to occur (Fig. 3b). Therefore, measurements of carbon retained by the organo-mineral and extent of mineral transformation, that portray organo-mineral destabilisation, were distinguishable between the different organo-mineral treatments. These

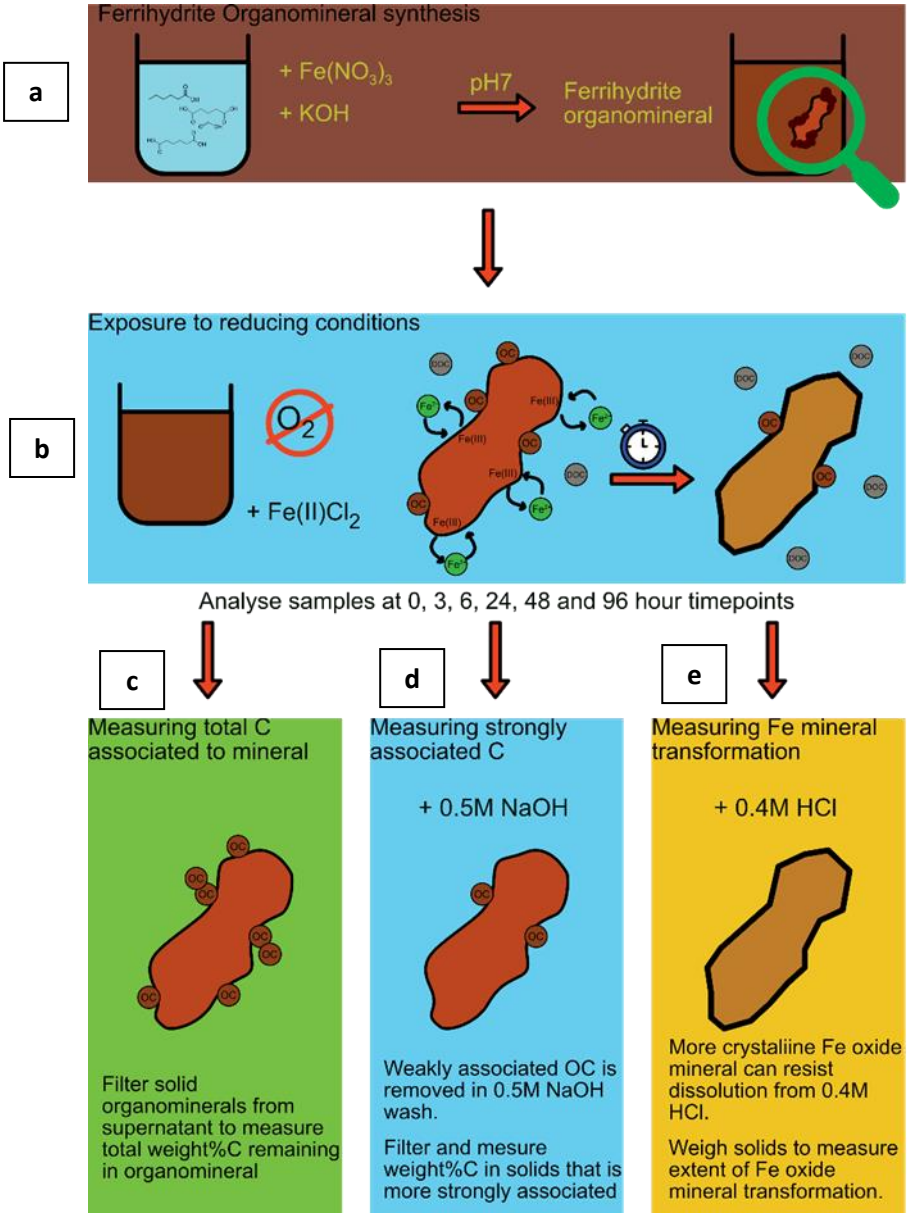

Figure 3 - Workflow for experiment; Beginning with the synthesis of organo-minerals (b) followed by the abiotic incubation in an anoxic glovebox (b), before wt%C (c), non-desorbable wt%C (d) and mineral transformation (e) was measured

measurements would be obtained destructively. The timepoints of destructive harvesting were selected as 0, 3, 6, 24, 48 and 96 hours, based on a similar previous experiment investigation (ThomasArrigo, Kaegi and Kretzschmar, 2019). Therefore, 90 small aliquots of each organo-mineral type were needed for this incubation.

The Aliquots contained 0.1g of organo-mineral pellet that was suspended within 10ml of a solution of 30mM MOPS buffer and 0.01M $NaNO_3$ contained within 12ml airtight exertainers. $NaNO_3$ acted to assist with cationic bridging utilised in the organo-mineral. The MOPs buffer was selected as it does not interact with the mineral surface (Bradbury and Baeyens, 1999) and buffers pH to between pH6 and 7 (Zhao *et al.*, 2022). The suspended organo-mineral pellets were disrupted and homogenised using a vortex mixer for 60 seconds each.

Before the incubation began, dissolved O_2 was removed from each sample by removing the airtight exertainer caps and exposing each sample to an anoxic 0ppb O_2 atmosphere for 24 hours within the anoxic glovebox at the Cohen geochemistry lab at Leeds University. This anoxic glovebox was located and utilized after extensive pilots at UKCEH Lancaster (see section 2.2.5). The glovebox is an airtight container with a vacuum box entry port and two pairs of glovebox gloves for handling samples within the glovebox (Fig. 4). The anoxic chamber was filled and pressurised with 95% N_2 and 5% H_2 gas.

Figure 4 – Anoxic glovebox at Cohen laboratory at the University of Leeds

The H_2 works to react with and remove any remnant O_2, producing water, which was removed absorbed by fresh silica desiccant. At the beginning of the incubation (T0), and Fe(II)Cl_2 was added to each sample within the anaerobic glovebox to make a solution of 100mM Fe(II). The Fe(II) within Fe(II)Cl_2 acted as the electron donor, initiating the abiotic reduction of ferrihydrite.

After T0, the exertainers were removed from the chamber with airtight caps screwed back on tight to maintain an anoxic N_2 headspace. The samples were agitated to allow for even exposure of the Fe(II) to the organo-mineral, by being placed on an oscillatory shaker at 150 rpm. The aliquots remained on the oscillatory shaker for 3, 6, 24, 48 and 96 hours before being brought back to the anaerobic chamber. Here the samples were harvested to measure weight % carbon (wt%C) remaining on the solid fraction and wt%C remaining on the solid fraction that is not desorbed by 0.5NaOH, which explored the fate of organo-mineral C. The 0.5M NaOH wash caused a significant increase in pH, mimicking natural soil processes that can induce raised pH of microsites in soils (Yan, Schubert and Mengel, 1996; Shi *et al.*, 2011; Li *et al.*, 2021), bringing about the solubilisation of weakly bound organo-mineral OC (Kaiser and Guggenberger, 2003; Kleber, Sollins and Sutton, 2007).Samples were also harvested to explore the extent of mineral transformation through measuring the weight of solid fraction that is resistant to dissolution by 0.4M HCl.

2.2.3. Analyses of solid fraction

The solid fraction of each sample was retained for measurements for measurements of destabilisation of organo-mineral OC and the extent of mineral transformation of the organo-mineral. At timepoints 0, 3, 6, 24, 48 and 96, 15 samples were harvested within the anoxic chamber for each organo-mineral treatment; 5 replicates for measuring wt%C remaining in the organo-mineral, 5 replicates that measured wt%C of OC more strongly associated and resistant to desorption by 0.5M NaOH, and 5 replicates that measured a proxy for the amount of non-ferrihydrite mineral that is able to resist dissolution by 0.4M HCl. The solid mineral fraction was obtained by passing the exertainer contents through a 0.22µm cellulose nitrate filter using a vacuum filter apparatus, with the

supernatant disposed of. The solid particles were rinsed with 10ml of milliQ H_2O to remove residual $Fe(II)Cl_2$.

Samples that measured the total OC remaining in solid organo-mineral (Fig. 3c), were taken from the anoxic chamber, and immediately stored in a -20°C freezer. The samples were later freeze dried for measuring the wt%C of the solid organo-mineral using COSTECH ECS 4010 (Costech Analytical Technologies, USA). The solid samples are combusted at 980°C and carried through a gas chromatography (GC) column with a helium carrier gas to chromatographically separate combusted elements measured on a thermal conductivity detector (TCD) calibrated with EDTA standards.

Samples that were measured for NaOH non-desorbable organo-mineral OC (Fig. 3d), remained in the anoxic chamber, where the solid fraction was inserted into 10ml of 0.5M NaOH solution within a new 12ml exertainer. The samples were then shaken for 24 hours on an oscillatory shaker at 150 rpm to enable full desorption of organo-mineral OC that is vulnerable to destabilisation by NaOH (Kaiser and Guggenberger, 2000). Once more, the samples were passed through a 0.22µm PES filter using vacuum filter apparatus within the anoxic chamber to retrieve the solids from the supernatant before being washed with 10ml milliQ H_2O. The solid organo-mineral fraction was removed from the anoxic chamber and immediately stored within a -20°C freezer. Then the sample was freeze-dried for to be measured for the wt%C of 0.5M NaOH non-desorbable OC fraction of the organo-mineral using COSTECH ECS 4010.

Samples that used for measuring the extent of iron oxide mineral transformation (Fig. 3e), also remained within the anoxic chamber. The organo-mineral solids were re-suspended within 10mL of 0.4M HCl in a 12ml exertainer and shook at 150 rpm on an oscillatory shaker for 24 hours to allow for dissolution of amorphous Fe oxide phases including ferrihydrite (Reddy et al., 2015; Wang et al., 2020). The sample was then passed through a pre-weighed 0.22µm PES filter to separate any solids from the supernatant. The Fe-oxide that was adhered to the PES filter was then left to air-dry for 24 hours before being reweighed. The difference between the pre and post filtered weights of the filter was used to

quantify the weight of Fe oxide mineral that does not dissolve in 0.4M HCl ($WtFe\text{-}O_{0.4M\ HCl\ wash}$). This (DW mineral post 0.4M HCl wash) was normalised with the total weight of Fe-oxide mineral in each sample (DW ferrihydrite in sample at T0) into the proportion of total ferrihydrite mineral that was resistant to dissolution by 0.4M HCl (%0.4M HCl resistant FeO mineral) (Equation 2).

$$(Equation\ 2)\ \%\ 0.4M\ HCl\ resistant\ FeO\ mineral = \frac{DW\ mineral\ post\ 0.4M\ HCl\ wash}{DW\ ferrihydrite\ in\ sample\ at\ T0}$$

Crystalline iron oxide minerals such as goethite are more resistant to dissolution by 0.4M HCl compared to amorphous iron oxide minerals such as ferrihydrite (Reddy *et al.*, 2015; S. Wang *et al.*, 2020; Zhao *et al.*, 2022). The $WtFe\text{-}O_{0.4M\ HCl\ wash}$ was used as a proxy for mineral transformation that took place. The method was developed for this experiment during pilots (see section 2.2.5).

2.2.4. Data analysis

Two-way analyses of variance (ANOVA) with a Tukey post-hoc test was used at the 96-hour datapoint to measure if there is any significant difference between the organo-minerals of mono-, di- and tri-carboxyl-richness in the measurements taken. The 96-hour timepoint was used for statistical analysis as this is the final timepoint in the time series and should be the point at which the extent of organo-mineral destabilisation due to reducing conditions is at its greatest. Statistical tests were performed using R through R studio software.

2.2.5. Pilots to the experiment

To optimise the process for synthesising carboxylic acid organo-minerals, a series of pilot experiments were conducted. This first refined the standard protocol (Schwertmann and Cornell, 2008; Zhao *et al.*, 2022) and then optimised the proportions of OC and mineral needed for the three organo-mineral treatments to achieve a standard wt%C for each. The organo-minerals were synthesised to achieve an environmentally relevant weight % C for each organo-mineral treatment at 5 wt%C (Crow *et al.*, 2007; Sollins *et al.*, 2009). To be able to synthesise a consistent 5 wt%C organo-mineral for the experiment, several batches of each organo-mineral treatments were made, with increasing carboxylic

acid weight added with 20g $Fe(NO_3)_3.9H_2O$ prior to KOH addition. The resulting organo-minerals were centrifuged to a pellet then freeze-dried, weighed, and measured for C using COSTECH ECS 4010. The resulting wt%C fed into constructing an isotherm that helped decipher the weight of each carboxylic acid that was needed to be added to the reactants for the organo-mineral synthesis.

A second-hand anaerobic glovebox (DW scientific compact anaerobic chamber) was purchased to progress to the experiment. N_2 gas was connected and pumped into the anaerobic chamber, where O_2 and CO_2 meters measured O_2 and CO_2 concentrations within the chamber. An O_2 concentration below 0.6ppm could not be achieved, too high for anaerobic conditions. This highlighted that there was either a leak in the chamber, an ineffective scrubber or both. Alternative arrangements were made to conduct the experiment at the Wolfson lab at Leeds University. Here, the anaerobic glovebox could achieve 0ppb O_2, satisfying the needs for the experiment.

A method to indicate the extent of mineral transformation was required to supplement the measurement of C in the organo-minerals. Common methods to measure mineral transformation include measuring the crystallinity of the mineral directly by x-ray diffraction analysis (XRD) (Zhao *et al.*, 2022) or by sequential dissolution of Fe-oxides (Heckman, Lawrence and Harden, 2018). XRD analysis was not available in my lab and the sequential dissolution agents of Na-pyrophosphate, hydroxylamine, and dithionite-HCl are aggressive chemicals that I was not comfortable to use in the communal lab, so an alternative method to determine mineral transformation was sought for.

An alternative method to common methods that indicate mineral transformation (such as dissolution by diothonite or measurement on XRD) was decided to be used. The alternative method used was to measure the weight of mineral that is not dissolved by 0.4M HCl ($WtFe\text{-}O_{0.4M\ HCl\ wash}$). This is as amorphous Fe-oxide minerals including ferrihydrite is dissolved by 0.4M HCl, leaving more crystalline Fe-oxide minerals remaining as the solid phase (Reddy *et al.*, 2015; S. Wang *et al.*, 2020; Zhao *et al.*, 2022). Therefore, fe-oxide minerals that have undergone mineral transformation into more crystalline forms will be measured, giving an indication of the extent of mineral transformation.

A protocol was developed as this method had not been conducted before. PES membrane filters were selected as it resists adsorption by OC and other compounds, but a pore size that retains the non-dissolved Fe-oxide mineral but allows for dissolved ferrihydrite to pass through was needed. A pore size of 0.22µm was selected as geothite mineral that was synthesised using protocol by Schwertmann and Cornell (2008), could not pass through the 0.22µm PES filter. Freshly synthesised geothite consisted of very fine particles, confirming that some more crystalline iron-oxide minerals were being retained by the 0.22µm PES filter.

2.3. Results

2.3.1. Fate of C in Organo-mineral

The amount of total C associated to ferrihydrite mineral differed between the different organo-mineral treatments (Fig. 5a). This corresponded with the carboxyl-richness of the OC, with greater amount of carbon associated to the mineral for di- and tri-carboxylic acid organo-minerals (4.47-5.06 wt%C and 4.30-4.95 wt%C respectively) compared to the mono-carboxylic acid organo-mineral (1.59-2.60 wt%C).

The differences between the carboxyl richness OC for the total C associated to the mineral at the 96 hour time point was statistically significant ($F(2)=56.97$, $p < 0.001$). Here a post-hoc Tukey test revealed that all organo-mineral treatments were significantly different from each other at 96 hours (all $p < 0.05$).

The wt%C of NaOH non-desrobable OC (Fig. 5b), defined as OC remaining after a 0.5M NaOH wash ($C_{0.5M\ NaOH}$), was less than the wt%C of the organo-mineral for each treatment (Fig. 5a). Differences remained between the wt%C of each organo-mineral treatment for $C_{0.5M\ NaOH}$ (0.54-1.03 wt%C for mono-carboxylic acid, 0.76-1.76 wt%C for di-carboxylic acid and 1.01-2.28 wt%C for tri-carboxylic acid). At the 96 hour time point, a two-way ANOVA revealed that there were statistically significant differences between organo-mineral treatments for $C_{0.5M\ NaOH}$ ($F(2)=36.8$, $p<0.001$). The post-hoc Tukey test at 96 hours revealed that there were statistical differences between mono-carboxylic acid organo-mineral treatment compared to both the di- and tri-carboxylic acid organo-mineral $C_{0.5M\ NaOH}$ (both $p<0.05$), whereas there was no clear statistical difference between di- and tri-carboxylic acid organo-mineral $C_{0.5M\ NaOH}$ ($p=0.153$). However, the statistically significant differences of $C_{0.5M\ NaOH}$ between mono-carboxylic acid organo-mineral treatment compared to both di- and tri-carboxylic acid organo-minerals was greatly reduced compared to the wt%C of the organo-minerals (Fig. 5a), where wt%C of $C_{0.5M\ NaOH}$ had a total range of 1.72wt%C (0.54-2.26wt%C) compared to 3.47wt%C (1.59-5.06 wt%C) of the organo-mineral.

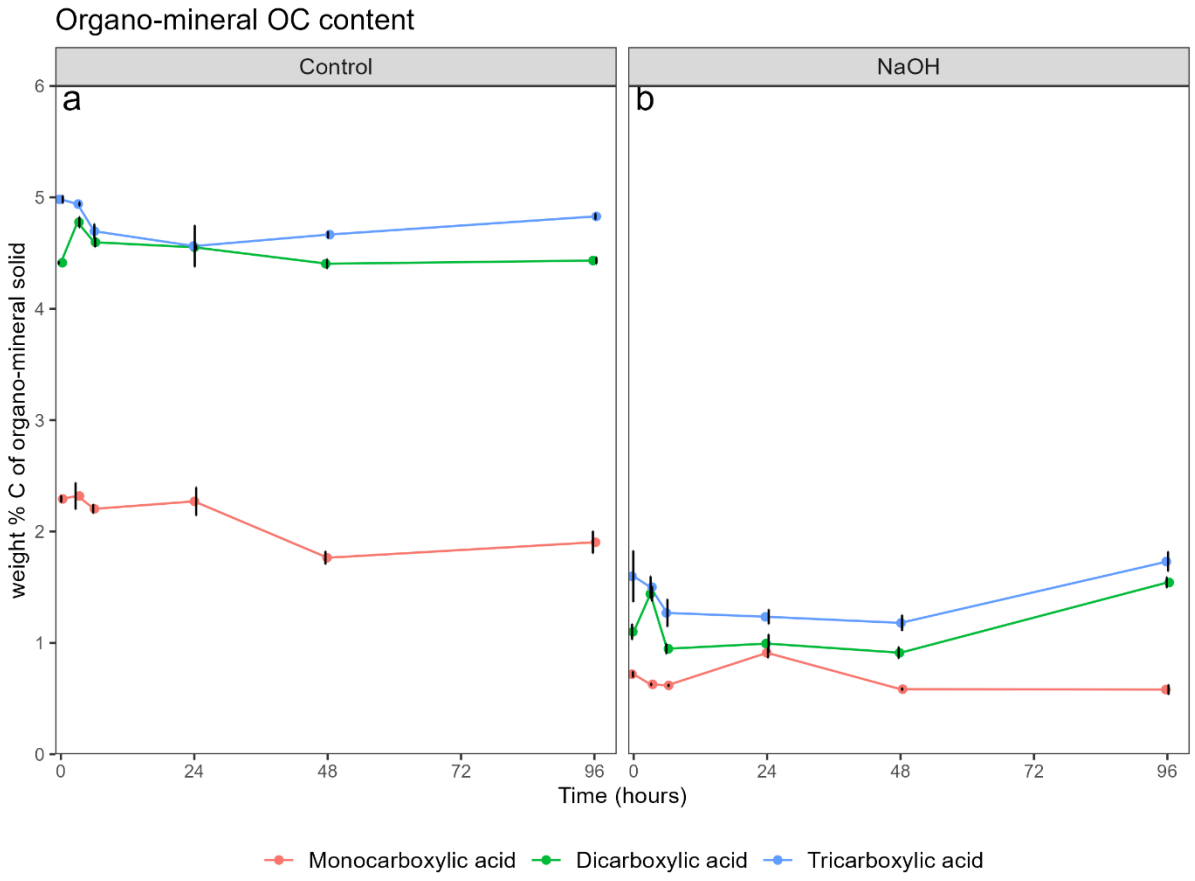

Figure 5 – Line graphs showing the temporal change of wt%C in the solid fraction of each organo-mineral treatment over time for both the control treatment (a) and the NaOH wash treatment (b). Each data point is shown at 0, 3, 6, 24, 48, and 96 hours shows the mean ± SE (n=5). The OC content of the organo-mineral for the NaOH wash treatment (b) was measured after a 24 hour 0.5M NaOH wash ($C_{0.5M\ NaOH}$)

2.3.2. Transformation of ferrihydrite mineral in reducing conditions

There was a clear difference in the change of WtFe-$O_{0.4M\ HCl\ wash}$ between the three organo-mineral treatments over the course of the incubation (Fig. 6). The tri-carboxylic acid organo-mineral treatment inhibited change in WtFe-$O_{0.4M\ HCl\ wash}$ (a range of 2.12mg (1.06-3.18mg)) compared to the mono- and di-carboxylic acid organo-mineral treatments (range of 7.99mg (2.55-10.44mg) and 8.39mg (1.61-9.00mg) respectively). At hour 96, after the 0.4M HCl wash, the WtFe-$O_{0.4M\ HCl\ wash}$ was significantly different between the organo-mineral treatments ($F(2)=53.8$, $p<0.001$). The post-hoc tukey test showed that the WtFe-$O_{0.4M\ HCl\ wash}$ for the tri-caboxylic acid organo-mineral treatment was significantly less than both the mono- and di-carboxylic acid organo-minerals (both $p<0.05$). However, there was no significant difference between the WtFe-$O_{0.4M\ HCl\ wash}$ between the mono- and di-carboxylic acid organo-mineral treatments ($p=0.125$).

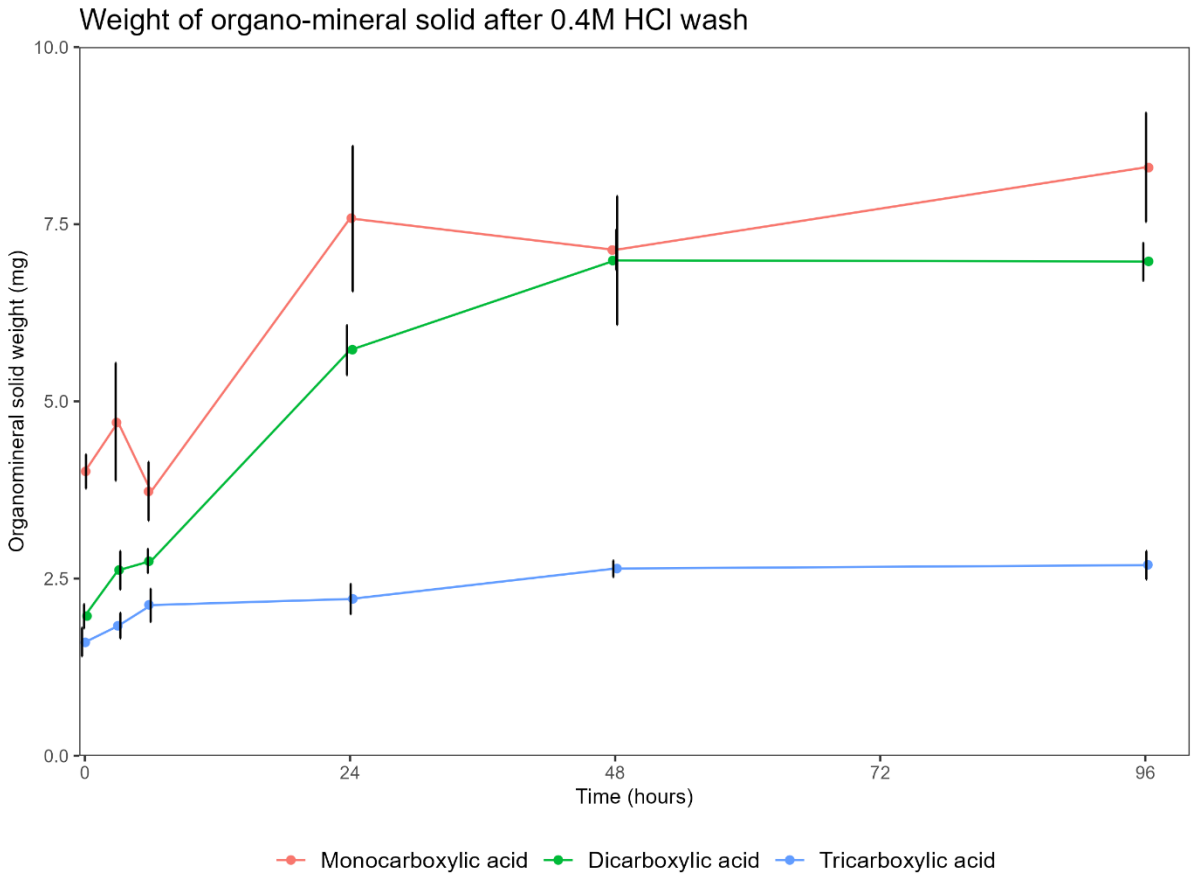

Figure 6 - A line graph showing the weight of solids after a 0.4M HCl wash for each organo-mineral treatment over the course of the incubation. This is a proxy to show Fe-oxide mineral transformation. Each datapoint shows the mean ± SE (n=5) for each organo-mineral treatment.

2.4. Discussion

This study set out to explore the research question **does the carboxyl-richness of organo-minerals affect their vulnerability to destabilisation by reductive dissolution?** This question was tackled through an experiment where model ferrihydrite organo-minerals of increasing carboxyl-richness were incubated in reducing conditions to induce abiotic reductive dissolution of the mineral. The hypothesis that the experiment tested was **carboxyl-poor organo-minerals have greater vulnerability to destabilisation by reductive dissolution compared to carboxyl-rich organominerals**. Measurements of the organo-mineral weight % C highlighted the fate of carboxylic acid OC throughout the incubation and measurements representative of mineral transformation helped to indicate the reductive dissolution that has occurred.

In this experiment, carboxyl-richness of the organo-mineral influenced its response to destabilisation in reducing conditions. The more carboxylic acid functional groups the OC molecule contains, the greater the retention of OC associated to ferrihydrite and with less transformation of the ferrihydrite mineral over time by reductive dissolution, indicating that the hypothesis has been proven.

2.4.1. Carboxyl poor organo-minerals contained less carbon

At the beginning and throughout the 96 hours of incubation, the mono-carboxylic acid organo-mineral contains significantly less C compared to the di- and tri-carboxylic acid organo-minerals (Fig. 5a). This is despite the fact that organo-minerals used in the experiment contained similar amounts of C when the organo-minerals were synthesised, at about 8 weight % C, tested during the pilot (see section 2.5.5).

This is likely due to more OC being desorbed for carboxyl-poor organo-minerals when rinsing of the solids with milliQ H_2O prior to freeze-drying for C analyses. Organo-minerals of lower carboxyl-richness have greater water extractable C compared to carboxyl-rich organo-minerals (Heckman *et al.*, 2011; Possinger, Bailey, *et al.*, 2020). This is due to the mechanisms of organo-organic associations

(Kleber, Sollins and Sutton, 2007) of carboxyl-poor organo-minerals being weaker than the more carboxyl-rich organo-minerals. The single carboxyl group in the mono-carboxylic acid (Fig. 2a) is occupied by the direct association to the mineral surface through ligand exchange (Kleber, Sollins and Sutton, 2007; Kleber *et al.*, 2021), leaving only the aliphatic tail free to form interactions with other OC. Therefore, weak hydrophobic and van der waals interactions between the aliphatic tails of hexanoic acid drive organo-organic associations in these carboxyl poor organo-minerals, which can be easily interrupted by rinsing with H_2O. In comparison, di- and tri-carboxylic acids have multiple carboxylic acid functional groups, which enables there to be a free carboxyl group available to interact with other OC even when one carboxyl group is occupied in direct association to the mineral surface. These 'free' carboxylic groups enable stronger mechanisms of organo-organic association, such as through cation bridging (Kleber, Sollins and Sutton, 2007). These interactions will be more resistant to a H_2O rinse.

2.4.2. Similar amount of NaOH non-desorbable OC between organo-minerals was independent of carboxyl-richness

There is little difference of 0.5M NaOH non-desorbable OC between the organo-minerals of different carboxyl-richness, where NaOH non-desorbable OC remains at 1-2 wt% C (Fig. 5b). This suggests that the quantity of this more stable organo-mineral OC is not dependant on the carboxyl-richness. This is opposes some recent research showing that as the carboxyl-richness increases, the stability against chemical washes such as NaOH and NaOCl increases (Curti *et al.*, 2021; Zhao *et al.*, 2022). This could be explained through the 0.5M NaOH wash used in this experiment, could overcome the differences in OC stability of organo-minerals of increasing carboxyl-richness that was seen in research using 0.1M NaOH wash (Curti *et al.*, 2021; Zhao *et al.*, 2022).

NaOH enhances the solubilisation of OC by causing ionisation of OC functional groups, including carboxylic acid (Lopez-Sangil and Rovira, 2013), enabling desorption of OC from the organo-mineral. The 0.5M NaOH wash is less able to destabilise OC involved in inner-sphere complexes, where

the OC is directly associated to the iron oxide surface through covalent bonds (Kleber, Sollins and Sutton, 2007). These inner-sphere complexes dominate direct organo-mineral interactions between carboxylic acid functional groups and the hydroxyl groups found on metal oxides such as ferrihydrite (Kleber, Sollins and Sutton, 2007; Kögel-Knabner *et al.*, 2008; Newcomb *et al.*, 2017; Kleber *et al.*, 2021). However, organo-mineral complexes also contain organo-organic associations, which is dominated by weaker mechanisms of association such as cation bridging, hydrophobic and van der waals interactions (Sollins *et al.*, 2006; Kleber, Sollins and Sutton, 2007; Newcomb *et al.*, 2017; Gao *et al.*, 2020). The NaOH wash can desorb and solubilise this OC. Therefore, the remaining non-desorbed OC after the 0.5M NaOH wash was predominantly OC involved in direct organo-mineral associations via inner-sphere complexes. There appeared to be a capacity of the mineral surface to host these 0.5M NaOH non-desorbable interactions that was not dependent upon the OC carboxyl richness, as this did not vary greatly between the different organo-minerals treatments. These results reflected the finite surface on minerals for direct organo-mineral to occur (Schweizer, 2022) irrespective of OC carboxyl-richness.

2.4.3. No change in organo-mineral OC content over time

Destabilisation of the organo-mineral complex is expected with the onset of reducing conditions, by adding ferrous iron (Fe(II)) in anaerobic conditions, through the reductive dissolution of ferrihydrite (Han *et al.*, 2019; ThomasArrigo, Kaegi and Kretzschmar, 2019). However, this experiment shows very little to no change of weight % carbon over the course of the time series (Fig. 5a), suggesting that there is no destabilisation of the organo-mineral complex occurring by the reductive dissolution of the ferrihydrite mineral. However, the transformation of iron oxide mineral from ferrihydrite to a more crystalline phase of iron oxide resistant to dissolution by 0.4M HCl (Fig. 6), shows that reductive dissolution and subsequent reprecipitation of Fe(III) has occurred.

Earlier research suggests that reductive dissolution of Fe(III)-oxides is inhibited by direct organo-mineral inner-sphere interactions (Schwertmann and Cornell, 2008; Henneberry *et al.*, 2012),

meaning that no destabilisation of organo-mineral OC would occur. This could explain the absence of a trend of decreasing weight % C in organo-minerals within this experiment. However, later research has shown that Fe(II)-ferrihydrite electron transfer can occur in carboxylic acid containing organo-minerals (Jones *et al.*, 2009; ThomasArrigo *et al.*, 2017; Zhou *et al.*, 2018). Furthermore, the inner-sphere complex between the carboxyl group of the OC and the Fe(III)-oxide mineral surface is able to be terminated during the exchange between Fe(II) and Fe(III) (Chen *et al.*, 2014). This is supported in further investigations (ThomasArrigo, Kaegi and Kretzschmar, 2019).

The lack of change in weight % C of the organo-minerals across the time series can be attributed to the abiotic nature of the experimental design, as previously seen in a similar experiment (Chen, Kukkadapu and Sparks, 2015). In an abiotic system, the OC that has been destabilised is unchecked from immediately re-adsorbing onto mineral surfaces that have re-precipitated following from reductive dissolution (Chen, Kukkadapu and Sparks, 2015), resulting in no change in weight % C over the course of the incubation. In a real soil system, microbes would be able to take advantage of the organo-mineral C that had become more accessible due to reductive dissolution of the mineral. Other experiments (Chen *et al.*, 2020) see a decrease in weight % C of organo-minerals when reductive dissolution of ferrihydrite is induced, suggesting that the results seen in our experiment is due to its abiotic nature.

There is no change in the amount of 0.5M NaOH non-desorbable OC in the organo-minerals over the course of the abiotic incubation. Any change in the binding strength of the direct organo-mineral interaction as has been highlighted in previous investigations (Chen, Kukkadapu and Sparks, 2015), is not realised in this experiment when measuring 0.5M NaOH non-desorbable OC over the course of the incubation.

2.4.4. Organo-mineral carboxyl-richness controlled the extent of mineral transformation induced by reductive dissolution

The carboxyl-richness of organo-minerals does influence the extent of the mineral transformation of ferrihydrite that results from reductive dissolution. Greater mineral transformation occurs in the mono- and di-carboxylic acid organo-minerals compared to the tri-carboxylic acid organo-mineral (Fig. 6) in this experiment, even though previous experiments have shown that even carboxyl-poor organo-minerals inhibit mineral transformation compared to pure ferrihydrite (ThomasArrigo, Kaegi and Kretzschmar, 2019).

OC in organo-minerals have been seen to supress mineral transformation of the iron oxide caused by reductive dissolution in abiotic systems (Henneberry *et al.*, 2012; Chen *et al.*, 2014; ThomasArrigo *et al.*, 2017; Zhou *et al.*, 2018; Han *et al.*, 2019). Carboxyl groups are particularly able to slow down the action of reductive dissolution and coincident mineral transformation, by removing Fe(II) from solution through adsorption to unoccupied carboxylic acid functional groups, thus slowing down the progress of the Fe(II) to the Fe(III) containing mineral surface (Jones *et al.*, 2009; Catrouillet *et al.*, 2014; ThomasArrigo *et al.*, 2017; Zhou *et al.*, 2018; ThomasArrigo, Kaegi and Kretzschmar, 2019). Therefore, carboxyl rich OC with greater abundance of available free carboxyl functional groups may slow down the action of Fe(II) that causes reductive dissolution and mineral transformation to a greater extent compared to carboxyl poor OC. This mechanism may also decrease the destabilisation of carboxyl-rich organo-mineral OC due to a slowing down of Fe-oxide reductive dissolution compared to the carboxyl-poor organo-mineral.

Furthermore, the carboxyl-rich OC can inhibit a more structured crystalline arrangement of the iron-oxide mineral re-precipitating after reductive dissolution (Jones *et al.*, 2009; ThomasArrigo *et al.*, 2017). Iron oxide minerals are able to re-precipitate onto the carboxylic functional groups of OC, thus impacting the crystal structure of this re-precipitating Fe-oxide mineral (Chan *et al.*, 2009). Carboxyl-rich OC will enable precipitation of Fe-oxide mineral in many orientations, due to the

multiple carboxyl functional groups (Chan *et al.*, 2009; ThomasArrigo, Kaegi and Kretzschmar, 2019) fostering the re-precipitation of a disordered and amorphous mineral. In this experiment Adipic acid (the di-carboxylic acid) is symmetrical in structure, whereas tricarballylic acid (the tri-carboxylic acid) is asymmetrical in structure. Therefore, when reprecipitation of the iron oxide mineral occurs after reductive dissolution, co-precipitation with the di-carboxylic acid will form a more symmetrical ordered and crystalline iron oxide mineral, whereas the mineral will be unordered and amorphous when co-precipitating with tri-carboxylic acid. This combined with the retardation of the Fe(II) movement to the mineral surface acts to reduce the extent of mineral transformation of the tri-carboxylic acid organo-mineral in this experiment. A greater divergence in the Fe-oxide crystallinity between the tri-carboxylic acid organo-mineral from the mono- and di-carboxylic organo-minerals may become apparent if the abiotic incubation was maintained for longer.

2.4.5. Wider implications

In a long-term perspective, this experiment has shown that the carboxyl-richness of an organo-mineral is relevant for maximising and maintaining the surface area of Fe-oxides and other metal oxide minerals. This is as the carboxyl-rich organo-minerals retain an amorphous Fe-oxide mineral structure, indicating that carboxyl-rich organo-minerals will retain a greater mineral reactive surface area for longer compared to carboxyl-poor organo-minerals. This impacts on the ability of the soil to retain organo-mineral OC as with greater mineral surface area maintained, the carboxyl-rich organo-minerals retain a greater capacity for direct organo-mineral interactions (Kleber, Sollins and Sutton, 2007; Kleber *et al.*, 2021). These have the capability to be more strongly associated such as through ligand exchange and inner-sphere complexes, making the OC more stable when exposed to biotic destabilisation (Kleber, Sollins and Sutton, 2007; Newcomb *et al.*, 2017; Kleber *et al.*, 2021). Furthermore, slowing soil ageing by inhibiting metal oxide mineral transformation (Zhao *et al.*, 2022) could help in maintaining the size of the SOC mineral fraction into the future. Older soils are concurrent with lower soil mineral surface areas and lower mineral surface reactivity, that translates into a smaller pool of mineral fraction SOC such as seen in older soils such in the tropics (Kirsten *et al.*,

2021; Zhou *et al.*, 2024). An Fe-oxide mineral pool where mineral ageing is inhibited or slowed down by carboxyl-rich OC could enable soils to retain a large pool of SOC in the mineral fraction, which is conceptualised as the important long-term SOC pool (Cotrufo and Lavallee, 2022). However, the ageing of soil minerals may be relevant across a longer timescale compared to what is applicable to mitigating anthropogenic CO_2 emissions and climate change.

The transformation of iron oxide minerals due to reductive dissolution and subsequent reprecipitation may result in associated OC to become encapsulated within the structure of the mineral (Han *et al.*, 2019; ThomasArrigo, Kaegi and Kretzschmar, 2019; Zhao *et al.*, 2022). This occluded OC would be less accessible to microbes and more stable. Field investigations have shown that OC that is occluded within crystalline minerals are found to be much older, so accordingly more persistent compared to OC that is not occluded or associated to amorphous iron oxide minerals (McFarlane *et al.*, 2013; McFarland *et al.*, 2019). In this experiment, the effect of OC occlusion during mineral transformation is not seen, as there is no apparent change in quantity of $C_{0.5M\ NaOH}$ throughout the timeseries for each organo-mineral treatment (Fig. 5b). It is possible that not enough time had elapsed for sufficient mineral transformation in order to see this effect. However, this effect may be prevalent for carboxyl-poor organo-minerals due to greater mineral dissolution and re-precipitation, enabling the potential for more occlusion of organo-mineral OC. Therefore, occluded OC emanating from the mineral transformation of carboxyl-poor organo-minerals will be very persistent, assuring more long-term mitigation of anthropogenic CO_2 in soils. Furthermore, crystalline iron oxide minerals such as geothite are more thermodynamically stable compared to ferrihydrite, therefore reductively dissolve less readily (Larsen and Postma, 2001; Pedersen *et al.*, 2005; Chen, Dong and Thompson, 2023). This effect conflicts with the mechanism where carboxyl-rich OC is able to maintain a greater capacity of mineral associated OC fraction by preserving mineral surface area, compared to carboxyl-poor OC. . However, the magnitude of OC that can become occluded and persistent for up to millennia is miniscule compared to the OC in the MAOM pool (McFarlane *et al.*, 2013; McFarland *et al.*, 2019; Cotrufo and Lavallee, 2022). Therefore, as this mechanism where carboxyl-poor organo-minerals

maximising OC occlusion will have a smaller impact on the mitigation of climate change, it is more important to increase the stability of the MAOM pool at large. Therefore, the ability of carboxyl-rich OC to maintain a larger fe-oxide surface area is preferential to be able to sequester more carbon into soil, building towards the 4 per mille initative (Minasny *et al.*, 2017). This highlights the need for the application of carboxyl-rich soil amendments as a land management strategy to improve the persistence of the MAOM pool.

Although carboxyl-rich OC is unable to completely thwart the ability for Fe-oxides to reductively dissolve, this experiment indicates that carboxyl-rich organo-minerals result in less destabilisation by reductive dissolution. However, in this abiotic incubation, the effect of destabilisation by the soil microbial community is missing. In a soil setting where soil microbial community is active, the vulnerability of organo-minerals to destabilisation by reductive dissolution could be enhanced by biotic destabilisation (Kleber *et al.*, 2021). This would indicate that in a soil with a microbial community, there could be large differences between carboxyl-rich and carboxyl-poor OC in the loss of organo-mineral OC due to microbial respiration. Here, the effect of the carboxyl-richness on maintaining mineral-surface area or enabling the occlusion of OC due to mineral-transformation may be less important than the impact of organo-mineral carboxyl-richness on resisting biotic destabilisation. This was investigated in further detail in chapter 3 of this thesis.

2.4.5. Conclusions

This investigation has shown that carboxyl-rich organo-minerals are able to contain a greater amount of OC due to stronger organo-organic interactions, rather than through any increase in direct organo-mineral interactions.

The carboxyl-richness of the organo-minerals do not appear to impact the ability of the Fe-oxide mineral to reductively dissolve. However, the slowing down of Fe(II) diffusion towards the mineral surface in organo-minerals containing more available carboxyl groups may reduce the destabilisation of carboxyl-rich organo-mineral OC. The mineral transformation results are suggestive

of this mechanism, even though direct capture of this mechanism has been out of reach of this investigation. Here, carboxyl-rich OC inhibits mineral transformation from ferrihydrite into more crystalline iron-oxide minerals compared to carboxyl-poor organo-minerals, maintaining a disordered structure of the mineral phase during re-precipitation.

Therefore, the hypothesis of this experiment, predicting that carboxyl-rich ferrihydrite organo-minerals will be less vulnerable to destabilisation by reductive dissolution, has been proven.

3. How does carboxyl richness affect organo-mineral stability in a soil environment?

3.1. Introduction

In Chapter 2 of this thesis, carboxyl richness had a limited impact on the stability of organo-mineral C in abiotic reducing conditions. The tri-carboxyl organo-minerals did not completely inhibit destabilisation by reductive dissolution, although other investigations (Jones *et al.*, 2009; Catrouillet *et al.*, 2014; ThomasArrigo *et al.*, 2017; Zhou *et al.*, 2018; ThomasArrigo, Kaegi and Kretzschmar, 2019) have indicated that carboxyl-rich organo-mineral OC can slow down the diffusion of the Fe(II) reducing agent to the mineral surface compared to carboxyl-poor organo-mineral OC. The experiment in Chapter 2 supported this with evidence of inhibited mineral transformation in tri-carboxyl organo-minerals. The experiment investigated whether the OC carboxyl-richness is a mechanistic control on the organo-minerals vulnerability to destabilisation by reductive dissolution. This required a simple, highly controlled experimental set-up with the organo-minerals incubated in abiotic and constant reducing conditions.

However, soil systems in which organo-minerals are situated are much more complex environments. There are countless interactions between organo-minerals and other components of soils such as soil microbes, plant inputs and highly heterogeneous soil physical and chemical properties which vary in space and time (Kleber *et al.*, 2021; Song *et al.*, 2022). It is not clear whether the limited impact that carboxyl-richness had on the stability of organo-mineral C in Chapter 2 will remain the same in a real, biotic soil system where redox conditions vary widely.

An important component of soils that will impact the destabilisation of organo-mineral OC are soil microbial communities (Bailey, Pries and Lajtha, 2019). Most soil microbes are most active and able to metabolise soil OC under aerobic conditions (Possinger, Bailey, *et al.*, 2020), so the potential

for biotic destabilisation of organo-mineral OC may be greatest during aerobic conditions. Some well adapted microbial communities can metabolise soil OC in anaerobic conditions readily (DeAngelis *et al.*, 2010; Bhattacharyya *et al.*, 2018), although to a lower efficiency (LaRowe and Van Cappellen, 2011). Some anaerobic soil microbes such as *Geobacter spp.* can directly destabilise organo-minerals by mediating biotic iron oxide reduction, using this process to enable the oxidation of soil C for respiration (Kato, Hashimoto and Watanabe, 2013; Merino *et al.*, 2021).

Most real soil systems will tend to oscillate between aerobic and anaerobic conditions both spatially and temporally (Keiluweit *et al.*, 2017; Bhattacharyya *et al.*, 2018; Possinger, Bailey, *et al.*, 2020; Afsar *et al.*, 2023) due to the variation in soil moisture generated by topography, weather, and the pore structure of the soil itself. Therefore, organo-mineral stability in soils will be affected by both the reductive dissolution of Fe-oxides experienced in anaerobic conditions as well as enhanced microbial activity during aerobic conditions (Bhattacharyya *et al.*, 2018; Bailey, Pries and Lajtha, 2019). The combination of anaerobic, Fe-reducing microbial communities and biotic destabilisation mechanisms could increase rates of organo-mineral destabilisation compared to abiotic organo-mineral destabilisation by reductive dissolution explored in Chapter 2.

In addition to the direct effects of aerobic and anaerobic conditions on microbial processes, transitions from saturated to unsaturated conditions in soils are known to generate peaks in microbial activity and respiration, known as the 'Birch effect' (Bailey, Pries and Lajtha, 2019; Barnard, Blazewicz and Firestone, 2020). These peaks are experienced in the wetting period immediately after an extended dry period. The arrival of new moisture connects isolated soil pores, transporting oxygen and nutrient that microbes can utilize for anabolism and respiration (Barnard, Blazewicz and Firestone, 2020). This peak in microbial activity in the transition between dry to wet conditions could instigate biotic destabilisation of organo-minerals. Similar peaks in the destabilisation and respiration of organo-minerals may also occur immediately after transitions from wet anaerobic conditions to drier aerobic conditions due increased accessibility of reductively destabilised organo-mineral OC combined with

increased aerobic microbial activity (Bhattacharyya *et al.*, 2018). Microbial communities can adapt to redox fluctuations (DeAngelis *et al.*, 2010) and respond quickly to the return of aerobic conditions. Alternatively, there is evidence that less OC decomposition may occur in the anaerobic to aerobic transition due to association to re-precipitated Fe-oxide minerals (Zhao *et al.*, 2020).

The duration of the periodicity of redox conditions within soil that oscillate between aerobic and anaerobic conditions will have a significant impact on the dominant mechanisms of organo-mineral OC destabilisation (Bhattacharyya *et al.*, 2018; Possinger, Bailey, *et al.*, 2020). Aerobically adapted microbial communities will tend to outcompete anaerobically adapted microbial communities in most soils due to aerobic respiration being more energy yielding compared to anaerobic respiration (LaRowe and Van Cappellen, 2011). Unless anaerobic conditions continue for a sufficient length of time or oscillate frequently, the anaerobic microbial community will not respond sufficiently (Evans and Wallenstein, 2012) and the extent of microbially mediated iron oxide reductive dissolution could be minimal.

Several experiments have investigated the impact of redox oscillations on the stability of mineral associated OC (Bhattacharyya *et al.*, 2018; Possinger, Bailey, *et al.*, 2020; Afsar *et al.*, 2023). However, how the chemical identity of OC in organo-minerals influences their vulnerability to destabilisations, has not previously been tested. Increasing carboxyl-richness was shown to increase organo-mineral stability in aerobic conditions (Curti *et al.*, 2021) to a greater extent compared to under reducing conditions (Chapter 2). Therefore, organo-mineral carboxyl-richness could be important in controlling organo-mineral stability under variable redox conditions experienced in natural soils.

The aim of this study was to investigate whether carboxyl-richness controls organo-mineral stability under oscillating aerobic and anaerobic conditions, which impose different destabilisation forces. Organo-minerals were synthesised, composed of ferrihydrite and either mono- or tri-carboxylic acid isotopically labelled with ^{13}C. These organo-minerals were incubated in a soil mixture for 4 weeks and exposed to oscillating redox conditions and the ^{13}C was traced into soil fractions and respiration.

Two hypotheses were tested in this experiment. **H1. Organo-mineral stability will be greater with increasing carboxyl-richness** and **H2**. **The extent of organo-mineral OC destabilisation will be greatest in soil with oscillating redox conditions**. Here, the extent of destabilisation is expected to differ between the different redox conditions, where greatest organo-mineral destabilisation is experienced in oscillating conditions followed by aerobic and then anaerobic conditions. Aerobic conditions will result in greater destabilisation compared to anaerobic conditions due to greater microbial activity, whilst organo-minerals exposed to oscillating conditions will experience the greatest destabilisation due to the combined effects of destabilisation by reductive dissolution and higher microbial activity.

3.2. Methodology

An incubation experiment was designed to investigate whether carboxyl-richness controls organo-mineral stability in a soil system that experiences varying redox conditions. Prior to the experiment (section 3.2.7), a number of preparatory steps were needed. These included: 1) synthesis of ^{13}C-labelled and unlabelled carboxylic acid organo-minerals and creating soil-organo-mineral mixtures for parallel incubations (sections 3.2.1 to 3.2.3); 2) validation of the ferrozine assay (section 3.2.4); 3) designing a setup for controlled anaerobic incubations (section 3.2.5); and 4) pilot experiments to optimise the incubation duration (section 3.2.6).

3.2.1. Selection of organo-mineral C

The experiment aimed to test the differences in organo-mineral stability between carboxyl-poor and carboxyl-rich organo-minerals. Results from Chapter 2 showed that a mono-carboxylic acid and tri-carboxylic acid would best highlight these differences between carboxyl-poor and carboxyl-rich organo-minerals, as the mono-carboxyl organo-mineral did not retain as much OC over time and experienced greater mineral transformation compared to the tri-carboxyl organo-minerals.

The mono-carboxylic acid used in Chapter 2 was hexanoic acid and the tri-carboxylic acid used was tricarballylic acid.

For this experiment, hexanoic acid (1-^{13}C hexanoic acid (Fig. 7a)) was selected as the mono-carboxylic acid but tricarballylic acid could not be used due to the high price of ^{13}C enriched tricarballylic acid. Instead, citric acid (1,3,5–^{13}C3 citric acid (Fig. 7b)) was selected as the tri-carboxylic acid. The citric acid molecule contains 6 carbon atoms similar to hexanoic acid, enabling a 1:1 relationship of carbon between the organo-mineral treatments, facilitating easier interpretation of results where total C and ^{13}C are measured.

3.2.2. Synthesis of organo-minerals

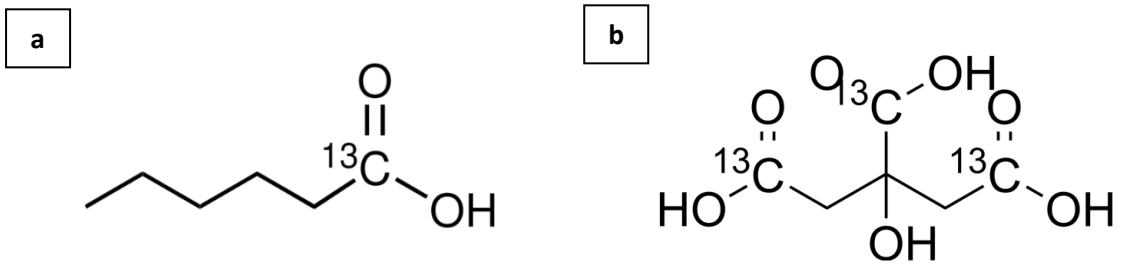

Figure 7 – ^{13}C labelled OC used to make ^{13}C enriched organo-minerals; 1-^{13}C Hexanoic acid (a) and 1,3,5-$^{13}C_3$ Citric acid (b)

Ferrihydrite organo-minerals were synthesised by coprecipitation with the carboxylic acid OC following the same method used in Chapter 2 (see sections 2.2.1 and 2.2.5) (Schwertmann and Cornell, 2008; Zhao *et al.*, 2022). Both ^{13}C labelled and unlabelled ferrihydrite organo-minerals were synthesised for use in parallel incubations (see section 3.2.7).

The organo-minerals were synthesised targeting a wt%C of 2wt% and ^{13}C enrichment of 5atm%. This wt%C target is lower than in Chapter 2 to minimise the costs of using ^{13}C labelled OC, however, a 2wt%C organo-mineral remains environmentally relevant (Crow *et al.*, 2007; Sollins *et al.*, 2009). The ^{13}C labelled carboxylic acids were diluted with the unlabelled carboxylic acid to produce a mixture of about 5atm% enriched carboxylic acid. A ^{13}C enrichment of 5atm% was chosen as this enrichment significantly exceeds the natural abundance of ^{13}C found in the soil matrix (see section 3.2.3). Therefore, the organo-mineral OC could be traced throughout the incubation. Here, 1-^{13}C Hexanoic acid (Fig. 7a) was mixed with unlabelled hexanoic acid at a ratio of 1:2.32, and 3.01g of the mix was added with 75g of $FeNO_3.9H_2O$ to make a ^{13}C enriched mono-carboxylic acid organo-mineral of 1.97wt%C at 5.31atm%^{13}C. For the ^{13}C enriched tri-carboxyl organo-mineral, 1,3,5–$^{13}C_3$ Citric acid (Fig. 7b) was mixed with unlabelled citric acid at a ratio of 1:5.61, and 1.15g of this mix was added to 75g of $FeNO_3.9H_2O$ to make a ^{13}C tri-carboxylic acid organo-mineral of 2.88wt%C at 5.80atm%^{13}C. Parallel mono- and tri-carboxyl organo-minerals were made to 1.67wt%C and 2.37wt%C, respectively.

3.2.3. Production of the soil-organo-mineral mix

B horizon soil (mineral horizon) was collected from Myerscough farm, Lancashire (53.848871, -2.784326). This site was adjacent to a farm runoff drainage ditch and so is frequented by flooding and saturation. Previous work at this site (McNamara, Mason and Oakley, Manuscript in preparation) as shown that the soil microbial community consists of both aerobic and anaerobic adapted communities, which are able to adapt to both aerobic and anaerobic conditions quickly. This is particularly important for the oscillating incubations as the soil microbiome was able to adapt and respond quickly to the changes between aerobic and anaerobic conditions. The soil was collected in November 2023 and stored at 5°C. The soil was at 33.25% max water holding capacity (WHC), with 8.79wt%C with a natural abundance of 1.08atm%^{13}C.

The soil was homogenised and airdried down to 29.90% max WHC at room temperature overnight then passed through a 0.4mm sieve. Soil organo-mineral mixtures containing 2.73wt% organo-minerals were created by mixing 9g DW equivalent of synthesised ferrihydrite into 330g DW equivalent of soil. This ratio was selected as soils often contain 2-4% iron oxides (Cornell and Schwertmann, 2003; Colombo *et al.*, 2014). This mixture was then passed through a 0.4mm sieve to homogenise and limit the size of soil aggregates. This process was completed for each organo-mineral treatment, creating four soil-organo-mineral mixtures (mono- and tri-carboxyl organo-minerals, ^{13}C labelled and unlabelled). The soil mixture containing ^{13}C enriched mono-carboxyl organo-mineral achieved 8.73wt%C at 1.11atm%^{13}C . The soil mixture containing ^{13}C enriched tri-carboxyl organo-mineral, achieved 8.75wt%C at 1.17atm%^{13}C.

3.2.4. Developing and validating the ferrozine assay method

Fe-oxide reductive dissolution mediated by soil anaerobic microbial communities was expected to be the main driver of organo-mineral destabilisation in the anaerobic conditions. This mechanism will reductively release Fe(III)-oxide into soil solution as Fe(II). Therefore, Fe(II)

accumulation within the soil-organo-mineral mix was measured by a ferrozine assay method, to validate the onset and extent of reductive dissolution within soil incubated in anaerobic conditions.

Ferrozine assays are a common method to measure total Fe (FeT) and Fe(II) in natural waters. The method uses a ferrozine reagent (sodium 4-[3-(pyridin-2-yl)-6-(4-sulfophenyl)-1,2,4-triazin-5-yl]benzene-1-sulfonate) that can complex with Fe^{2+} ions to form a purple coloured chelate (Huang and Hall, 2017). A colorimetric reader can be used to measure the absorbance (at 562nm wavelength) of the assay and the concentration of Fe^{2+} can be quantified by using a calibration of known Fe^{2+} concentrations. Here, the colorimetric reader emits light towards the sample which is contained in a transparent cuvette at a wavelength that is absorbed by the colorimetric reagent, which in the case of ferrozine is 562nm. A detector on the opposite side of the sample to the light source, measures the amount of light that has transmitted through the sample, and by deduction, the absorbance.

The ferrozine assay used for this experiment follows the method of Huang and Hall (2017). Here, 3g dry mass of soil-organo-mineral mix was shaken in 30 mL of 0.4M HCl for 1 hour to dissolve iron contained within the soil. Next, centrifugation of the sample at 4500rcf separated the solid soil particles from the supernatant and then centrifugation on a microcentrifuge at 10,000rcf removed any colloids from suspension. Then the soil extracts are added to an 8x12 microplate along with the ferrozine assay reagents, which differ between measurement of Fe(II) and FeT. For Fe(II) measurement, 40µL of soil extract was added to 40µL of milliQ H_2O, 100µL of acetate pH buffer, before 100µL of 1.46mM ferrozine reagent in 0.1M HCl was added. The acetate buffer maintained pH to near pH4. The same protocol was followed for measurement of FeT, except 40µL of 10% hydroxylamine hydrochloride was added instead of milliQ H_2O as a reduction reagent and left for 10 minutes to incubate. The reduction reagent worked to reduce Fe^{3+} to Fe^{2+} ions, so that the ferrozine reagent was able to complex with all the Fe in the sample. The calibration curve for FeT measurements on Ferrozine was satisfactory between 0.5mM and 0.01mM FeT, and the calibration curve of Fe(II) was very good between 0.01mM and 0.001mM Fe(II), setting the limits of detection for the ferrozine assay methods.

All glassware was washed in a 1% HCl acid bath for 24 hours to prevent contamination by residual Fe and pipette tips were changed each time to prevent cross-contamination.

A pilot experiment was devised to test the ferrozine method and investigate the ferrozine reagent incubation times for both the Fe(II) and Fe(T) ferrozine assays, as the ferrozine reagent incubation time can alter the accuracy of the results (Huang and Hall, 2017). The absorbance from two sets of samples were measured in triplicate and compared to test the accuracy of the assay at set ferrozine reagent incubation times. One set of samples consisted of just a 0.4M HCl soil-organo-mineral mix extract using the method outlined previously. The other set of samples were the same soil-organo-mineral mix extracts spiked with a known amount of Fe(II) from $FeCl_2$ solution, or Fe(III) from $Fe(NO_3)_3.9H_2O$ for the FeT test. Absorbance was measured using the microplate reader for ferrozine reagent incubation times of 5, 10, 20, 30 minutes and 1, 2 and 3 hours. The optimal incubation time was revealed where the % Fe recovery is nearest to 100%. The % recovery represents the difference between Fe concentration of a Fe spiked sample measured by the ferrozine assay and the known amount of Fe added manually through spiking the sample. This was calculated using equation 3 where C_{sample} was the concentration of the samples that have not been spiked measured by the microplate reader (µM), V_{sample} was the volume of the non-spiked sample (µL), C_{spike} was the concentration of the spike samples measured by the microplate reader (µM), V_{spike} was the volume of the spiked sample (µL), and Fe_{added} was the known amount of Fe(III) or Fe(II) added when spiking the sample (µmol).

$$(Equation\ 3)\ \%\ Recovery = \frac{Cspike\ \times Vspike}{(Csample\ \times Vsample) + Feadded} \times 100$$

Results from the pilot shows that a 1-hour ferrozine reagent incubation time gives the most accurate results for both the Fe(II) and FeT assays. Note that the soil extract was diluted by factor 1:15 with 0.4M HCl for the FeT ferrozine assay to keep the concentration within the limits of detection (0.01mM to 0.5mM of Fe).

Table 1 – Mean (n=3) % Fe recovery for both the FeT assay and the Fe(II) assay and their standard deviations for each selected ferrozine reagent incubation time. Green highlights the mean % Fe recovery closest to 100%

Incubation time	Average FeT % retained	Standard deviation	Average Fe(ii) % retained	Standard deviation
5 mins	105.61	3.28	102.00	1.55
10 mins	105.29	2.78	101.93	0.82
20 mins	105.07	2.31	100.61	0.84
30 mins	104.97	2.16	100.44	0.60
1 hour	104.79	2.82	100.00	0.61
2 hours	105.10	3.80	99.65	0.65
3 hours	105.42	4.53	99.43	0.52

3.2.5. Designing of controlled anaerobic incubations

Creating anaerobic incubations that led to the initiation of organo-mineral destabilisation by reductive dissolution of ferrihydrite was essential for this experiment. Thus, it was imperative that all O_2 was removed from the incubations and O_2 leaking inhibited for a sufficient time required for the soil microbial community to respond and adapt to anaerobic conditions enabling reductive dissolution of Fe-oxides mediated by the soil microbes.

A method was developed for removing O_2 without introducing O_2 during flushing or through leakage after flushing, and tested in a pilot. Customised Kilner jar lids were fitted with Apogee oxygen sensors to measure O_2 concentrations in the headspace, with septa to insert gas needles for N_2 flushing whilst the lid remains securely attached to the jar. The set up used a N_2 gas line that was split 20 ways, each inserted into a jar via a syringe needle (Fig. 8). N_2 gas flowed through this needle into

Figure 8 - Set-up to test the establishment of anaerobic incubations by N_2 flushing 20 kilner jars. Apogee O_2 sensors were attached to 8 of the kilner jars recording O_2 (%) within the kilner jar headspace

the soil headspace, creating a positive pressure within the jar, which pushed air out through another syringe needle into the fume cupboard. Apogee sensors connected to a CR1000X Series datalogger programmed to take O_2 measurements every 10 seconds, were inserted into 8 of the jars. O_2

measurements were viewed in real time using PC400 support software by Campbell Scientific on a connected computer.

N_2 gas was flushed through the jars for 45 minutes at a pressure of 5psi. The % O_2 in the jar headspace dropped rapidly within 5 minutes, followed by the O_2 % slowly levelling out for the next 10 minutes (Fig. 9). The Apogee sensors were not well calibrated for these low concentrations of O_2, as they showed negative O_2 % readings, so the sensor output (in mV) was used to observe changes in O_2 levels (Fig. 10). There was no change in O_2 concentration in the jar headspace after 20 minutes of N_2 flushing. This was defined as the required flushing time.

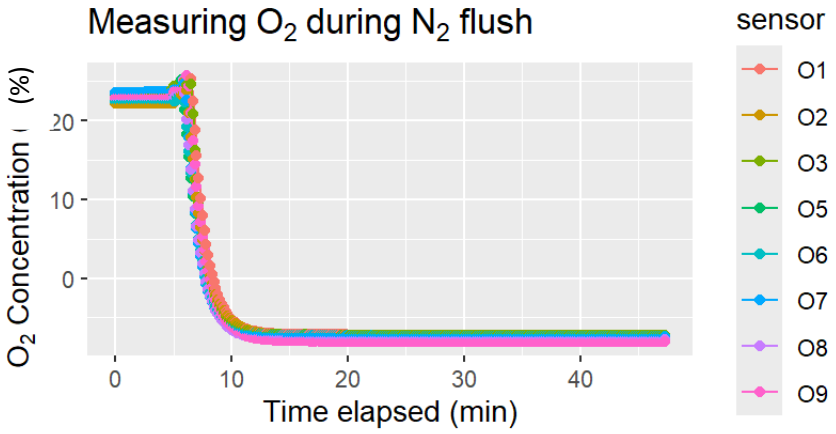

Figure 9 – Line graph showing measurements from each Apogee sensor of O_2 % concentration every 10 seconds in the headspace of kilner jars during flushing with N_2

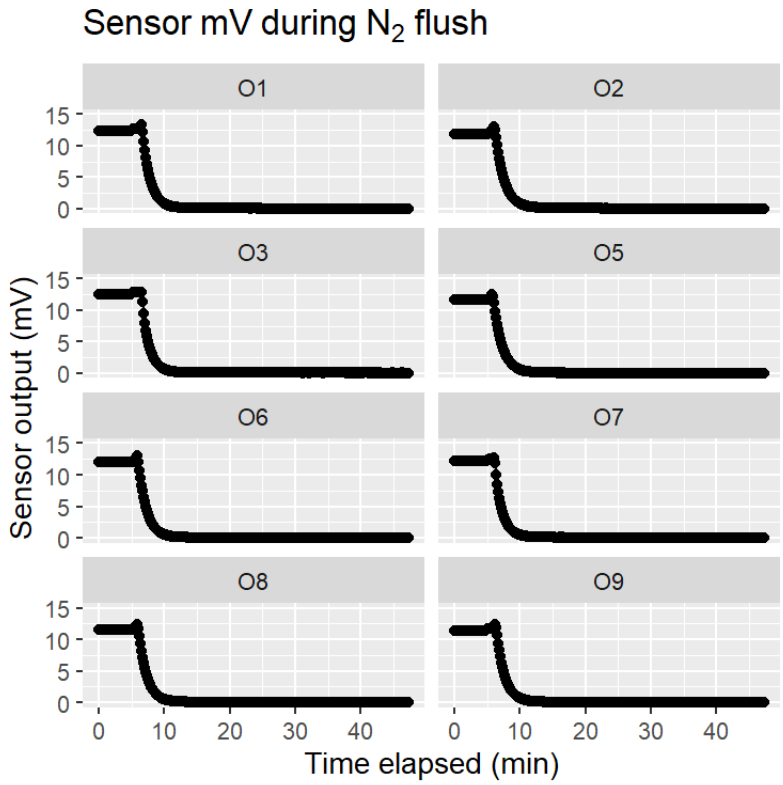

Figure 10 - Line graph showing measurements from each Apogee O_2 sensor (mV) every 10 seconds in the headspace of kilner jars during flushing with N_2

At the end of the flush, N_2 inflow needles were removed from the septa immediately before the gas outflow needle, so positive pressure inside the jars inhibited ambient O_2 from entering the headspace. The Apogee oxygen sensors remained in the jars as they were left overnight to incubate at 15°C, making O_2 measurements every minute. Melted paraffin wax was dripped onto the surface of the septa to seal any small punctures made by the syringe needles. These measures meant that the Apogee O_2 sensors recorded little to no change in mV output. The gradient of linear models created

on the mV output measurements were all <0.001 except Sensor O5 (Fig. 11), showing that the change

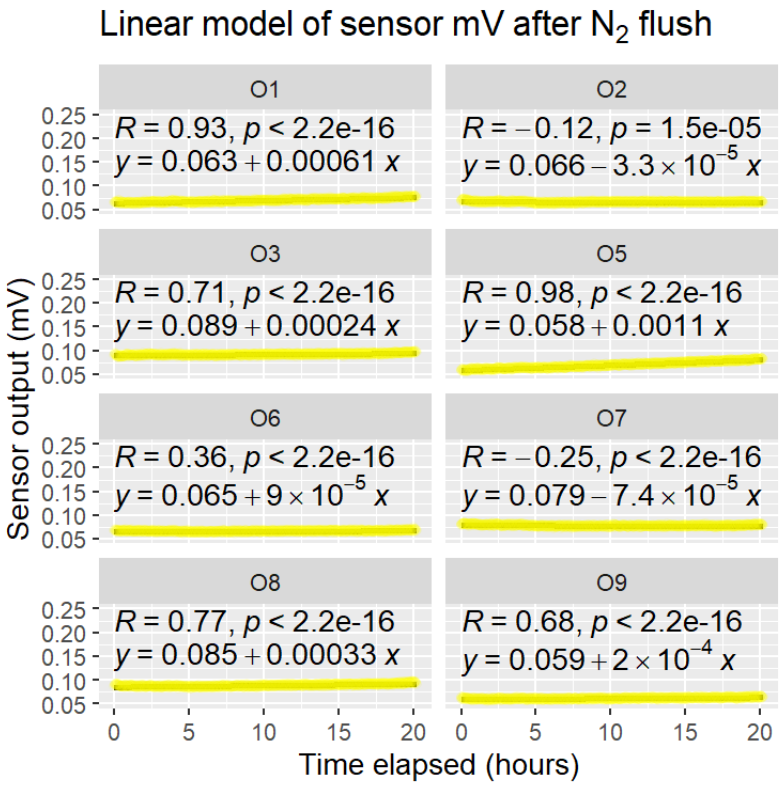

Figure 11 – Linear models made from Apogee O_2 sensor output (mV) of the 20 hours after N_2 flush. The gradient of the linear model shows the trend of O_2 entering the kilner jar headspace for 8 sensors named O1 to O9

in O_2 level was very small over time. Lab air entering the jar headspace could cause these small changes in O_2 sensor mV output. Alternatively, O_2 retained within the soil pore spaces after the N_2 flush could slowly equilibrate with the soil headspace, raising the O_2 concentration within negligible levels. This was able to be flushed out during the next N_2 flush, meaning that this method was sufficient to create anaerobic conditions for the incubation.

3.2.6. Optimising the anaerobic incubation period for constant and oscillating redox treatments

The anaerobic conditions created needed to be maintained for long enough for the soil microbial community to respond and adapt to anaerobic conditions, enabling the biotic mediation of Fe-oxide reductive dissolution. A pilot experiment was set up to measure Fe(II) in the soil-organo-

mineral mix to determine the length of time anaerobic conditions were required for Fe(II) to be detected by the ferrozine assay.

Soil-ferrihydrite mix (10g dry weight equivalent) was added to 12 jars for an anaerobic incubation. The soil-ferrihydrite mix was set to 80% of max WHC with N_2 purged milliQ H_2O, and anaerobic conditions were initiated following the method developed in section 3.2.5. The samples were incubated for 0, 1 and 2 weeks in triplicate at 15°C. FeT and Fe(II) measurements were taken on the samples using the ferrozine method (see section 3.2.4). The results were standardized to mmol of Fe per g of dry weight soil-ferrihydrite mix, so that the proportion of FeT that is Fe(II) could be visualised (Fig. 12). A one-way ANOVA and post-hoc Tukey test was used to support the results.

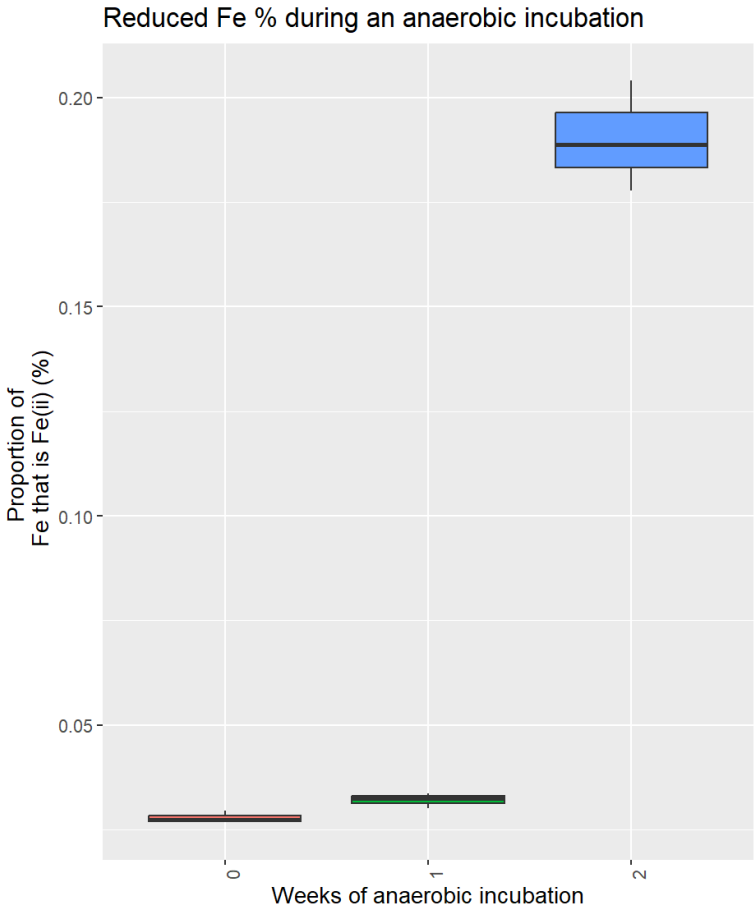

Figure 12 - Boxplot (mean ± IQR (n=3)) showing the percentage of FeT within the soil-ferrihydrite mix that is in reduced form (Fe(ii)) at 0, 1 and 2 weeks

The % of FeT that is Fe(II) remained small throughout the two weeks of anaerobic incubation, however, there was a significantly greater proportion of Fe(II) after 2 weeks of incubation (mean = 0.19%) compared to 0 days of incubation (mean = 0.028%) ($p<0.01$). Whereas, at 1 week of anaerobic incubation (mean = 0.032%) the proportion of Fe(II) was not significantly different to day 0 ($p = 0.79$).

Greater potential for Fe-oxide reductive dissolution is likely with increasing length of time of anaerobic conditions, as it is likely that the proportion of Fe(II) will increase over a longer period. However, the anaerobic conditions in the oscillating incubation was limited to the two weeks in order to keep the size of the experiment manageable but enabling enough time for Fe-oxide reductive dissolution and the potential for organo-mineral destabilisation.

3.2.7. Incubation experiment

Based on the outcomes from the pilot-scale work in sections 3.2.6, an incubation experiment was conducted to investigate whether carboxyl-richness controls organo-mineral stability in a soil system under varying redox conditions (Table 2). Soils were amended with ^{13}C labelled mono- or tri-carboxylic acid organo-minerals, and exposed to constant aerobic, constant anaerobic and oscillating conditions within airtight Kilner jars at 15°C. The destabilisation of the ^{13}C enriched organo-mineral OC was measured by tracing organo-mineral derived ^{13}C throughout the incubations with $^{13}CO_2$ gas concentration measurements and ^{13}C solid sample measurements. Further measurements of total CO_2 concentration, pH and Fe(II) abundance did not require ^{13}C enriched soil-organo-mineral mix.

*Table 2 - Table showing the timeline of each sample treatment for the incubation experiment. Yellow colour shows aerobic conditions; blue colour shows anaerobic conditions; * represents CO_2 and $^{13}CO_2$ gas sampling days; ○ represents sampling of solid soil mineral fraction for wt%C and ^{13}C measurements; □ represents sampling for ferrozine*

Day of incubation	Mono- or tri-carboxyl organo-mineral samples					
	13C enriched			Unlabelled		
	Aerobic	Anaerobic	Oscillating	Aerobic	Anaerobic	Oscillating
0	*	*	*	*	*	*
1	*	*	*	*	*	*
2						
3	*	*	*	*	*	*
4						
5						
6						
7	*	*	*	*	*	*
8						
9						
10	*	*	*	*	*	*
11						
12						
13						
14	*	*	*	*	*	*
15						
16						
17	*	*	*	*	*	*
18						
19						
20						
21	*○	*○	*○	*□Δ	*□Δ	*□Δ
22						
23						
24	*	*	*	*	*	*
25						
26						
27						
28	*○	*○	*○	*□Δ	*□Δ	*□Δ

Therefore, parallel incubations containing unlabelled soil-organo-mineral mix were conducted. This minimised the use of ^{13}C labelled OC to reduce costs. Aerobic, anaerobic and oscillating treatments

were run in parallel for 4 weeks, accommodating one full oscillation in the oscillating treatment; 1 week aerobic, 2 weeks anaerobic and 1 week of aerobic conditions. The incubation was split into two time-staggered blocks to make the experiment easier to manage.

In total, 112 Kilner jars were used. This included 28 jars each for 4 organo-mineral treatments (mono- and tri-carboxyl organo-minerals, ^{13}C labelled and unlabelled). From these 28 jars for each organo-mineral treatment, 4 were used for measurements at the start (T0) of the incubation, and 8 jars were exposed to each of 3 redox treatments (aerobic, anaerobic and oscillating). Half of these jars were incubated for the full 4 weeks, with half the jars destructively harvested after 3 weeks, at the end of the anaerobic stage of the oscillating incubation. All the jars were destructively sampled for the measurement of ^{13}C solid fraction, pH and Fe(II) abundance.

To prepare for the incubations, 10.3g of soil-organo-mineral mixture (10g dry weight equivalent soil + 0.3g dry weight equivalent organo-mineral) were added to each 250mL jar. Then MilliQ H_2O was added to the soils to set the soil water saturation dependent upon the aerobic or anaerobic conditions. Soil for the aerobic treatment was set to 50% max WHC, and for the anaerobic treatment to 80% max WHC. The water saturation was adjusted gravimetrically with MilliQ H_2O. For the anaerobic conditions, 80% max WHC was achieved with MilliQ H_2O that was sparged with N_2 gas for 30 minutes to remove dissolved O_2. Furthermore, O_2 was removed from the soil headspace by flushing with N_2 for 30 minutes at 5PSI (see section 3.2.5). For the oscillating treatment, soils were aerobic for 7 days then transitioned anaerobic. To achieve this, N_2 sparged MilliQ H_2O was added to the soil to 80% max WHC before the headspace was flushed with N_2 for 30 minutes (see section 3.2.5). At day 21, the oscillating incubations transitioned from anaerobic back to aerobic conditions. Here, the soil was dried for 36 hours at 15°C with the lids removed to lower the water saturation to 50% max WHC. After 36 hours, the jars were re-sealed.

CO_2 and $^{13}CO_2$ gas concentrations of the soil headspaces were sampled intermittently throughout the incubations. Samples were taken through septa using a 50mL syringe and needle that

had been flushed 3 times to prevent cross-contamination. For CO_2, a 10mL sample was withdrawn and injected into pre-evacuated 3mL exetainers, and $^{13}CO_2$ samples were taken by extracting 30mL of headspace gas injected into pre-evacuated 12mL exetainers. The CO_2 samples were analysed on a PerkinElmer Autosystem XL gas chromatograph (GC) calibrated to 500ppm, 1000ppm, 4000ppm and 8000ppm CO_2 concentrations. Here, the over pressurised sample gas within the exetainers enters the GC with an Argon and Hydrogen carrier gas through to a stainless steel Porapak Q 50–80 mesh column (length 2 m, outer diameter 3.17 mm) maintained at 60 °C that separates out constituent gases by molecular mass. Then CO_2 was detected by a Flame Ionisation Detector operating at 130°C (Elias *et al.*, 2024). The respired CO_2 (ppm) values were compiled and normalised to µg of CO_2 per g of dry weight equivalent soil-organo-mineral mix, using Equation 4 then Equation 5. Equation 4 normalised the GC measured ppm CO_2 concentration (Cv) into µg of CO_2-C per litre of headspace (Cm), where M was the molecular weight of carbon (12.011 g mol^{-1}), p was the barometric pressure in the incubation headspace (taken as 1 atm), R was the gas constant (0.08206 L atm K^{-1} mol^{-1}) and T was the air temperature of the incubation (set at 288.15°K or 15°C). Equation 5 further normalised Cm into µg of CO_2-C per gram of DW of organo-mineral soil mixture, where V was the volume of headspace in the incubation (0.25 L) and DW_{soil} was the DW equivalent of organo-mineral soil mixture within each incubation (g). $^{13}CO_2$ samples were analysed using a Picarro cavity ring-down spectrometer (model: G2201-I, Picarro, Inc. CA, USA) coupled with a custom-built auto-sampler. The $\delta^{13}CO_2$ measurements were recorded relative to the Vienna Pee Dee Belemnite standard (Elias *et al.*, 2024) and calibrated using 3 working standards of -26.21‰, 426.19‰ and 3974.36‰ $\delta^{13}CO_2$ values.

$$(Equation\ 4)\ Cm = \frac{Cv\ \times M \times\ p}{R\ \times T} = \frac{Cv\ \times 12.011\ \times 1}{0.08206\ \times 288.15}$$

$$(Equation\ 5)\ Cr = \frac{Cm\ \times \frac{V}{1000}}{DW_{soil}}$$

At the beginning of each incubation, the soil headspace was flushed with N_2 gas at 5PSI for 30 mins for anaerobic treatments (see section 3.2.5), or with synthetic air at 5PSI for 1 minute for aerobic

treatments. Then, T0 sample was taken to measure remaining CO_2 and $^{13}CO_2$ concentrations within the soil headspace. The lids remained air-tight on the jars, accumulating CO_2 from soil microbial activity and $^{13}CO_2$ from organo-mineral until the next sampling point where a T1 sample was taken. The net CO_2 (ppm) between T0 and T1 measurements for each timepoint equated to the CO_2 respired from the soil during the length of time since the last flush (T0). The soil headspace was then reset by being flushed, removing legacy CO_2 and $^{13}CO_2$, before another T0 sample was taken. This method of sampling soil headspace gas enabled all respiration and organo-mineral destabilisation to be captured so that a mass balance of ^{13}C was possible. The sampling for CO_2 and $^{13}CO_2$ were taken on days 0, 1, 2, 4 of the first week to capture any spike in microbial activity during the start of the experiment, followed by days 7, 10, 14, 17, 21, 24 and 28 for the last 3 weeks of the experiment.

To measure soil pH, reduced Fe(II) quantity and ^{13}C in the fine fraction of the soil-organo-mineral mixture, destructive samples were taken before the beginning of the incubation, at the end of the anaerobic phase in the oscillating incubations (21 days of incubation) and at the end of the incubation (28 days of incubation). For pH measurements, 6g of fresh weight unlabelled soil-organo-mineral mix were taken, added to 15ml of MilliQ H_2O, stirred and left to settle for 30 mins. Then the pH of the mixture was measured using a Hanna pH meter.

To measure Fe(II) in the soil mixture, the ferrozine assay method based upon Huang and Hall (2017) was used (see section 3.2.4). These results were then standardised to mmol of Fe or Fe(II) per gram of dry weight equivalent soil-organo-mineral mix. The proportion total Fe (FeT in mmol g^{-1} DWsoil) that was Fe(II) (Fe(ii) mmol g^{-1} DWsoil) was presented as a % using Equation 6.

$$(Equation\ 6)\ Proportion\ of\ reduced\ iron\ (\%\ Fe) = \frac{Fe(ii)\ mmol\ per\ g\ DW\ soil}{FeT\ mmol\ per\ g\ DW\ soil} \times 100$$

The soil-organo-mineral mix from the ^{13}C enriched incubations were destructively harvested to measure the ^{13}C in the fine fraction (<45µm). Immediately after harvesting, the soil-organo-mineral mix were immediately oven dried at 40°C for 24 hours, and 5g of this dried soil was taken for physical

soil fractionation following a method developed from Lopez-Sangil and Rovira (2013). Soil microaggregates within the 5g of soil-organo-mineral mix was disrupted by shaking the soil mixture in a 125mL bottle with 5 marbles and 40mL of MilliQ H_2O for 1 hour on a horizontal rotary shaker at 150rpm. This soil water mixture was then passed through a 200µm-sieve into a beaker to remove the sand fraction. This beaker containing the <200µm fraction was then sonicated at 60W for 5 minutes (or until 440 J cm^{-3} is reached) using a VCX 130 W model sonicator. The dispersed microaggregates enclose fine POM particles. The beaker was placed in a bucket of ice during sonication to counteract intense heating, keeping the temperature <40°C. This soil water mix was then passed through a 45µm sieve into a pre-weighed tin tray. The tray was then moved to the soil oven at 40°C for several days to evaporate the water before being weighed. The <45µm fraction of the soil-organo-mineral mix was calculated by subtracting the weight of the tin from the weight of the tin and soil once it had been removed from the oven. The proportion of the soil-organo-mineral mix that was <45µm was calculated from the known dry weight of soil-organo-mineral mix that was added to the bottle before any physical fractionation. The wt%C of the oven dried <45µm fraction was measured using a COSTECH ECS 4010 (see section 2.2.3). The $\delta^{13}C$ of the oven dried <45µm fraction was measured using the COSTECH ECS-4010 coupled to a Picarro cavity ring-down spectrometer (CDRS) (model : G-2131i) isotopic analyser (Picarro Inc. CA, USA) via a split-flow interface (Maddison *et al.*, 2017; Elias *et al.*, 2024). Here, the COSTECH ECS 4010 combusted the sample into CO_2 which bypassed the TCD, being carried straight to the picarro in a N_2 carrier gas, where the isotopic ratio of the $^{13}CO_2$ relative to the Vienna Pee Dee Belemnite standard was measured. The optimal weight of sample required for using the COSTECH-picarro was calculated using Equation 7 and the wt%C measured from the COSTECH ECS 4010, so that the concentration of CO_2 that was carried into the picarro would enable accurate $\delta^{13}C$ measurements.

$$(Equation\ 7)\ Weighed\ sample\ (mg) = \frac{0.4}{wt\%C} \times 100$$

The ^{13}C <45µm solid fraction Delta (δ ‰) CDRS output from the COSTECH-picarro was converted to atm % ^{13}C using Equation 8, where $R_{standard}$ was the $^{13}C/^{12}C$ ratio of the Vienna Pee Dee Belemnite primary standard ($R_{standard}$ = 0.0112372) and δ was the measured δ ‰ output from the COSTECH-picarro. This equation was constructed by combining the equations 9 and 10. Equation 9 calculated the δ ‰ by using the $^{13}C/^{12}C$ ratio of a sample (R_{sample}) and the $R_{standard}$, and equation 10 used δ and $R_{standard}$ to calculate atm% ^{13}C.

$$(Equation\ 8)\ Atm\ \%\ ^{13}C\ = \frac{R_{standard}(1 + \frac{\delta}{1000})}{1 + R_{standard}(1 + \frac{\delta}{1000})} \times 100$$

$$(Equation\ 9)\ \delta = \frac{R_{sample} - R_{standard}}{R_{standard}} \times 1000$$

$$(Equation\ 10)\ atm\%^{13}C = \frac{^{13}C}{^{13}C + ^{12}C} \times 100\ \ or\ \frac{R}{R+1} \times 100$$

The atm % ^{13}C values of the samples were calibrated using working standards of beet sugar, cane sugar and Refcen which had atom % ^{13}C values of 1.08, 1.1 and 1.33, respectively.

3.2.8. Data analysis and statistical analyses

A one-way anova followed by a post-hoc tukey test was used to test whether there were significant differences of atom%^{13}C in the <45µm solid fraction between the mono-carboxyl organo-mineral and tri-carboxyl organo-mineral treatments at the end of the incubation (day 28).

The mass of CO_2-C per µg of organo-mineral soil mixture was cumulatively added at each time point to reveal the cumulative respiration of CO_2 over the course of the incubation. Also, the respiration rate of samples were revealed by calculating the mass of respired CO_2-C standardized to the DW of the organo-mineral soil mixture over time. One-way anovas and post-hoc tukey tests were used to reveal differences in the cumulative CO_2 respiration and respiration rate between the organo-mineral treatments and between the redox treatments. These tests were conducted when the

oscillating incubations changed redox treatment at day 7, 21 and at the end of the incubation at day 28.

The isotopic composition of the ^{13}C enriched organo-mineral (δ values of 4477.17‰ and 3990.81 ‰ for tri-carboxylic acid and mono-carboxylic acid organo-minerals respectively) and natural abundance soil (δ value of -29.63‰) were distinct enough, that the $\delta^{13}CO_2$ measurement were able to be used for source partitioning of the respired CO_2, using isotopic mixing model equations (Cotrufo and Pressler, 2023). Therefore, the amount of CO_2-C that was derived from organo-mineral OC was calculated at each timepoint using equation 11, where Co was the organo-mineral derived respired C (μgCO_2-C g^{-1} DW soil), Cr was the total respired C (μgCO_2-C g^{-1} DW soil), $\delta^{13}CO_2$ was the picarro δ‰ output of the $^{13}CO_2$ gas sample, δSoil was the mean natural abundance δ‰ of the soil (-29.63‰, n=3) and δOrgmin was the mean δ‰ of the ^{13}C mono-carboxylic acid organo-mineral (3990.81‰, n=3) and ^{13}C tri-carboxylic acid (4477.17‰, n=3) measured on the COSTECH-picarro. The proportion of organo-mineral OC that remains within the organo-mineral soil mixture at each timepoint can be calculated by subtracting the cumulative organo-mineral derived OC respired from the known value of total amount of organo-mineral OC within each sample.

$$(Equation\ 11)\ Co = \left(\frac{\delta^{13}CO_2 - \delta Soil}{\delta Orgmin - \delta Soil} \right) \times Cr$$

One-way anovas and post-hoc tukey tests were conducted at day 7, 21 and 28 on the proportion of organo-mineral OC that remains within the organo-mineral soil mixture to reveal if differences between organo-mineral and redox treatments were significant.

3.3. Results

3.3.1. Total CO_2 respiration

The mean (n = 4) cumulative respired CO_2 differed between incubation treatment both for mono- (Fig 13b) and tri-carboxyl organo-minerals (Fig. 13a), as well as between both organo-mineral treatments (Fig.13) ($p<0.01$ between each treatment for each timepoint throughout the incubation). The aerobic treatments had greatest mean cumulative respired CO_2, followed by oscillating treatments and then the anaerobic treatments for both organo-mineral treatments. The mono-carboxyl organo-mineral incubations saw greater mean cumulative respired CO_2 compared to tri-carboxyl organo-mineral incubations for the aerobic (132.2 compared to 115.4 μg CO_2 g^{-1} DW soil) and oscillating treatments (112.4 compared to 83.3 μg CO_2 g^{-1} DW soil) by the end of the incubation at day 28. However, the mean cumulative respired CO_2 of the mono-carboxyl organo-mineral treatment was greatly suppressed compared to tri-carboxyl organo-mineral treatment for the anaerobic treatments throughout the incubations (29.3 compared to 60.2 μg CO_2 g^{-1} DW soil at day 28).

The aerobic and oscillating treatments have close but significantly different ($p<0.01$ at day 7) mean cumulative respired CO_2 for the first week for both organo-mineral treatments. Here, the cumulative respired CO_2 during this week is greater for the mono-carboxyl compared to tri-carboxyl organo-mineral treatments for both aerobic (60.1 compared to 36.0 μg CO_2 g^{-1} DW soil) and oscillating treatments (67.9 compared to 38.2 μg CO_2 g^{-1} DW soil). The mean cumulative respired CO_2 of aerobic and oscillating treatments diverge from each other from day 7 to 21 during onset of anaerobic conditions in the oscillating treatments for both mono-carboxyl (difference of 7.8 μg CO_2 g^{-1} DW soil at day 7 compared to 22.2 μg CO_2 g^{-1} DW soil at day 21) and tri-carboxyl (difference of 2.2 μg CO_2 g^{-1} DW soil at day 7 compared to 16.9 μg CO_2 g^{-1} DW soil at day 21) organo-mineral treatments. The return of aerobic conditions during the final week of the incubations led to an increase in the mean cumulative respired CO_2 for oscillating incubations of mono-carboxyl (difference of 14.2 μg CO_2 g^{-1} DW

soil at day 28) but not tri-carboxyl (difference of 17.6 µg CO_2 g^{-1} DW soil at day 28) organo-mineral treatments.

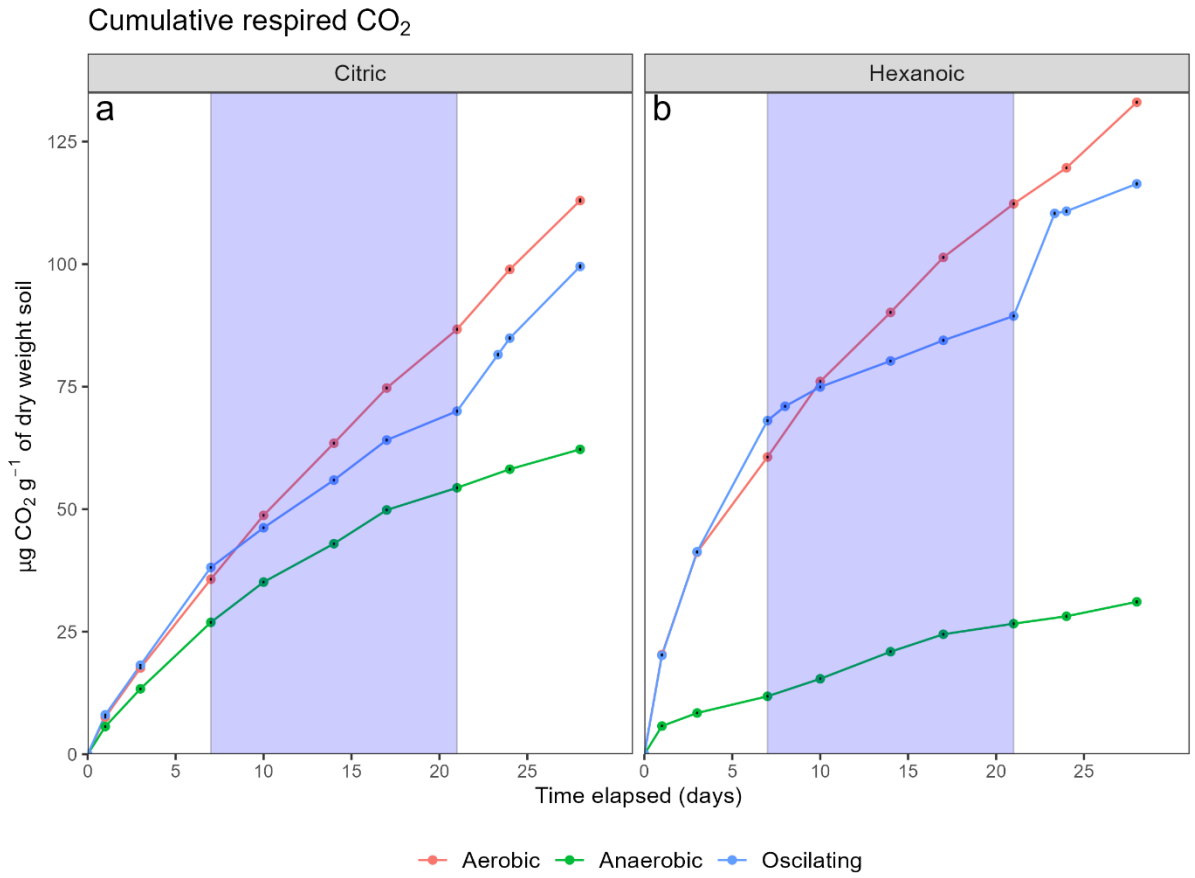

Figure 13 – Line graph showing datapoints of mean ±SE (n = 4) cumulative respired CO_2 (µg CO_2 g^{-1} DW soil) across time for each of aerobic, anaerobic and oscillating incubation treatments for both tri-carboxyl (a) and mono-carboxyl (b) organo-minerals. The blue shaded area shows the period of the incubation (days 7 to 21) when the oscillating treatments are in anaerobic conditions

3.3.2. Respiration rate

The pattern of mean (n=4) respiration rate differs between aerobic (Fig. 14a), anaerobic (Fig. 14b), and oscillating treatments (Fig. 14c) across the whole timeframe of the incubations. Aerobic, anaerobic, and oscillating treatments for both organo-mineral treatments experience a peak in respiration rate day 1 of the incubation. This peak in mean respiration rate at day 1 for the aerobic and oscillating treatments were greater for mono-carboxyl (20.28 and 20.15 μg CO_2 g^{-1} DW soil day^{-1} respectively) compared to tri-carboxyl (7.63 and 8.07 μg CO_2 g^{-1} DW soil day^{-1} respectively) organo-mineral treatments (both $p<0.01$). Here, there was no significant difference between to aerobic and anaerobic treatments for both mono-carboxyl ($p = 0.942$) and tri-carboxyl ($p = 0.471$) organo-mineral treatments. However, this peak at day 1 was much smaller for anaerobic treatments for both mono-carboxyl (5.78 μg CO_2 g^{-1} DW soil day^{-1}) and tri-carboxyl (5.67 μg CO_2 g^{-1} DW soil day^{-1}) organo-mineral treatments, which are not significantly different from each other ($p = 0.575$). After the peak on day 1, the mean respiration rate for each treatment decreases towards a more stable respiration flux for the rest of the incubation. For both organo-mineral treatments, the respiration rate remained similar between aerobic and anaerobic treatments from day 1 until after day 7, when the oscillating treatment was transferred to anaerobic conditions (all $p>0.170$). The exception is that there was a second peak for the oscillating treatments breaks this immediately after the return to aerobic conditions at day 21. The respiration rate at this second peak is greater than the respiration rate experienced at the first peak during the oscillating incubations for both mono-carboxyl (91.26 μg CO_2 g^{-1} DW soil day^{-1}) and tri-carboxyl (30.56 μg CO_2 g^{-1} DW soil day^{-1}) treatments.

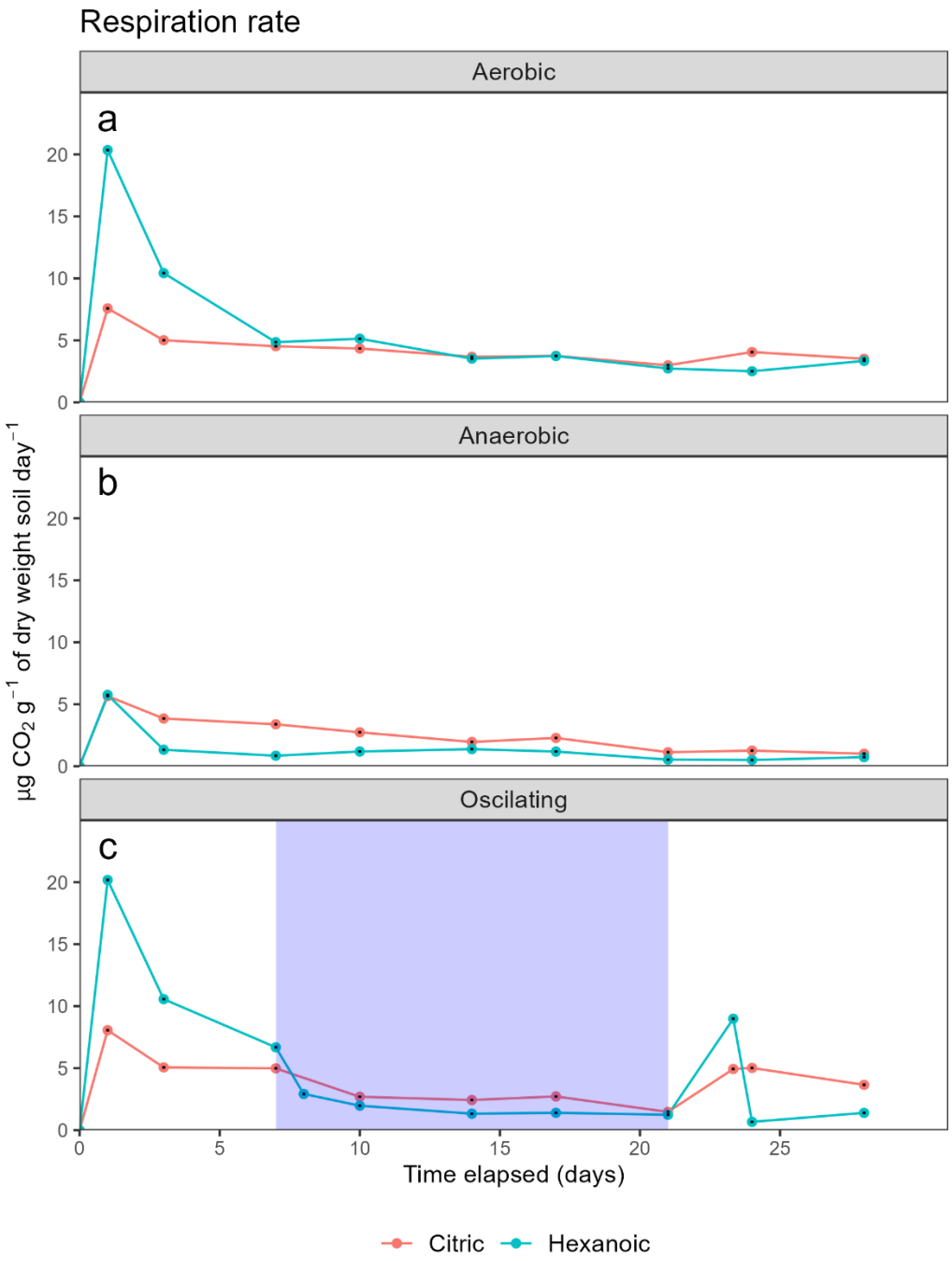

Figure 14 – Line graph showing datapoints of mean ± SE (n = 4) respiration rate (µg CO_2 g^{-1} DW soil day^{-1}) for mono- and tri-carboxyl organo-mineral treatments of aerobic (a), anaerobic (b) and oscillating (c) redox conditions. The blue shaded area shows the period of the incubation (day 7 to day 21) when the oscillating treatments are in anaerobic conditions

3.3.3. Proportion of CO_2 derived from organo-mineral C

The proportion of total CO_2 that has derived from mono-carboxyl organo-minerals is much greater compared to tri-carboxyl organo-minerals (Fig. 15) for aerobic, anaerobic, and oscillating treatments (all $p<0.01$). The proportion of total CO_2 that has derived from mono-carboxyl organo-mineral range between 14.04 – 59.70% over the entire incubations, whereas the proportion of total CO_2 that has derived from tri-carboxyl organo-minerals all remain below 2.99%.

Tri-carboxyl organo-minerals provide a greater proportion of total respired CO_2 under anaerobic conditions, compared to aerobic conditions within the aerobic and oscillating treatments. The proportion of total respired CO_2 derived from the mono-carboxyl organo-mineral in the anaerobic treatment increases over the length of the incubation (from 0.53 to 2.99%). At day 28, the proportion of total respired CO_2 derived from the mono-carboxyl organo-mineral in the anaerobic treatment is significantly different to the aerobic and oscillating treatments (both $p<0.01$). The mono-carboxyl organo-minerals provide a smaller proportion of total respired CO_2 in the anaerobic treatment (26.12 – 47.57%) compared to aerobic (58.87 – 90.08%) and oscillating (50.40 – 89.78%) treatments for the first 17 days of the incubation. However, by day 28 the mono-carboxyl organo-minerals provide a greater proportion of total respired CO_2 in the anaerobic treatment (63.58%) compared to aerobic (39.13%) and oscillating treatments (14.04%).

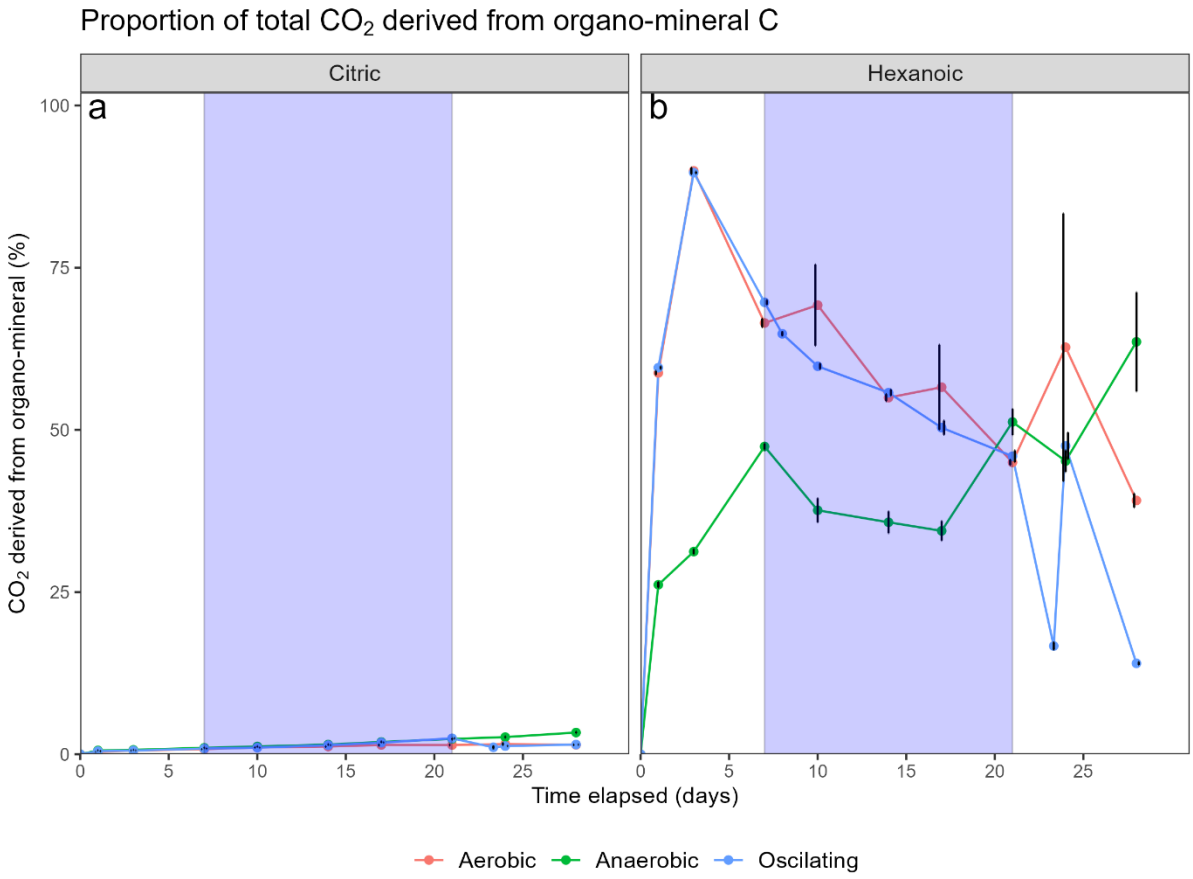

Figure 15 – Line graph showing datapoints of the mean ± (n = 4) of the proportion (%) of respired CO_2 that was derived from both the tri-carboxyl (a) and mono-carbo (b) organo-minerals in aerobic, anaerobic and oscillating treatments. The blue shaded area shows the period of the incubation (day 7 to day 21) when the oscillating treatments are in anaerobic conditions

3.3.4. Rate of organo-mineral derived C being respired

The CO_2 respiration rate that has derived from the organo-minerals were statistically different between mono- and tri-carboxyl organo-mineral for each treatment type throughout the incubation (all $p<0.01$). The CO_2 respiration rate derived from tri-carboxyl organo-minerals were supressed compared to mono-carboxyl organo-mineral incubations (Fig. 16). The CO_2 respiration rate that derived from tri-carboxyl organo-mineral remained very consistent for the length of the incubation for each treatment type, by remaining between 0.02 and 0.06 μg CO_2 g^{-1} of DW soil day^{-1}. An exception occurs at day 21 for the oscillating treatment. Here, where the oscillating treatment incubation was returned to aerobic conditions, the CO_2 respiration rate derived from the tri-carboxyl organo-mineral reached a rate of 0.36μg CO_2 g^{-1} of DW soil day^{-1}. There was greater variability in CO_2 respiration rate derived from mono-carboxyl organo-minerals compared to tri-carboxyl organo-minerals for aerobic (1.23 – 11.99 μg CO_2 g^{-1} of DW soil day^{-1}), oscillating (0.20 - 15.30 μg CO_2 g^{-1} of DW soil day^{-1}), and anaerobic treatments (0.23 - 1.50 μg CO_2 g^{-1} of DW soil day^{-1}). There was also more statistical difference between aerobic, oscillating, and anaerobic treatments for mono-carboxyl (5 out of 9 timepoints $p>0.01$ between treatments) compared to tri-carboxyl organo-minerals (8 out of 9 timepoints $p>0.01$ between treatments). There was a trend of going from a greater CO_2 respiration rate derived from mono-carboxyl organo-minerals at the beginning of the incubation to a lower rate by the end of the incubation for the aerobic (11.99 at day 1 to 1.31 μg CO_2 g^{-1} of DW soil day^{-1} at day 28 of the incubation) and oscillating treatments (12.05 at day 1 to 0.20 μg CO_2 g^{-1} of DW soil day^{-1} at day 28 of the incubation). The exception to this trend was at day 22 in oscillating treatment. Here, as the incubation was returned to aerobic conditions, there was a peak in the CO_2 respiration rate derived from the mono-carboxyl organo-mineral of 15.30μg CO_2 g^{-1} of DW soil day^{-1}.

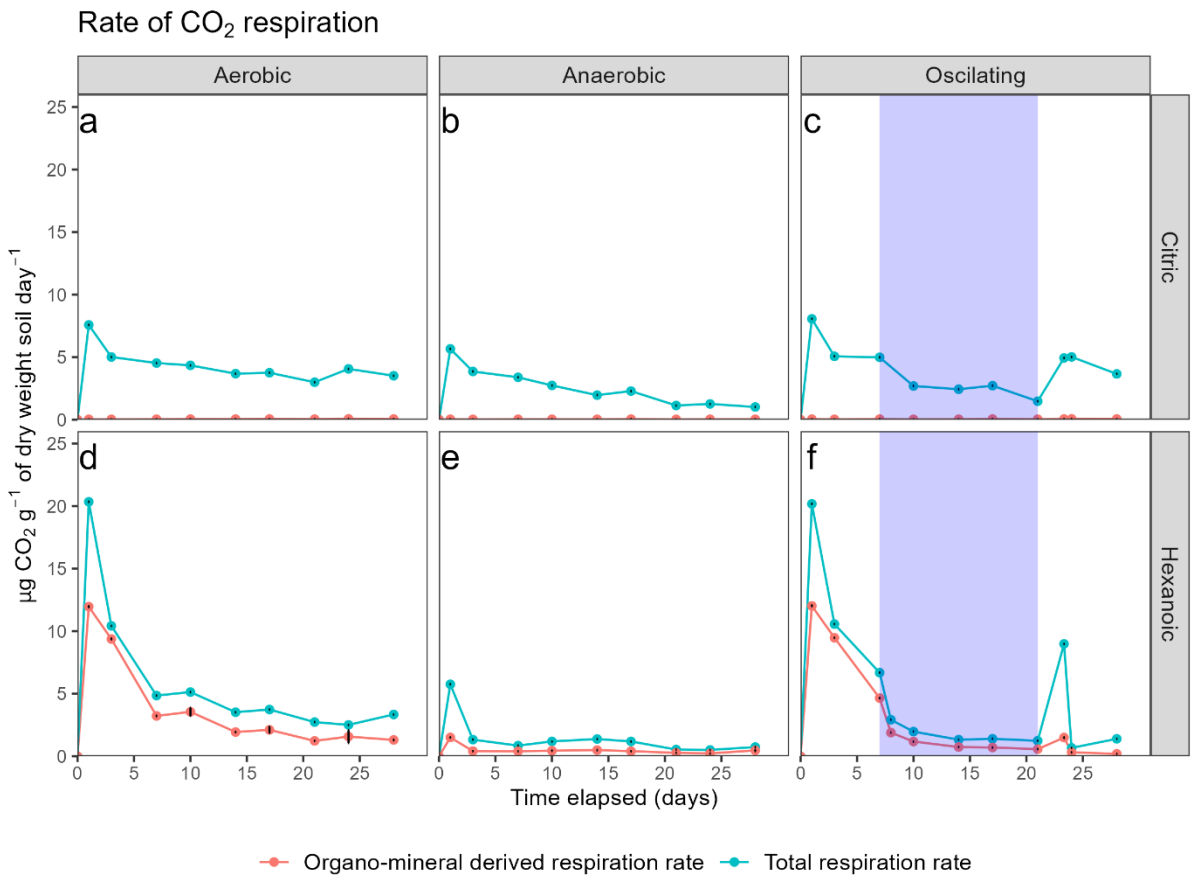

Figure 16 – Line graph showing datapoints of the mean ± SE (n = 4) of the respiration rate (µg CO_2 g^{-1} DW soil dat^{-1}) of organo-mineral derived OC (red lines) and total respiration rate (blue lines) for tri-carboxyl (a, b, c) and mono-carboxyl (d, e, f) organo-mineral treatments. The blue shaded area shows the period of the incubation (day 7 to day 21) when the oscillating treatments are in anaerobic conditions

3.3.5. Proportion of organo-mineral C respired

The proportion of total mono-carboxyl organo-mineral OC that was respired greatly exceeds that of tri-carboxyl organo-minerals during the incubations (Fig. 17A). The mean proportion of total mono-carboxyl organo-mineral OC respired by the end of the incubation at 28 days, was 13.15% for the aerobic treatment, 10.07% for the oscillating treatment and 1.89% for the anaerobic treatment. This compares to the proportion of total tri-carboxyl organo-mineral respired being less than 0.14% for every treatment (0.13% in the aerobic treatment, 0.12% for the oscillating treatment, and 0.09% for the anaerobic treatment). Therefore, 99.86% or greater of the total tri-carboxyl organo-mineral OC remains unrespired. Here, a factor of 20 to 100x more organo-mineral C was respired for mono-carboxyl compared to tri-carboxyl incubations, so the proportion of total organo-mineral OC that was respired between mono- and tri-carboxyl organo-minerals is statistically different for every treatment (all $p<0.01$).

The proportion of total organo-mineral OC respired were statistically different at day 28 between each treatment for both mono- and tri-carboxyl organo-mineral incubations (all $p<0.01$). Here, the aerobic treatments attributed to greatest proportion of total organo-mineral C respired followed by the oscillating and then the anaerobic treatments. This difference between treatment types was greater for the mono-carboxyl compared to the tri-carboxyl organo-mineral incubations. The amount of organo-mineral C respired in aerobic treatments is 6.97 times greater than anaerobic treatments for the mono-carboxyl treatments compared to 1.45 times greater in the tri-carboxyl organo-mineral treatments.

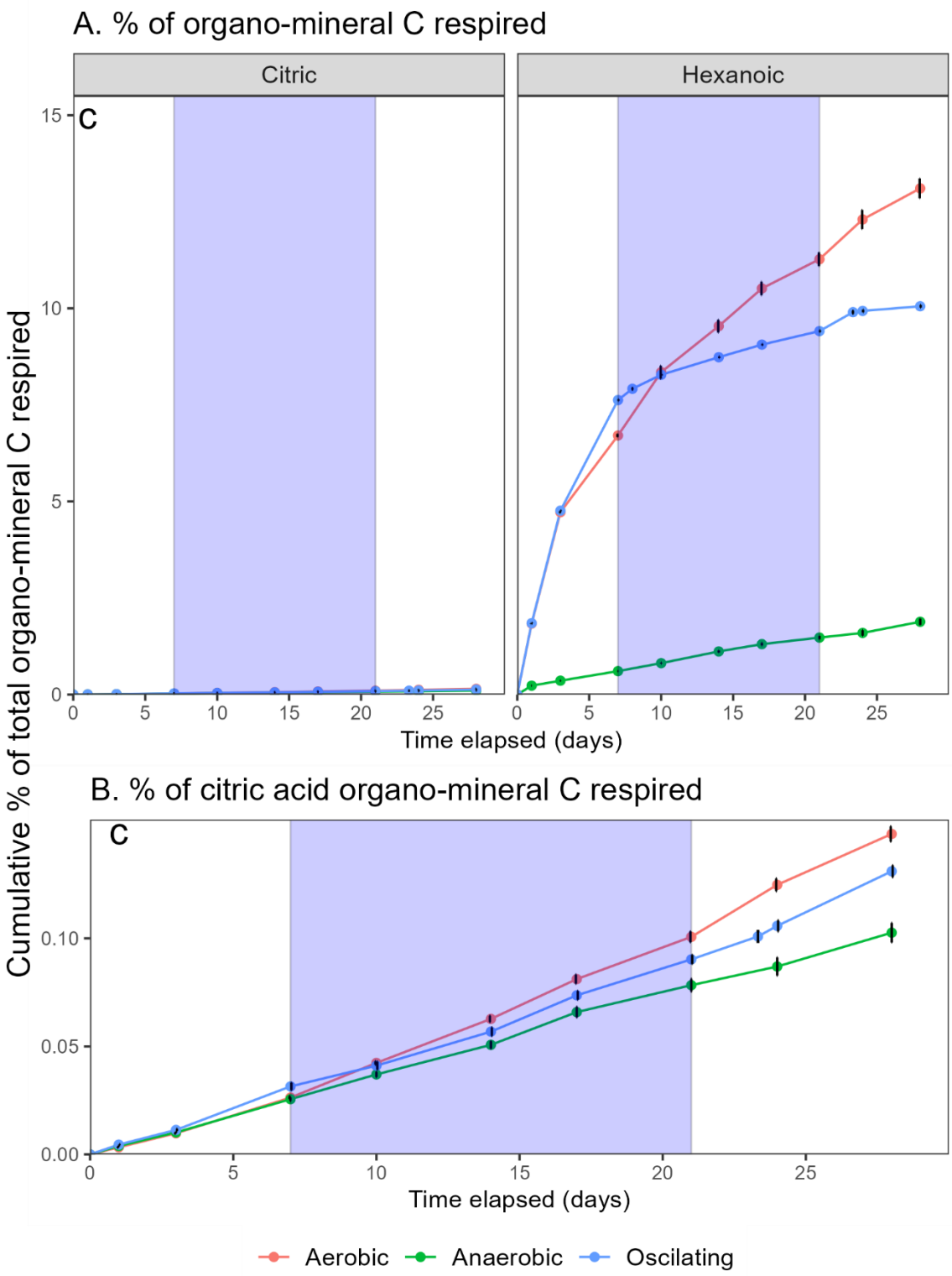

Figure 17 – Line graph showing datapoints of the cumulative mean ± SE (n = 4) proportion (%) of total organo-mineral C respired during the incubations. (A) a line graph of proportion (%) of total tri-carboxyl (a) and mono-carboxyl total organo-mineral C respired. (B) a zoomed in version of the line graph for proportion of tri-carboxyl organo-mineral C respired during the incubations. The blue shaded area shows the period od the incubation (day 7 to day 21) when the oscillating treatments are in anaerobic conditions.

3.4. Discussion

This experiment set out to investigate **whether carboxyl-richness controls organo-mineral stability under oscillating, aerobic, and anaerobic conditions, which impose different destabilisation forces**. This was explored through an experiment where ^{13}C labelled organo-minerals of increasing carboxyl richness were added to soils and incubated under aerobic, anaerobic, and oscillating conditions. Two hypotheses were tested. **Organo-mineral stability is greater with increasing carboxyl richness (H1)**, and **the extent of organo-mineral OC destabilisation will depend upon the redox conditions of the soil (H2).** Measurements of CO_2 and $^{13}CO_2$ throughout the incubation, which were processed by a mixed model, revealed the amount of respired CO_2 that derived from the organo-mineral. This highlighted the extent of destabilisation of organo-mineral throughout the incubations.

3.4.1. Carboxyl-rich organo-minerals were most stable

The results of this experiment showed that more organo-mineral destabilisation occurred in the mono-carboxyl organo-mineral incubations compared to the tri-carboxyl organo-mineral incubations. Despite the total cumulative respiration within both organo-mineral treatments being within the same order of magnitude of each other, the respired CO_2 that derived from the organo-mineral OC greatly differs between the two organo-mineral treatments. Respired CO_2 deriving from the mono-carboxyl organo-minerals were about 2 orders of magnitude greater than the tri-carboxyl organo-minerals, for all redox treatment types. Therefore, the mono-carboxyl organo-mineral OC is more available to microbes for respiration compared to tri-carboxyl organo-mineral OC. This is clear evidence that the stability of carboxyl-rich organo-minerals are greater than carboxyl-poor organo-minerals, proving the hypothesis (H1).

3.4.2. Aerobic conditions enabled greatest destabilisation of organo-mineral

Results of this experiment show that by the end of the incubation, the greatest amount of organo-mineral destabilisation occurred in the aerobic treatments for both mono- and tri-carboxyl organo-mineral treatments. This disproves the hypothesis (H2), where the oscillating treatment was

predicted to cause the greatest amount of organo-mineral destabilisation. In this experiment, the oscillating treatments did induce greater organo-mineral destabilisation compared to the anaerobic treatments for both mono- and tri-carboxyl organo-mineral treatments.

3.4.3. Biotic destabilisation of organo-organic interactions dominate

The greater magnitude of organo-mineral destabilisation during the aerobic phases of the incubations coincided with greater total respiration. This highlights that increased soil microbial activity helped to drive organo-mineral destabilisation. In comparison, destabilisation by reductive dissolution is low during the timeframe of the incubation. This reduced level of respired CO_2 deriving from the organo-minerals derived OC in anaerobic conditions could be explained by the absence of O_2 supressing soil microbial activity. However, the spike in respired CO_2 following the transition from anaerobic to aerobic conditions in the oscillating treatments, is predominantly derived from the soil matrix rather than organo-mineral OC, even in the mono-carboxyl organo-mineral treatment. Therefore, reductive dissolution of ferrihydrite during the anaerobic phase of the oscillating treatment did not replenish the pool of destabilised OC.

Therefore, biotic destabilisation mechanisms greatly outweighed the abiotic destabilisation mechanisms. Here, a more active microbial community during aerobic conditions led to destabilisation of organo-mineral and organo-organic bonds enhancing the bioavailability of the OC for utilization by microbes (Keiluweit *et al.*, 2015; T. Wang *et al.*, 2020; Li *et al.*, 2021). The mono-carboxylic acid organo-organic interactions within this experiment were much weaker than that of tri-carboxyl acid (as discussed in section 2.4.1). Here, the hexanoic acid could only participate in organo-organic interactions through its aliphatic tail. These hydrophobic and van der Walls interactions are much weaker than the cation bridging or ligand exchange (Kleber, Sollins and Sutton, 2007; Kleber *et al.*, 2021) possible through the free hydroxyl and carboxyl groups found in citric acid. Therefore, mono-carboxylic acid involved in organo-organic interactions were a very bioavailable source of OC during this incubation. The active microbial community in aerobic conditions was able to utilise and respire

this source of organo-mineral OC to a far greater extent than that of the microbial community within anaerobic conditions.

3.4.4. Limitations to the bioavailability of mono-carboxyl OC

At the beginning of the experiment, mono-carboxyl organo-mineral OC was preferentially utilized in respiration by the soil microbes even over the soil matrix OC. During the first week of the incubations, 60-90% of total respired CO_2 derived from the mono-carboxyl organo-mineral compared to less than 5% for the tri-carboxyl organo-mineral treatment. Both citric and hexanoic acid are labile molecules able to be readily utilised by the soil microbes, so these results show that the tri-carboxyl OC was far less bioavailable to the microbial community compared to mono-carboxyl OC due to differences in the stability of the organo-minerals complex.

Towards the end of the aerobic and oscillating incubations, the microbes began running out of this easily available mono-carboxyl OC, utilizing a greater proportion of soil matrix derived OC for respiration, shown in the convex shape of proportion of total organo-mineral OC respired (Fig. 17A). This suggests that there is a finite resource of easily bioavailable carboxyl poor organo-mineral C that is being utilised preferentially and rapidly by the soil microbial community and once the most easily accessible organo-mineral C becomes less abundant, the soil microbes are returning to soil matrix OC for their C source.

If this trend continued onwards from the incubation, it would indicate that there is an inaccessible portion of C that cannot be utilized by the microbial community. There would be further investigation needed to unpick whether this trend is a demonstration of organo-mineral C that is inherently stable from biotic destabilisation mechanisms due to inner-sphere complexation (Kleber, Sollins and Sutton, 2007; Kögel-Knabner *et al.*, 2008; Newcomb *et al.*, 2017; Kleber *et al.*, 2021) or just an artefact of experimental design due to insufficient mixing of the organo-mineral into the soil matrix enabling by extensive physical protection.

3.4.5. Slow destabilisation by reductive dissolution of ferrihydrite

It takes time 2 weeks for the reductive dissolution of ferrihydrite and production of aqueous Fe^{2+} to become detectable by ferrozine assay. Therefore, the longer anaerobic conditions are maintained, the greater amount of reductive dissolution is possible. Therefore, destabilisation by reductive dissolution of ferrihydrite could become more significant under longer periods of anaerobic conditions than explored in this incubation. Therefore, if this experiment was conducted with a much longer anaerobic phase within the oscillating treatment, it is possible that greater reductive dissolution of ferrihydrite could enable some OC to become accessible to microbes that would otherwise be inaccessible to microbes due being in direct organo-mineral associations and OC that is physically protected in the aerobic incubations.

3.4.6. Wider implications

Despite differences of organo-mineral destabilisation between redox treatments, this study highlights that the carboxyl-richness of the organo-minerals has a greater importance determining organo-mineral stability. This has occurred for organo-minerals involving the amorphous redox reactive mineral ferrihydrite, for which destabilisation by reductive dissolution is deemed to be important (Chen *et al.*, 2020; Inagaki *et al.*, 2020; Possinger, Bailey, *et al.*, 2020). Here, a carboxyl-rich organo-mineral will be more stable than a carboxyl-poor organo-mineral independent of the redox conditions within the soil. Therefore, when focusing efforts on increasing the persistence of mineral fraction of soils, greater importance should be placed upon the chemistry of the OC (carboxyl-richness) compared to soil conditions (aerobic, anaerobic and oscillating). This does not dismiss effectiveness of these management practices, such as waterlogging to induce anaerobic conditions, to increase SOC persistence. In fact, the results of this experiment support that anaerobic conditions will suppress organo-mineral destabilisation irrespective of the carboxyl-richness. Therefore, the impact of management practices that manage redox conditions in specific sites cannot be dismissed, such as rewetting soils within a peatland will enhance SOC in the particulate SOC fraction (Mander *et al.*, 2024). However, any development of soil management practices that could increase the carboxyl-richness of

the SOC mineral fraction could have a transformational impact for enhancing the stability and persistence of the mineral associated SOC pool, and supplement existing management practices (Wiesmeier *et al.*, 2019). The soil management practice to increase carboxyl-richness could include the addition of oxidised organic amendments such as compost (Spaccini and Piccolo, 2007; Yu *et al.*, 2019), which is readily developed and available. Therefore focussing on investigating the impact of existing land management strategies on MAOM stability could provide evidence that there is a mechanism in which soils can be managed to become a viable nature-based CDR strategy in line with the 4 per mille initiative (Minasny *et al.*, 2017).

3.4.7. Conclusions

This incubation experiment has shown that the carboxyl-richness of the organo-minerals have a greater impact on the stability compared to redox conditions in soil systems, where carboxyl-rich organo-minerals were more stable in all redox treatments. Biotic destabilisation mechanisms generated by microbial activity were more impactful than reductive dissolution, resulting in greatest destabilisation occurring in aerobic conditions and suppressed destabilisation during anaerobic conditions, independent of organo-mineral carboxyl-richness.

Therefore, the first hypothesis of this experiment, predicting that carboxyl-rich organo-minerals will be more stable in a soil system, was proven. Whereas the second hypothesis that predicted for oscillating conditions to result in greatest destabilisation, was disproven as aerobic conditions resulted in the greatest organo-mineral destabilisation.

4. Microbe cell wall composition controls stability of necromass-derived mineral associated SOC

4.1. Introduction

Chapter 2 and 3 highlighted the importance of the carboxyl-richness of organo-minerals for organo-mineral stability. Chapter 2 showed that in reducing conditions tri-carboxyl organo-minerals can slow down the diffusion of Fe(II) ions to the iron oxide mineral surface (Jones *et al.*, 2009; Catrouillet *et al.*, 2014; ThomasArrigo *et al.*, 2017; Zhou *et al.*, 2018; ThomasArrigo, Kaegi and Kretzschmar, 2019), thus inhibiting the extent of organo-mineral destabilisation by reductive dissolution compared to mono-carboxyl organo-minerals. Chapter 3 revealed the stability of tri-carboxyl organo-minerals far exceeds the stability of mono-carboxyl organo-minerals in real soil conditions, where soil microbial communities adjust to aerobic and anaerobic conditions, as well as oscillations between the two. These two experiments were conducted where the organo-mineral OC was a homogenous mix of simple OC compounds of mono-, di- or tri-carboxylic acid.

Although OC compounds found in organo-mineral associations in natural soils tend to be simpler and more labile than POM (Lehmann and Kleber, 2015; Waring *et al.*, 2020), it is still heterogenous in composition (Kleber, Sollins and Sutton, 2007; Lehmann *et al.*, 2020; Kleber *et al.*, 2021), varying in the types of functional groups that the OC contains, their functional complexity, as well as the size of the OC molecule (Possinger, Zachman, *et al.*, 2020). This heterogeneity will affect how the OC molecule will interact within an organo-mineral, affecting the stability of the organo-mineral (Newcomb *et al.*, 2017; Kleber *et al.*, 2021). Some OC compounds will preferentially form direct organo-mineral interactions, whereas other OC compounds will preferentially form organo-organic interactions. This results in variation in the spatial structure of the organo-mineral complex (Kleber, Sollins and Sutton, 2007; Possinger, Zachman, *et al.*, 2020). Therefore, the composition of organo-mineral OC can vary significantly compared to the model OC compounds used in Chapter 2 and 3 of this thesis.

Previous investigations show that organo-mineral OC is dominated by microbially derived OC, particularly microbial necromass OC (Kopittke *et al.*, 2018, 2020; Klink *et al.*, 2022; Xuan *et al.*, 2024). This results in the carbon to nitrogen (CN) ratio of soil mineral fractions being lower than other fractions of soil (Kopittke *et al.*, 2018, 2020). Microbial necromass comprises of all the cellular components and degraded OC that derives from dead soil microbial cells (Buckeridge, Creamer and Whitaker, 2022; Camenzind *et al.*, 2023). Microbial necromass OC has a high abundance of reactive functional groups, which assists with interactions to soil minerals (Kleber *et al.*, 2021; Buckeridge, Creamer and Whitaker, 2022). Greater abundance of reactive functional groups could also favour greater stability when in organo-minerals, as seen in Chapters 2 and 3 with carboxyl-richness.

An important component of microbial necromass are microbial cell walls. The composition of cell walls can vary between soil microbes, most notably between gram positive (Gr^+) bacteria, gram negative (Gr^-) bacteria and fungi (Vollmer, Blanot and De Pedro, 2008; Garcia-Rubio *et al.*, 2020). All these cell walls contain phospholipid bilayers in their cell membranes, which contain phosphate groups that may associate to soil mineral surfaces very strongly via a bidentate coordination (Newcomb *et al.*, 2017). Whereas the hydrophobic lipid tails may be important in forming organo-organic interactions via hydrophobic interactions (Kleber, Sollins and Sutton, 2007; Possinger, Zachman, *et al.*, 2020; Kleber *et al.*, 2021). Otherwise, the cell walls between the microbial types vary, particularly fungi, which belongs to a different kingdom to Gr^+ and Gr^- bacteria, resulting in a vastly different cell wall structure (Fig. 18). Chitin dominates cell walls in Fungi (Garcia-Rubio *et al.*, 2020); a thick peptidoglycan layer is found in Gr^+ bacterial cell walls; and in Gr^- bacteria, cell walls contain a second phospholipid bilayer along with a thin peptidoglycan layer(Vollmer, Blanot and De Pedro, 2008). There are other components which are unique to the cell walls of each microbial type, such as β-glucans and

mannoproteins in Fungi, teichoic and lipoteichoic acids in Gr^+ bacteria, and lipopolysaccharides within Gr^- bacterial cell walls.

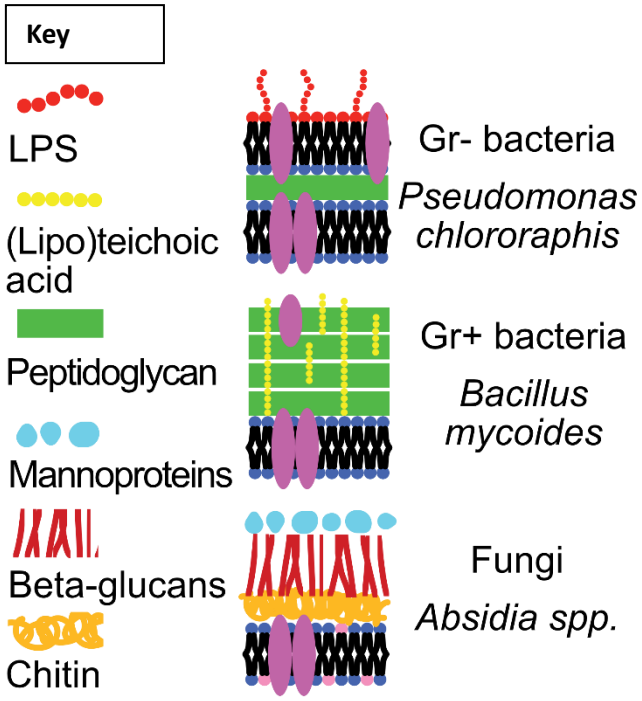

Figure 18 – Infographic showing the composition of Fungi, Gr^- and Gr^+ bacteria cell walls. The labels include the species of soil microbe used in this experiment for each microbe type.

Furthermore, cell wall components may become degraded in real soil systems (Cotrufo *et al.*, 2013; Lehmann and Kleber, 2015). These degradation OC products will be smaller, more labile and will have a greater abundance of reactive functional groups compared to the cell wall components from which they originated (Hu *et al.*, 2018). Therefore, these degradation products may be able to interact with soil minerals to a greater extent (Kleber *et al.*, 2021). When cell wall components and their degradation products associate to soil minerals, these different compositions between Fungi, Gr^+ and Gr^- bacteria will likely result in differences in organo-mineral stability.

Previous research investigating the effect of OC composition on the stability of organo-minerals has used simple OC compounds (ThomasArrigo, Kaegi and Kretzschmar, 2019; Curti *et al.*, 2021; Zhao *et al.*, 2022) such as those used in Chapters 2 and 3. Therefore, there remains a knowledge

gap in how differences in the composition of more complex and heterogeneous OC, such as microbial necromass, can affect the organo-mineral stability. As this is more relevant to a real soil system, these knowledge gaps are important to pursue.

This study aimed to investigate whether there are differences in organo-mineral stability when they are composed of necromass from different microbial groups. Organo-minerals composed of necromass from a single species of fungi, Gr^+ bacteria or Gr^- bacteria were synthesised and their stabilities were tested using NaOH and NaOCl chemical washes. These chemical washes induce differing degrees of organo-mineral destabilisation through desorption and oxidation. Three hypotheses were tested in this experiment. **(H1) organo-minerals derived from gram-negative necromass will have the greatest stability.** This is due to the second phospholipid bilayer and thus the additional phosphate groups being able to strongly bind to mineral surfaces via ligand exchange (Newcomb *et al.*, 2017). **(H2) The most stable fraction of the organo-mineral will have lower nitrogen content.** Although microbial necromass has a high N content, the OC functional groups that most strongly associate to the minerals are carboxyl and phosphate groups (Newcomb *et al.*, 2017) which do not contain N.

4.2. Methodology

An experiment was designed to test whether the stability of necromass-organo-minerals are affected by the source and thus the composition of the necromass. This required growing microbial cultures of different types to harvest their necromass (section 4.2.1), which was then used to synthesise organo-minerals (section 4.2.2). The stabilities of these synthesised organo-minerals were compared using two chemical washes (section 4.2.3).

4.2.1. Preparing the microbial necromass

Fungi, Gr^+, and Gr^- bacteria isolates of single species were cultured from soil used in an experiment at UKCEH Wallingford (Goodall and Griffiths, In progress). These isolates were *Absidia spp.* (fungi), *Bacillus mycoides* (Gr^+ bacteria) and *Pseudomonas chlororaphis* (Gr^- bacteria). Cultures of these soil microbes were grown using autoclave sterilised lab equipment in a containment level 2 microbiology lab within sterilised class 2 microbiological safety cabinets. *Absidia spp.* (fungi) cultures were grown in a sterilised potato dextrose broth for 7 days and both *Bacillus mycoides* (Gr^+ bacteria) and *Pseudomonas chlororaphis* (Gr^- bacteria) cultures were grown in in sterilised R2A broth for 3 days sat upon an oscillatory shaker within an incubator set at 25°C. These cultures were converted into necromass by chloroform fumigation using an adapted protocol (Buckeridge, La Rosa, *et al.*, 2020).

Table 3 – Compositions of insoluble and soluble Fungi, Gr^+ and Gr^- bacterial necromass; Mean (n=5) wt%C, wt%N and CN ratio measured using COSTECH ECS 4010 (see section 4.2.3)

Necromass solubility	Microbe type	wt%C	wt%N	CN
Insoluble	Fungi	49.42	4.18	11.82
Insoluble	Gr+	40.24	9.13	4.39
Insoluble	Gr-	37.28	9.69	3.84
Soluble	Fungi	38.25	1.95	19.61
Soluble	Gr+	21.7	6.37	3.41
Soluble	Gr-	29.56	8.71	3.4

Here, solid microbial biomass pellets were created by centrifuging the microbial cultures, which were then resuspended in sterile MilliQ H_2O before 0.5ml of chloroform ($CHCl_3$) was added behind a fume cupboard. Then the chloroform spiked samples were shaken on an oscillatory shaker for 30 minutes to bring about cell lysis for all the biomass in the sample. Here, the microbial cell walls

disintegrated, simultaneously releasing intracellular material into solution, killing the microbes. Once cell lysis was complete, the biomass within the sample was necromass, composed of intracellular components, soluble intracellular material, and lysed cell walls. The chloroform was evaporated by degassing the sample for 20 minutes using compressed air, before the samples were centrifuged to separate insoluble necromass within a pellet from the soluble necromass in the supernatant. The soluble necromass fraction within the supernatant was passed through a 0.22um PES vacuum filter, to remove any insoluble necromass particulates. Both necromass fractions (Table 3) were freeze-dried and ground into a homogenous powder ready to be used in making the synthetic organo-minerals.

4.2.2. Synthesis of necromass-OC derived organo-minerals

In this experiment, the stability of ferrihydrite and montmorillonite necromass organo-minerals was investigated. The predominant mechanism by which OC associates to the mineral differs between smectite clays such as montmorillonite, and the iron-oxides such as ferrihydrite. OC tends to interact with smectite clays through cation bridging, whereas OC tends to interact with iron-oxides through ligand exchange (Kleber *et al.*, 2021). This results in the mineral surfaces preferentially selecting different compounds for direct organo-mineral interactions (Lehmann *et al.*, 2008), leading to different OC composition of the organo-mineral with different stabilities.

Nine organo-mineral types were synthesised for this experiment; 6 ferrihydrite-necromass organo-minerals and 3 montmorillonite-necromass organo-minerals. These comprised of ferrihydrite and insoluble necromass, ferrihydrite ad soluble necromass and montmorillonite and soluble necromass.

The insoluble necromass fraction (see section 4.2.1) predominantly consists of lysed cell wall components (Buckeridge, La Rosa, *et al.*, 2020). Insoluble necromass can be incorporated into organo-minerals via co-precipitation (Schwertmann and Cornell, 2008). Therefore, insoluble necromass organo-minerals were only synthesised with ferrihydrite as OC can only interact to the montmorillonite by adsorption. However, the soluble necromass fraction (see section 4.2.1) is able to adsorb onto

montmorillonite, so both montmorillonite and ferrihydrite organo-minerals are synthesised with the soluble necromass fractions.

Ferrihydrite insoluble necromass organo-minerals were synthesised by coprecipitation following the same method used in Chapters 2 and 3 (see sections 2.2.1 and 2.2.5)(Schwertmann and Cornell, 2008). The insoluble necromass organo-minerals were synthesised targeting 3wt%C (Table 4).

Soluble necromass organo-minerals were synthesised by adsorbing the soluble necromass onto an already formed mineral of ferrihydrite or montmorillonite. (1) For ferrihydrite, the mineral was synthesised in the absence of OC using the same methods described in section 2.2.1 and 2.2.5. Once the ferrihydrite had precipitated out of solution and been washed several times with MilliQ H_2O, the ferrihydrite was decanted into several 50mL centrifuge tubes ready for soluble necromass to be added for organo-mineral synthesis via adsorption. (2) For montmorillonite, a calcium saturated montmorillonite (Ca-montmorillonite) was synthesised following adapted protocols from Wang and Xing (2005). This was done to maximise the ability of montmorillonite to adsorb OC, as divalent cation saturated clays tend clays have a higher sorption affinity ((Yu *et al.*, 2004; Wang and Xing, 2005; Aggarwal *et al.*, 2006; Yan, Hu and Jing, 2012). Here, 20g of dry montmorillonite was added to 5L of 1M $CaCl_2$ and stirred for 24 hours for the mineral surface to absorb and equilibrate with $CaCl_2$ in solution. Chlorine impurities were removed by washing with MilliQ H_2O several times until the EC of the supernatant is less than 100µs. The Ca-montmorillonite was then freeze-dried and homogenised with a pestle and mortar ready to be used for synthesising an organo-mineral via adsorption.

An adsorption isotherm was created using pilot studies, which revealed the concentration of soluble necromass that needed to be added for each necromass type and mineral type to achieve an organo-mineral of 2wt%C. The soluble necromass of each microbial types were added and dissolved into separate centrifuge tubes containing 0.5g dry weight equivalent of ca-montmorilonite or ferrihydrite containing a 0.1M $NaNO_3$ solution. The pH was adjusted to pH7 (+-0.5) using dilute HCl and NaOH. The centrifuge tubes were placed on a rotary shaker for 24 hours. This allows for enough time

for an equilibrium to be achieved between the dissolved soluble necromass in the solution and necromass adsorbed to the mineral surfaces. The samples were then centrifuged at 4500rcf to harvest the newly synthesised soluble necromass organo-mineral pellets.

The soluble necromass containing organo-minerals were synthesised targeting 2wt%C (Table 3). However, this was difficult to achieve particularly for the montmorillonite organo-minerals due to a more limited saturation capacity resulting from a lower surface area compared to ferrihydrite (Huang and Schnitzer, 1986).

Table 4 - Compositions of ferrihydrite and montmorillonite organo-minerals composed of insoluble and soluble Fungal, Gr^+ and Gr^- bacterial necromass; Mean (n=5) wt%C, wt%N and CN ratio measured using COSTECH ECS 4010 (see section 4.2.3)

Mineral type	Necromass solubility	Microbe type	wt%C	wt%N	CN
Ferrihydrite	Insoluble	Fungi	2.99	0.3	10.17
Ferrihydrite	Insoluble	Gr+	3.05	0.8	3.91
Ferrihydrite	Insoluble	Gr-	3.47	0.89	3.92
Ferrihydrite	Soluble	Fungi	2.04	6.53	6.53
Ferrihydrite	Soluble	Gr+	1.56	2.74	2.74
Ferrihydrite	Soluble	Gr-	2.68	2.9	2.9
Montmorillonite	Soluble	Fungi	0.51	2.06	2.06
Montmorillonite	Soluble	Gr+	2.29	3.86	3.86
Montmorillonite	Soluble	Gr-	1.47	2.88	2.88

4.2.3. Chemical stability tests of organo-minerals

The stability of organo-minerals with 9 different compositions (Table 4) were tested through NaOH and NaOCl chemical washes. NaOH and NaOCl chemical washes mimicked desorption and oxidation organo-mineral destabilisation processes that occur in natural soils (Mikutta and Kaiser, 2011; Lopez-Sangil and Rovira, 2013). The NaOH (see section 2.2.2) wash caused a significant increase in pH, which mimics natural soil processes such as root and microbial exudates, and dry-wet cycling that can induce raised pH of microsites in soils (Yan, Schubert and Mengel, 1996; Shi *et al.*, 2011; Li *et al.*, 2021), bringing about the solubilisation of weakly bound organo-mineral OC (Kaiser and Guggenberger, 2003; Kleber, Sollins and Sutton, 2007). The NaOCl wash is a strong oxidising agent that oxidatively reduced labile SOC into CO_2, thus mimicking the action and substrate selectivity of microbial degradation (Mikutta and Kaiser, 2011). The NaOCl wash left behind more stable SOC that is

involved in strong association to minerals, occluded within aggregate structures or has intrinsic chemical recalcitrance (Mikutta *et al.*, 2006). Here, aliquots of 0.1g dry weight equivalent of each organo-mineral pellet were added to centrifuge tubes for a NaOH wash, NaOCl wash and a no wash control with 5 replicates. The protocol for the chemical washes were based upon work by Curti *et al.* (2021).

For the NaOH wash, 10ml of 0.1M NaOH was added to the aliquots and shaken for 24 hours to simulates destabilisation by desorption (Curti *et al.*, 2021). For the NaOCl wash, 10ml of 1M NaOCl was added to the aliquots and shaken for 24 hours, destabilising the organo-mineral through oxidation (Mikutta *et al.*, 2005; Kaiser and Guggenberger, 2007; Curti *et al.*, 2021). Solid material from the chemical washes were retained after being filtered out of the wash by a 0.2µm PES filter. The solid organo-minerals from the chemical washes and no wash control were freeze dried to analyse the quantity of carbon and nitrogen in the samples using the COSTECH ECS 4010 (see section 2.2.3).

4.2.6. Data processing and statistical analysis

The proportion (%) of organo-mineral C and N that was retained after the NaOH and NaOCl washes were evaluated by calculating the fraction of C or N measured for the NaOH and NaOCl treatments compared to the C or N measured for the control treatment for each organo-mineral type.

Multiple one-way ANOVAs with post-hoc Tukey tests to a 95% confidence interval, were used to determine any significant differences of all organo-mineral measurements (wt%C, wt%N, CN ratio, % of C and N retained) between organo-mineral types within the same treatment, and between treatments within the same organo-mineral type.

Welch's t-test was used to determine significant differences in wt%C, wt%N and CN ratio between the necromass and the organo-mineral control treatment.

4.2.7. FTIR Spectral analysis

The chemistry of fungal, gram-positive and gram-negative bacteria was investigated using Attenuated Total Reflectance Fourier Transform Infrared (ATR-FTIR) spectral analysis. ATR-FTIR spectra were taken at the microbiology laboratory at UKCEH Wallingford. This was used to link whether differences in the chemical composition of each necromass treatment explained differences in organo-mineral stability for each necromass treatment.

Four replicate ATR-FTIR spectra were taken from each of fungi, gram-positve and gram-negative bacterial raw insoluble necromass samples. Here, infra-red spectra at wavelengths of 600cm^{-1} to 4000cm^{-1} with an aperture of 2cm^{-1} were directed at the interface of the sample and high-refractive-index diamond crystal which enables the sample to absorb some infra-red light. The amount of infra-red absorbed by the sample changes at different wavelengths depending on the chemistry of the sample (Griffiths, 1983; Stuart, 2004; Smith, 2011). An attenuated infra-red light is reflected back being intercepted by a Mercury Cadmium Tellurid (MCT) detector, which converted the signal into the FTIR spectra that can be analysed. Each spectra was averaged over 32 scans in order to remove noise.

The resulting FTIR spectra were processed using the packages “PlotFTIR” and “ChemoSpec” in RStudio to perform qualitative and semi-quantitative analyses. Each spectra were normalised so that the minimum measured absorbance measure zero, before being averaged to remove further noise. A baseline correction using the interquartile range (IQR) method to enable qualitative analyses through interpreting the peaks of the spectra to indicate what functional groups are present within the insoluble necromass samples. In particular focus was peaks near 3000cm^{-1} and 1700cm^{-1} wavenumbers, where hydroxyl and carbonyl groups from carboxylic acids are identified (Klein, 2020).

Conversion of the baseline corrected spectra to second derivative transformed spectra with Savitzky-Golay smoothing to perform semi-quantitative analyses on the abundance of the chemical functional groups of interest (Puissant *et al.*, 2017). The second derivative transformation sharpened

and narrowed absorbance bands and completely removed baseline drift, and the Savitzky-Golay smoothing removed further noise from the spectra (Rinnan, Berg and Engelsen, 2009). From this spectra, calculations of absolute area under the curve for the spectral ranges of interest enabled semi-quantitative comparison of the carboxyl-richness between insoluble fungi, gram-positive and gram-negative bacterial necromass. The spectral ranges selected for the area under the curve calculations were 2800-3000cm^{-1} for the hydroxyl group and 1480-1780cm^{-1} for the carbonyl group (Fig. 25). These are broad ranges that were selected to take account for shifts in the wavenumbers of spectral peaks caused by the heterogeneous chemical structure of the necromass, such as adjacent aliphatic ring structures (Klein, 2020).

4.3. Results

4.3.1. CN composition of necromass and their organo-minerals

The CN ratio of both the insoluble and soluble fungal necromass was significantly higher than the CN ratio of the Gr^+ and Gr^- bacterial necromass ($p<0.01$) (Table 2; Fig. 19a. Fig. 19d). The CN ratio of Gr^+ and Gr^- necromass fractions were more similar to each other than to fungi, where the soluble necromass fractions were similar to each other ($p = 0.99$), but the insoluble fractions were still significantly different from each other ($p<0.01$).

The CN ratios of all the organo-minerals (Table 3; Fig. 19b, Fig. 19c, Fig. 19e) were marginally lower than the necromass from which the organo-minerals were synthesised (Table 2; Fig. 19a, Fig. 19d). The CN ratio of the insoluble necromass organo-minerals from Fungal, Gr^+ and Gr^- bacteria were not significantly different to the necromass before co-precipitation with ferrihydrite ($p=0.15$, $p=0.31$ and $p=0.43$ respectively). Whereas the CN ratio of the soluble necromass organo-minerals were significantly different ($p<0.05$) but particularly for fungal necromass organo-minerals (Table 3).

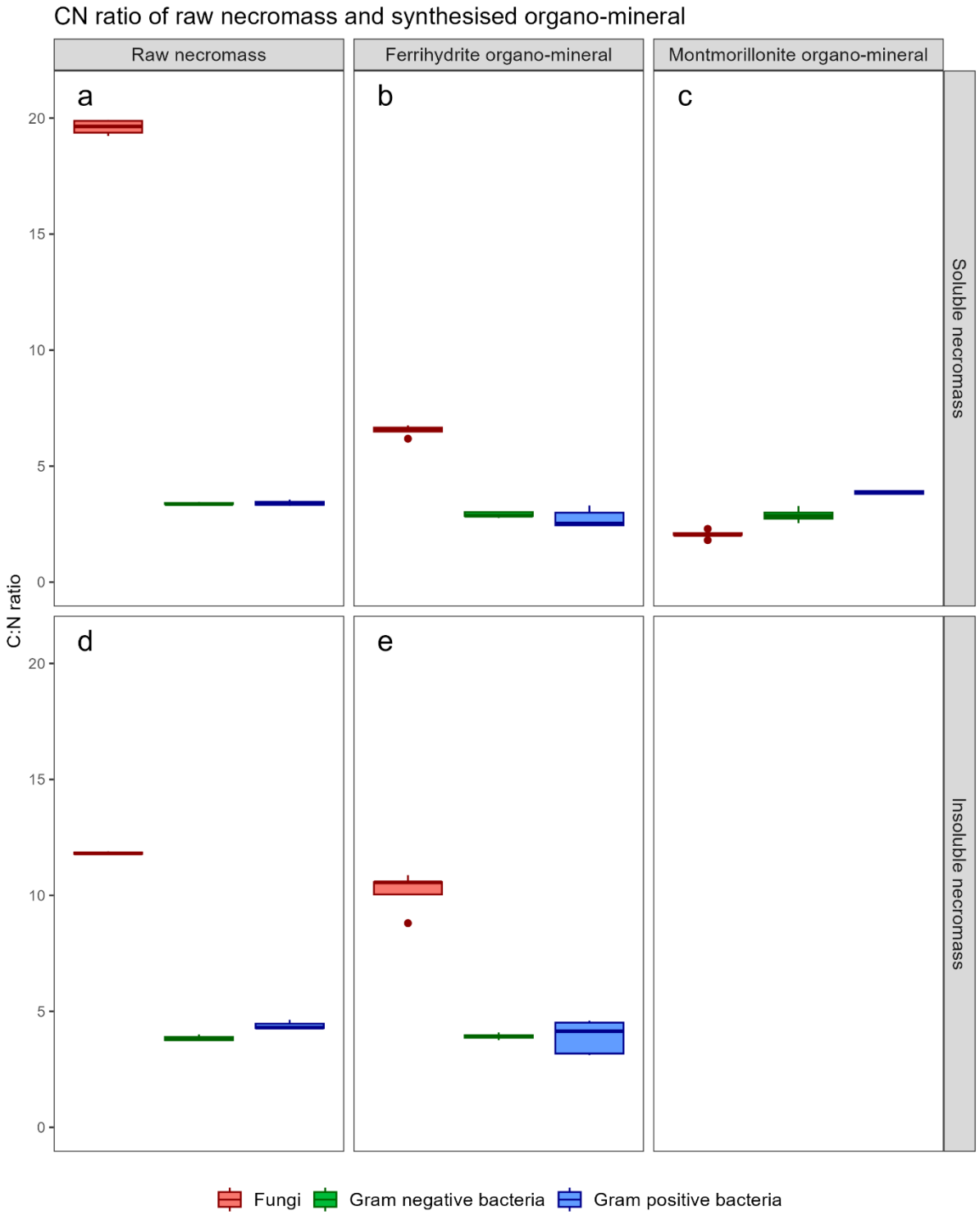

Figure 19 – Boxplots showing the mean (n=3) CN ratio of soluble and insoluble necromass for each microbe type (a and d) and the mean (n=5) CN taio of each synthesised organo-mineral (b, c and e)

4.3.2. Organo-mineral carbon retention after destabilisation

The NaOH and NaOCl chemical washes removed some C from every organo-mineral type, with the NaOCl removing more than the NaOH wash (Fig. 20A, Fig. 20B). The wt%C after both the NaOH and NaOCl chemical washes were significantly different from the wt%C of the control for every organo-mineral type ($p<0.01$) except for the soluble Gr^- montmorillonite organo-mineral ($p = 0.06$) and the insoluble fungi organo-mineral ($p=0.67$) after NaOH destabilisation (Fig. 20B). There were significant differences in the wt%C of NaOH destabilised fungal organo-minerals (all $p<0.05$) compared to Gr^+ and Gr^- organo-minerals, but not between Gr^+ and Gr^- organo-minerals (all $p>0.05$). After the NaOCl wash, only the insoluble fungal necromass organo-mineral had significantly different carbon content at 1.24wt%C compared to its equivalent Gr^+ and Gr^- bacteria necromass organo-minerals (Fig. 20B) at 0.98 and 0.90wt%C respectively ($p<0.05$). The wt%C of NaOCl destabilised soluble necromass organo-minerals (Fig. 20A) were very similar between all microbial types, all being 0.76±0.03 wt%C and 0.38±0.01 wt%C for the ferrihydrite and montmorillonite organo-minerals, respectively (all $p>0.12$).

The proportions (%) of organo-mineral C that were retained (Fig. 21) were significantly different between both NaOH and NaOCl treatments for all organo-mineral types ($p<0.05$). Fungal necromass organo-minerals retained more C compared to Gr^+ and Gr^- bacteria in all treatments except after NaOCl destabilisation of the ferrihydrite soluble necromass organo-minerals. After the NaOCl treatment, between 17-72% of C was retained across all organo-mineral types.

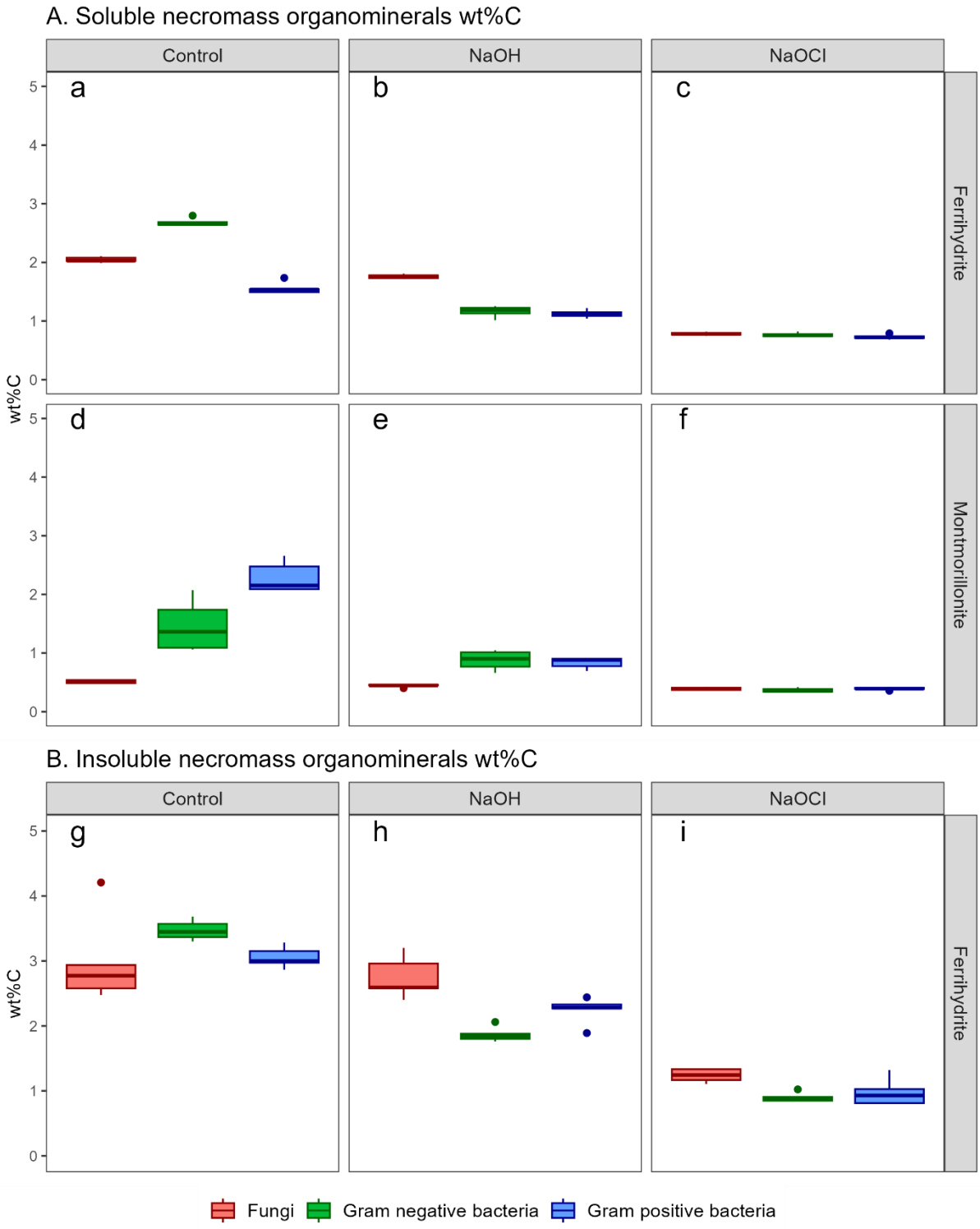

Figure 20 – Boxplot (mean ±IQR (n=5)) showing the wt%C of organo-minerals under control, NaOH wash and NaOCl wash treatments, for both soluble (A) and insoluble (B) necromass types.

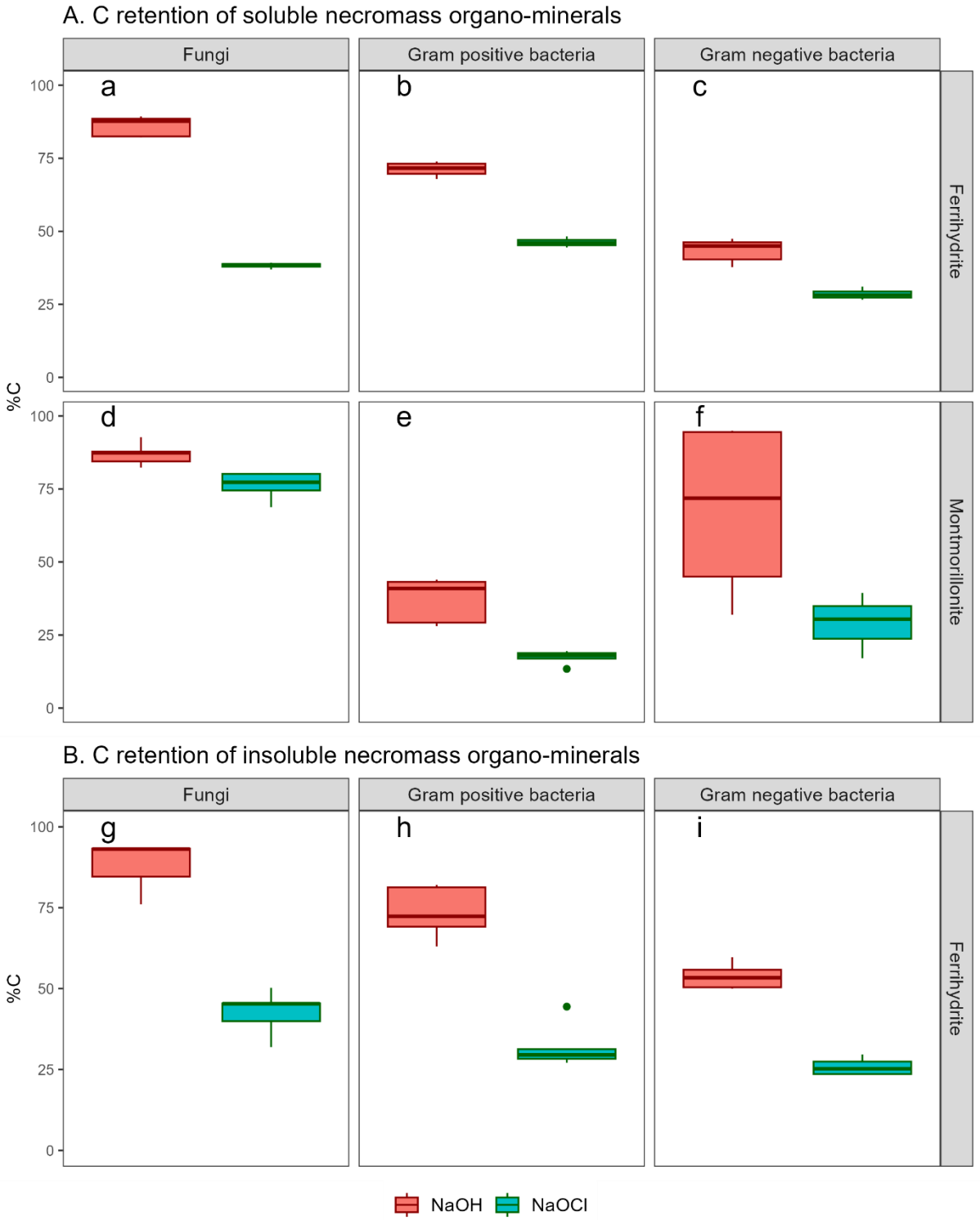

Figure 21 – Boxplot (mean ± IQR (n=5)) showing the retention of organo-mineral C after the chemical washes through proportion (%) of C measured in the control treatment retained on both soluble necromass (A) and insoluble necromass (B) organo-minerals after NaOH and NaOCl washes

4.3.3. Organo-mineral nitrogen retention after destabilisation

The wt%N of each organo-mineral type decreased after the NaOH and NaOCl wash (Fig. 22) compared to the control (all significant at $p<0.05$). This follows the same pattern as wt%C loss (Fig. 20) except the loss of wt%N was greater. There was almost complete removal of all nitrogen from the NaOCl wash for all organo-minerals (all 0.01±0.01 wt%N) with no significant difference of wt%N between the necromass types (all $p>0.12$).

There was more organo-mineral N retained after the NaOH wash within the insoluble necromass, at 37.1 to 78.6 %N retained (Fig. 23A), compared to soluble necromass organo-minerals, at 5.68 to 27.63 %N retained (Fig. 23B) ($p<0.05$). Although some significant difference between organo-mineral types remained for N retained after the NaOCl wash ($p<0.05$ to $p = 1.00$) only 0.5-3% of N was retained across all organo-mineral types.

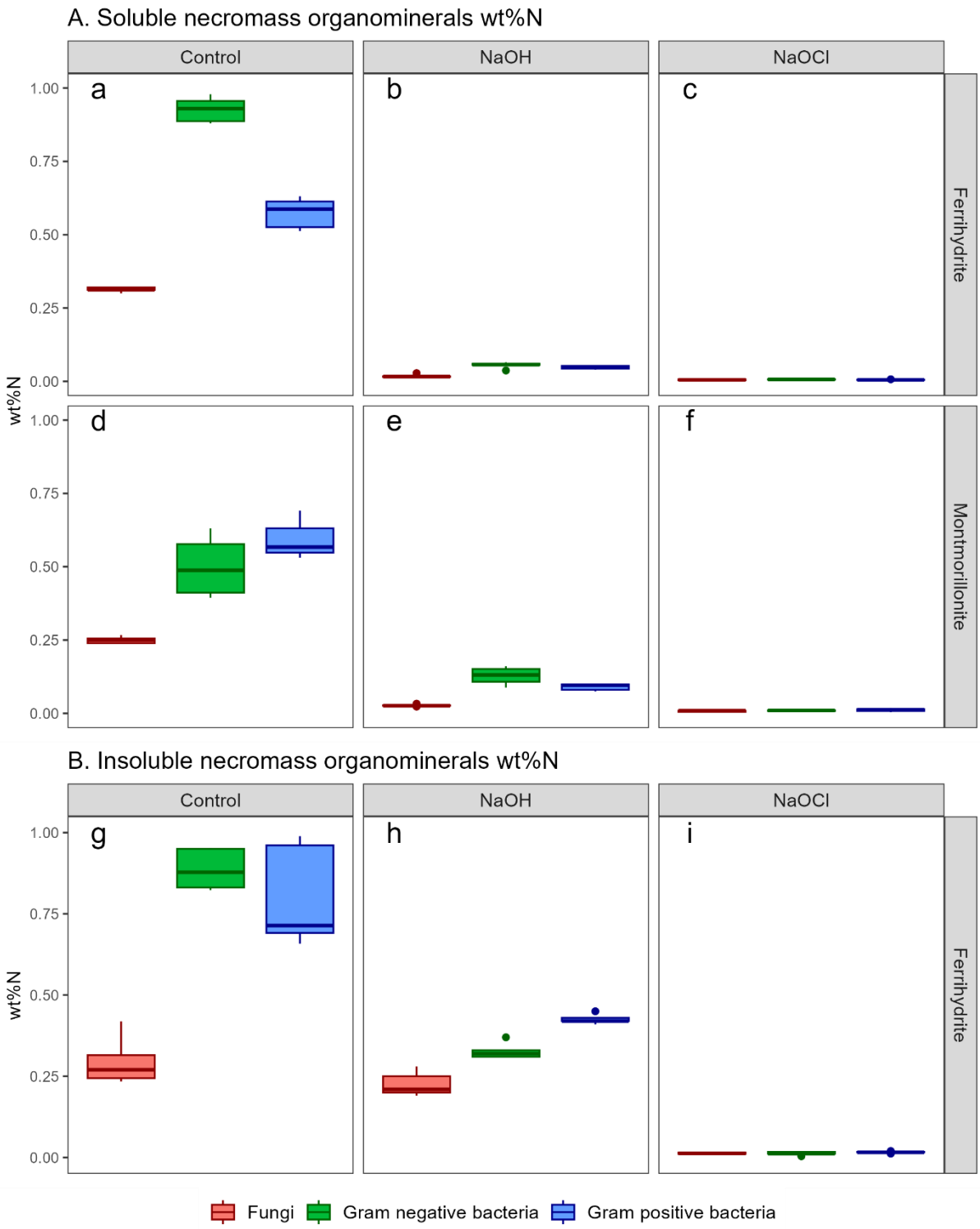

Figure 22 – Boxplot (mean ± IQR (n=5)) showing the wt%N of organo-minerals under control, NaOH wash and NaOCl wash treatments, for both soluble (A) and insoluble (B) necromass types

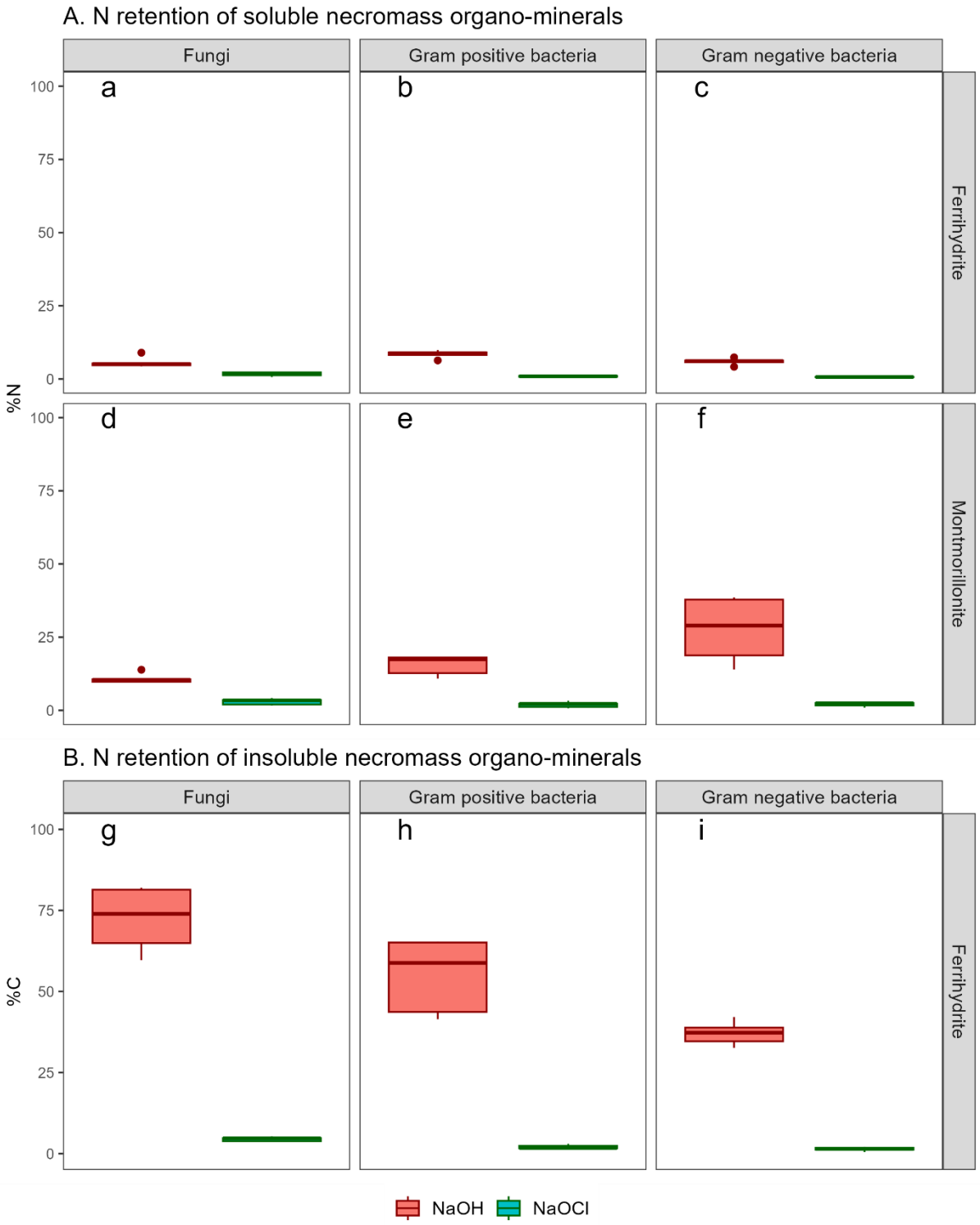

Figure 23 – Boxplot (mean ± IQR (n=5)) showing the retention of organo-mineral N after the chemical washes through proportion (%) of N measured in the control treatment retained on both soluble necromass (A) and insoluble necromass (B) organo-minerals after NaOH and NaOCl washes

4.3.4. Organo-mineral CN ratio after destabilisation

The CN ratio of all soluble necromass organo-minerals (Fig. 24A) increased compared to the control after the NaOH wash, and further after the NaOCl wash. However, for the insoluble necromass organo-minerals (Fig. 24 B), the CN ratio was not significantly altered by the NaOH treatment ($p = 0.97$, $p = 0.85$, $p = 0.99$ for fungi, Gr^+ and Gr^- organo-minerals respectively). However, the NaOCl treatment increased the CN ratio of these insoluble necromass organo-minerals significantly ($p<0.05$) to 98.83, 60.58 and 62.20 for Fungi, Gr^+ and Gr^- organo-minerals, respectively.

The CN ratio of fungal necromass organo-minerals exceeds both Gr^+ and Gr^- organo-minerals for every treatment ($p<0.05$) except following the NaOCl wash for the soluble necromass organo-minerals ($p = 0.36$ to $p = 0.69$).

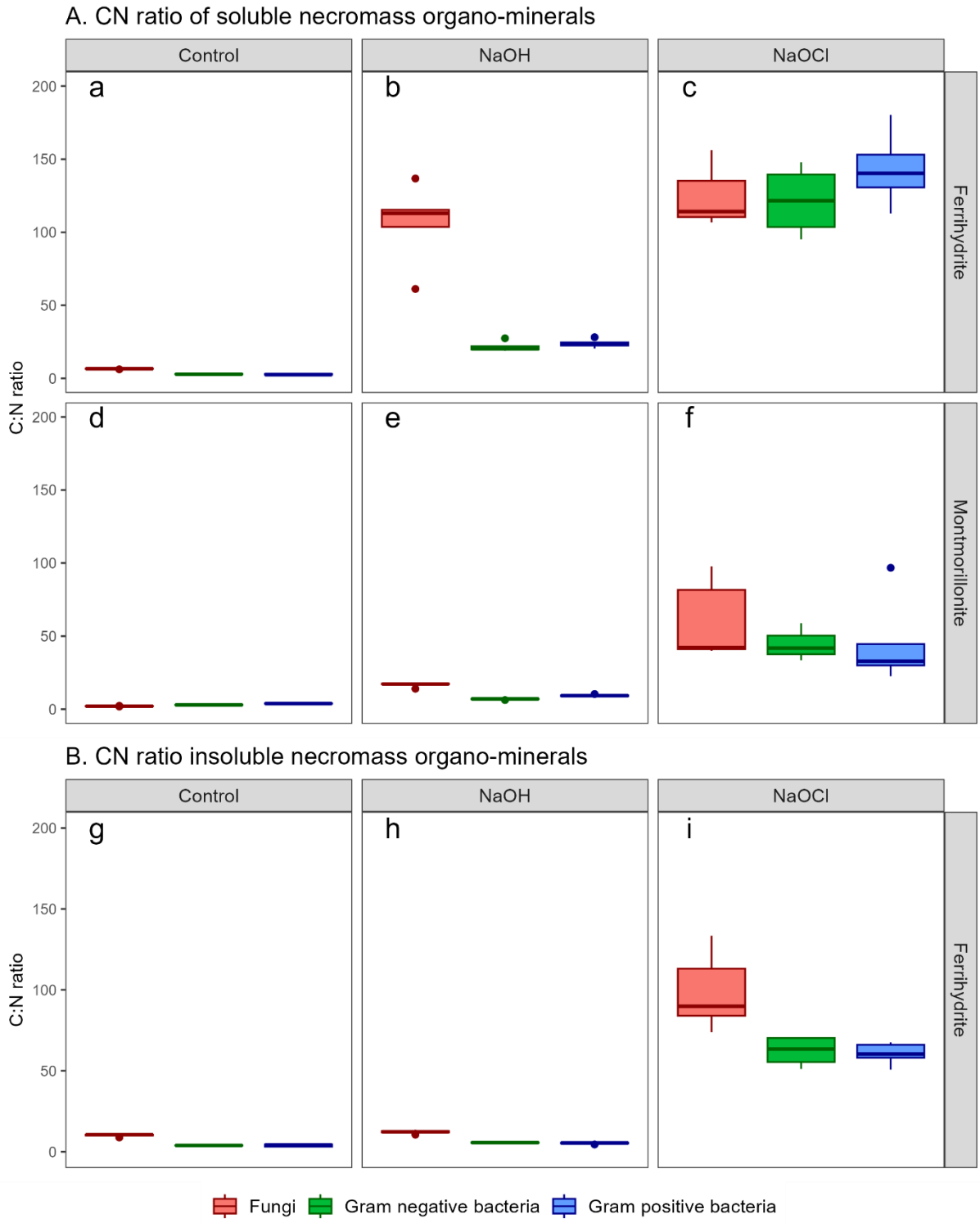

Figure 24 – Boxplot (mean ± IQR (n=5)) showing the CN ratios of organo-minerals under control, NaOH wash and NaOCl wash treatments for both soluble (A) and insoluble (B) necromass types

4.3.5. FTIR spectra

The baseline corrected spectra (Fig.25A) displays strong dual hydroxyl peaks at 2917cm^{-1} and 2850cm^{-1}, and strong peaks in the carbonyl region of FTIR spectra at 1540cm^{-1} and 1625cm^{-1}. The spectra of the gram-positive and gram-negative bacterial necromass follow closely to each other over the spectra, whereas the fungal necromass spectra contain peak intensities that differ greatly. Fungal necromass has peaks of greater absorbance in the 2800-3000cm^{-1} hydroxyl group region of the spectra (Fig. 25Ai) compared to the gram-positive and gram-negative bacterial necromass. This pattern is reversed for the peak intensities in the 1480-1780cm^{-1} carbonyl region of the spectra (Fig. 25Aii).

The area under of the curve calculations of the second derivative transformed spectra (Fig. 25B) show that the fungal necromass has over four times greater absorbance of the infra-red spectra in the 2800-3000cm^{-1} hydroxyl group spectral range 0.157 Abs$(cm^{-1})^{-1}$ compared to gram-positive and gram-negative bacterial necromass at 0.031 and 0.039 Abs$(cm^{-1})^{-1}$ respectively. For the 1480-1780cm^{-1} carbonyl group spectral range the gram-negative bacterial necromass has greater absorption of the infra-red at 0.171 Abs$(cm^{-1})^{-1}$ followed by gram-positive bacterial necromass at 0.139 Abs$(cm^{-1})^{-1}$ and fungal necromass at 0.116 Abs$(cm^{-1})^{-1}$. However, if this spectral region is split into 1650-1780cm^{-1} and 1480-1650cm^{-1}, then the fungi necromass at 0.057Abs$(cm^{-1})^{-1}$ absorbs more infra-red at the higher 1650-1780cm^{-1} wavenumber, but absorbs much less infra-red at the lower 1480-1650cm^{-1} wavenumber compared to both gram-positive and gram-negative bacterial necromass.

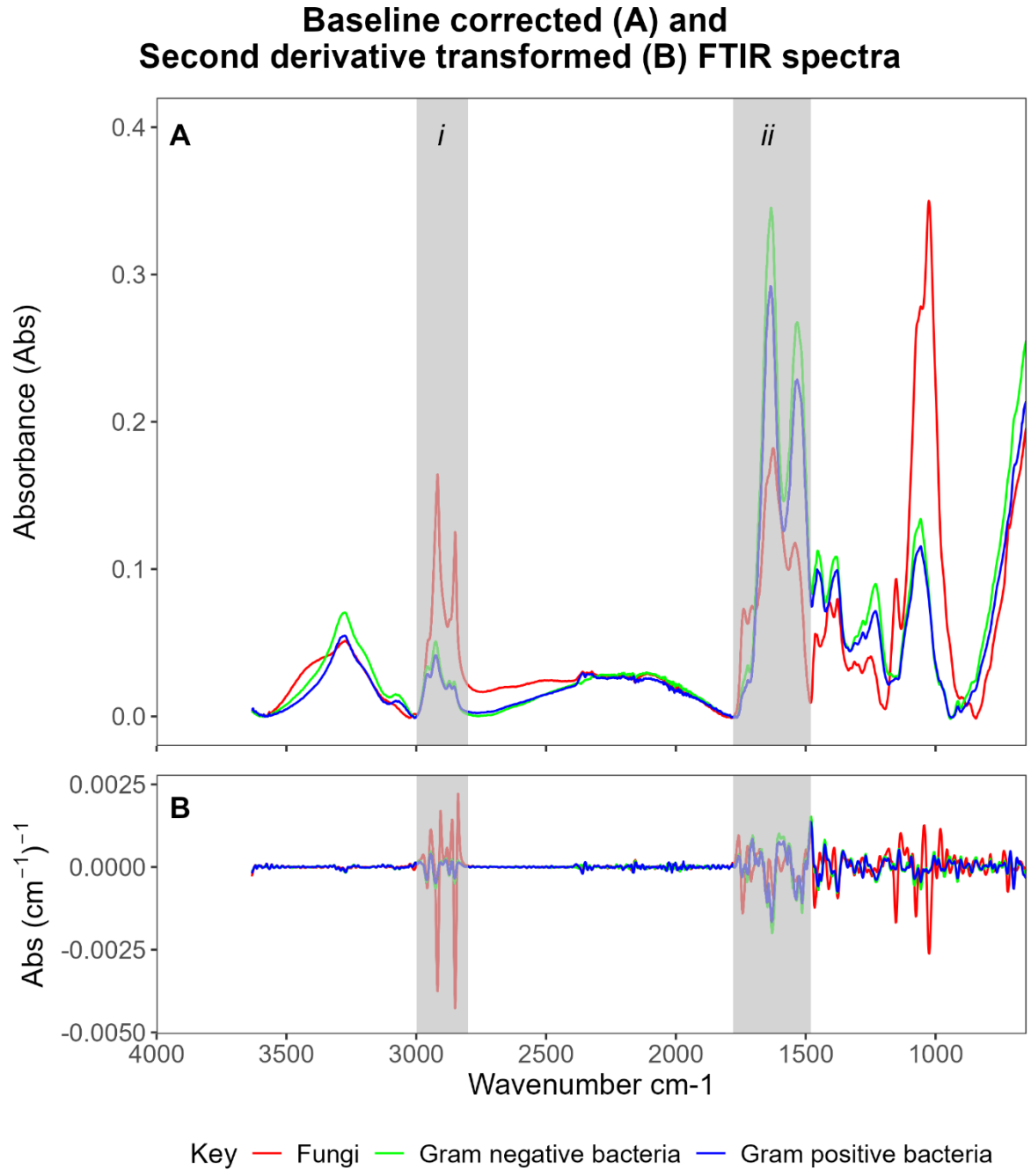

Figure 25 – Baseline corrected (A) and second derivative transformed (B) FTIR spectra of insoluble Fungi, Gram positive and Gram negative bacterial necromass. Grey higlights the spectral regions for hydroxyl functional groups between 2800-3000cm^{-1} (i) and carbonyl functional groups between 1480-1780cm^{-1} (ii), that make up carboxylic acid functional groups.

4.4. Discussion

This experiment set out to investigate **whether there are differences in the stability of organo-minerals when composed of necromass from different microbial types**. This was explored using chemical washes which desorb (NaOH) or oxidise (NaOCl) OC within the organo-mineral. This tests the stability of organo-minerals composed of fungal, Gr^+ and Gr^- bacterial necromass. Two hypotheses were tested. **Organo-minerals derived from gram-negative necromass will have the greatest stability (H1)**, and **the most stable fraction of the organo-minerals will have a lower nitrogen content (H2)**. Measurements of wt%C and wt%N of the organo-mineral solids in the control treatment and after NaOH and NaOCl washes revealed the extent of C and N destabilisation between the different organo-minerals.

4.4.1. Fungal necromass organo-minerals were the most stable

The results from this experiment showed that fungal necromass organo-minerals retained a greater amount of necromass OC after destabilisation by NaOH wash compared to Gr^+ and Gr^- organo-minerals. The wt%C of organo-minerals after NaOH wash was greatest in fungal necromass organo-minerals, except for the montmorillonite organo-mineral (Fig 20). Here, the saturation of soluble fungal necromass on the montmorillonite surface when synthesising the organo-mineral was a much lower wt%C than the saturation of soluble Gr^+ and Gr^- necromass, leading to less wt%C in the fungal organo-mineral after the NaOH wash even though little was destabilised. In fact only 13% of necromass OC was lost due to NaOH wash in the montmorillonite organo-minerals, compared to over 30% for both Gr^+ and Gr^- necromass (Fig 21). The lower saturation level of soluble fungal necromass on montmorillonite achieved during organo-mineral synthesis was likely due to its composition (see section 4.4.4). There was little difference between necromass types in the wt%C of organo-minerals after the NaOCl wash (see section 4.4.3). The exception to this was for the insoluble fungi necromass organo-mineral (Fig. 20), where there was significantly more wt%C after the NaOCl wash compared to insoluble Gr^+ and Gr^- organo-minerals.

Therefore, fungal necromass organo-minerals retained more OC after destabilisation by desorption (NaOH) and oxidation (NaOCl) compared to Gr^+ and Gr^- bacterial necromass organo-minerals, disproving the hypothesis (H1) predicting that gram-negative bacterial necromass would be the most stable. In fact, the fungal necromass is the most stable in an organo-mineral.

4.4.2. Fungal necromass has greater carboxyl-richness

In baseline corrected FTIR spectra (Fig. 25 A) both the hydroxyl and carbonyl peaks are shifted to lower wavenumbers compared to the expected 3000cm^{-1} for hydroxyl and 1700cm^{-1} for carbonyl groups of simple carboxylic acids. This is due to the presence of aliphatic ring structures (Mobaraki and Hemmateenejad, 2011; Klein, 2020) of N-acetylglucosamine and N-acetylmuramic acid found in chitin and peptidoglycan. The spectral peaks in the carbonyl region of the spectra are further shifted to lower wavelengths due to the presence of amide groups (Klein, 2020), which are particularly abundant in the peptide chains of the peptidoglycan contained in gram-positive and gram-negative necromass (Vollmer, Blanot and De Pedro, 2008).

The results from the area under the curve calculations (section 4.3.5.) on the second derivative transformed spectra (Fig. 25B) suggest that fungal necromass is more abundant in carboxylic acid functional groups, and thus has greater carboxyl-richness, compared to gram-positive and gram-negative bacterial necromass. Fungal necromass absorbs more infra-red in the 2800-3000cm^{-1} hydroxyl group region and the higher wavenumber 1650-1780cm^{-1} carbonyl region of the spectra, highlighting greater abundance of carboxylic acid functional groups (Hay and Myneni, 2007; Klein, 2020). The gram-negative and gram-positive necromass absorb much more infra-red at the lower wavenumber 1480-1650cm^{-1} carbonyl region of the spectra where the peaks from carbonyls in amide functional group appear (Klein, 2020). The FTIR spectral confirmation of the presence of these N-containing amide groups along with the results showing that gram-negative and gram-postive bacterial necromass have lower CN ratios (section 4.3.1.) reflects the abundance of amide groups found within the peptide chains of peptidoglycan within gram-positive and gram-negative necromass.

4.4.3. NaOCl stable organo-mineral fractions were nitrogen poor

The results show that almost all of the nitrogen is destabilised during the NaOCl wash for all organo-mineral types. Here, only 0.01 wt%N or less is retained by the organo-minerals after destabilisation by NaOCl (section 4.3.3). Thus less than 5% of nitrogen was retained by the organo-mineral in the NaOCl stable fraction, which was far less than the 17% or more carbon retained.

Even though the lower CN ratio of the organo-mineral controls compared to the raw necromass suggest a preferential uptake of nitrogen containing components by the minerals (section 4.3.1), the high CN ratio of the NaOCl stable organo-mineral fraction (section 4.3.4) suggests that nitrogen containing OC was not important in the most stable organo-mineral OC fraction. This supports the hypothesis (H2) predicting that the most stable fraction of the organo-minerals will have a lower nitrogen content.

4.4.4. NaOH stable organo-mineral OC dependent upon necromass chemistry

Both Gr^+ and Gr^- bacteria cell walls contain peptidoglycan, making their composition more similar to one another compared to fungi, whose cell walls are dominated by chitin. The CN ratios of raw insoluble and soluble necromass (section 4.3.1) highlight this pattern of necromass composition, which also translated into the composition of synthesised organo-minerals, where there was greater similarity between Gr^+ and Gr^- necromass organo-minerals compared to fungal necromass organo-minerals. The composition of these organo-minerals influenced their vulnerability to desorption by 0.1M NaOH wash. Here, the wt%C of the Gr^+ and Gr^- necromass organo-minerals were similar to each other but significantly different to the fungal necromass organo-minerals after the NaOH wash, where the fungal necromass organo-minerals were more stable (section 4.4.1).

This NaOH wash destabilises organo-mineral OC by solubilising the OC through ionisation of the OC functional groups (Lopez-Sangil and Rovira, 2013) such as amines and carboxyl groups. This will not affect organo-mineral OC involved in inner-sphere complexes (Newcomb *et al.*, 2017), so primarily will destabilise OC in organo-organic interactions, where weaker interactions such as cation bridging

occur to a greater extent (Sollins *et al.*, 2006; Kleber, Sollins and Sutton, 2007; Newcomb *et al.*, 2017; Gao *et al.*, 2020; Kleber *et al.*, 2021). The 0.1M NaOH wash used in this experiment revealed differences in stability between organo-mineral compositions similar to experiments testing the stability of organo-minerals of increasing carboxyl richness (Curti *et al.*, 2021; Zhao *et al.*, 2022). Therefore, supporting that fungal necromass contain more carboxyl groups (see section 4.4.2.), that enable greater stability to NaOH wash compared to Gr^+ and Gr^- bacterial necromass.

4.4.5. Chitin enabled greater organo-mineral OC retention after NaOCl wash

The most stable fraction of organo-mineral in this experiment was the organo-mineral OC that was retained after the NaOCl wash. The amount of the NaOCl-stable OC was dependent upon the type of mineral, as the wt%C of the organo-minerals after the NaOCl wash was the same between soluble necromass types, yet differed between montmorillonite and ferrihydrite minerals. Montmorillonite has a smaller surface area available for ligand exchange compared to ferrihydrite (Huang and Schnitzer, 1986; Guo *et al.*, 2020; Kleber *et al.*, 2021), so consequently the montmorillonite has a smaller capacity for direct organo-mineral interactions to occur. Therefore, montmorillonite had a smaller capacity to contain NaOCl wash resistant organo-mineral OC compared to the ferrihydrite, independent of OC chemistry.

In contrast to soluble necromass organo-minerals, the wt%C of NaOCl-stable OC within insoluble necromass organo-minerals differed between necromass compositions. The fungal necromass organo-mineral retained a greater wt%C after destabilisation by the NaOCl wash compared to insoluble Gr^+ and Gr^- necromass organo-minerals. The cell walls of the microbes which constituted the majority of the insoluble necromass, differ between Fungi compared to Gr^+ and Gr^- (Vollmer, Blanot and De Pedro, 2008; Garcia-Rubio *et al.*, 2020). Carboxylic acid containing Chitin (section 4.4.2.), which dominates the fungal cell walls, enabled greater organo-mineral stability to NaOCl oxidation compared to peptidoglycan, which constituted a significant part of both Gr^+ and Gr^- bacterial cell walls. Here, the NaOCl wash was able to oxidise and degrade chitin and peptidoglycan without altering the ferrihydrite

mineral (Siregar *et al.*, 2005). Chitin and peptidoglycan have some similarities in chemical structure as both are composed of O-linked glycans (Hu *et al.*, 2018; Liang *et al.*, 2019) (Fig. 26), however, a major difference in the composition is that peptidoglycan contains peptide chains (Vollmer, Blanot and De Pedro, 2008). This could be the difference in the NaOCl stability seen between insoluble Fungi, Gr^+ and Gr^- bacteria necromass in this experiment. The oxidation of chitin by NaOCl can create carboxyl-rich degradation products (Yoo *et al.*, 2005; Yang *et al.*, 2012) enhancing the stability of the degraded OC through inner-sphere complexation to the mineral surface, as seen in Chapters 2 and 3.

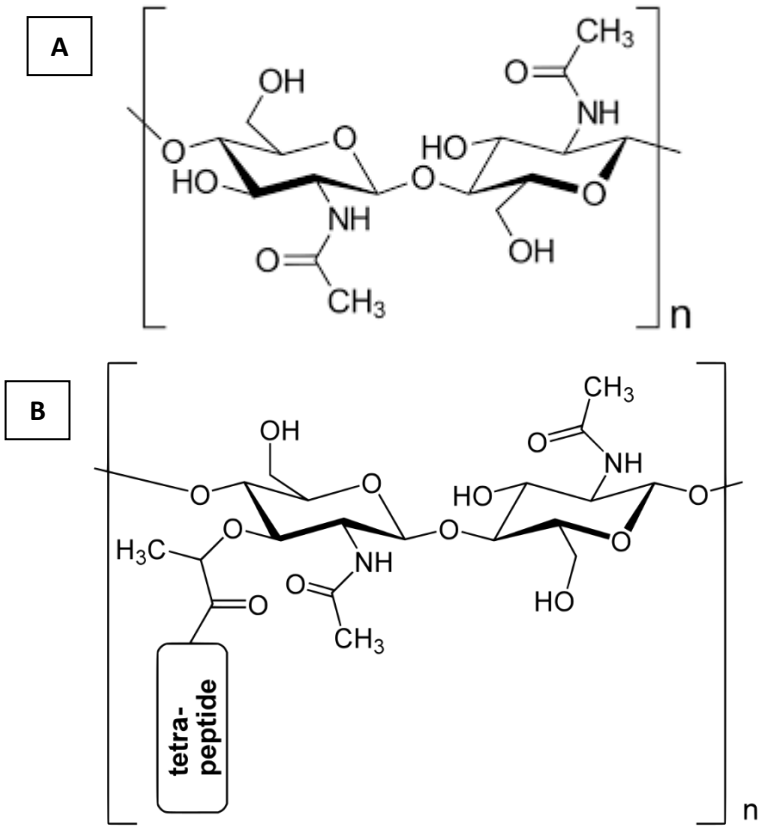

Figure 26 – Chemical structure of Chitin (A) consisting of O-linked N-acetylglucosamine monomers. The chemical structure of Peptidoglycan (B) consisting of O-linked N-acetylglucosamine and N-acetylmuramic acid with an attached tetra-peptide chain.

4.4.6. Wider implications

As oxidation of chitin by NaOCl can create carboxyl-rich degradation products (section 4.4.4) which may have helped fungal insoluble necromass to have the greater stability in this experiment (section 4.4.1), this exemplifies the importance of carboxylic acid functional groups and OC carboxyl-richness on organo-mineral stability. This supports the conclusions of Chapters 2 and 3 of this thesis, where greater stability occurred for carboxyl-rich organo-minerals. In this experiment, phosphate groups that are predicted to form strong direct organo-mineral interactions (Newcomb *et al.*, 2017) were not examined but could also have a significant impact on the stability of heterogenous OC in organo-minerals.

The results of this experiment suggest that soil microbial community composition and the associated composition of microbial necromass could be important in impacting the stability of

organo-mineral OC. The results that show that fungal necromass organo-minerals are more stable than Gr^+ and Gr^- necromass organo-minerals (section 4.2.1), meaning that a microbial community composition rich in fungi could translate to greater abundance of fungal necromass, greater proportion of fungal necromass derived OC associated to soil minerals, thus a greater stability of the organo-minerals.

The soil microbial community composition of intensively managed agricultural land tends to be low in fungi (Hannula *et al.*, 2017). Land management practices such as reduction in soil fertilisation and no-tillage (Blanco-Canqui and Lal, 2008; dos Reis Ferreira et al., 2020; Jilling et al., 2020) could be utilised to increase the fungal contribution to the soil microbial community (de Vries *et al.*, 2006; Di Lonardo *et al.*, 2020), which could translate into the creation of more fungal necromass and greater organo-mineral stability. Alternatively, a soil microbial inoculant (Hart *et al.*, 2018) could be developed for the purpose of increasing fungal abundance in the soil microbial community and increase fungal necromass input into MAOM. There is opportunity to research how land management strategies can impact the soil microbial community in the context of MAOM stability, including with through increasing carboxyl-richness. This would provide a platform to transfer knowledge of the mechanisms of MAOM stability into land management techniques that can be applied to have a real-world impact.

The soil microbial community could also impact the ability for biotic destabilisation of organo-minerals (Bailey, Pries and Lajtha, 2019). Further research would be needed to quantify the balance between stabilisation of necromass OC on organominerals and biotic destabilisation of organo-minerals in different soil microbial communities.

4.4.6. Conclusions

This experiment has shown that fungal necromass organo-minerals have greater stability compared to organo-minerals containing necromass derived from Gr^+ and Gr^- bacteria. Following destabilisation by NaOH and NaOCl washes, the organo-minerals retained a N-poor stable fraction of

necromass OC. This included retaining a greater proportion of fungal derived chitin compared to peptidoglycan derived from Gr^+ and Gr^- bacteria.

The first hypotheses of this experiment, predicting that Gr^- bacterial necromass would be the most stable, was not supported by the experiments as fungi was the most stable necromass OC within organo-minerals. However, the second hypothesis that predicted for the most stable fraction of necromass OC within organo-minerals to be N-poor, was supported by the experiments.

5. General discussion

Enhancing the MAOM soil carbon store is seen as a potential long-term solution as a nature-based CDR technology to mitigate anthropogenic climate change (Minasny *et al.*, 2017; Fuss *et al.*, 2018; Cotrufo *et al.*, 2019; Wiesmeier *et al.*, 2019; Lehmann *et al.*, 2020; Georgiou *et al.*, 2022). However, to succeed in long-term MAOM carbon storage, the stability of organo-mineral complexes should be maximised (Bailey, Pries and Lajtha, 2019), which requires the closure of knowledge gaps on the controls on the stability of organo-mineral complexes. This thesis has focused on investigating how the OC composition effects the stability of organo-mineral complexes, through three separate experiments.

Three overarching findings emerged from the results of the experiments. Firstly, the overall stability of organo-minerals increased with increasing carboxyl-richness. The second is that the OC composition was a significant control on the stability of organo-organic interactions within organo-mineral complexes. Finally, the OC composition played less of an important role in effecting the stability of the direct organo-mineral interactions within organo-mineral complexes.

5.1. Organo-mineral stability increased with increasing carboxyl-richness

Results from Chapters 2 and 3 of this thesis directly show that organo-mineral stability is enhanced with increasing carboxyl-richness. Furthermore, Chapter 4 of this thesis indicates the greater stability experienced by insoluble Fungal necromass could be driven by carboxyl-richness, where NaOCl oxidised chitin create carboxyl-rich degradation products (Yoo *et al.*, 2005; Yang *et al.*, 2012). Carboxyl-rich organo-minerals had greater stability when confronted with both physiochemical and biotic destabilisation mechanisms. This was exemplified in the incubation experiment in Chapter 3, where the carboxyl-rich organo-minerals had greater stability than the carboxyl-poor organo-minerals in both anaerobic and aerobic conditions, where destabilisation by reductive dissolution and by microbial activity dominated respectively.

The extra carboxyl groups in each OC molecule that coats the mineral in the carboxyl-rich organo-mineral complex were able to adsorb with and remove the Fe(ii) ion from solution OC (Jones *et al.*, 2009; Catrouillet *et al.*, 2014; ThomasArrigo *et al.*, 2017; Zhou *et al.*, 2018; ThomasArrigo, Kaegi and Kretzschmar, 2019). This reduces the quantity of Fe(ii) reaching the metal-oxide surface and lowering the rate of Fe-oxide reductive dissolution and the destabilisation of the organo-mineral complex, highlighted in the results in Chapters 2 and 3.

During the incubations with aerobic conditions (Chapter 3), the carboxyl-rich organo-mineral OC was not bioavailable for soil microbes to utilise in respiration, in contrast to carboxyl-poor organo-mineral OC. This difference in bioavailability can be attributed to the organo-organic interactions being more stable in carboxyl-rich organo-minerals compared to carboxyl-poor OC limited to weak hydrophobic interations (Kleber, Sollins and Sutton, 2007; Curti *et al.*, 2021; Kleber *et al.*, 2021). These weak hydrophobic organo-organic interactions drove greater water extractable OC in carboxyl-poor organo-minerals in Chapter 2 (Heckman *et al.*, 2011; Possinger, Bailey, *et al.*, 2020).

5.2. OC composition played an important role in the stability of organo-organic interactions

OC composition

The stability organo-organic interactions within the organo-mineral complex were influenced by the OC composition in each experiment within this thesis. The carboxyl-richness controlled the stability of organo-organic interactions in Chapter 2 and 3 by controlling the type of interactions possible between 2 OC molecules. Organo-organic interactions in carboxyl-poor organo-minerals were limited to hydrophobic and van der Waals interactions, whereas carboxyl-rich organo-organic interactions could facilitate more stable interactions such as cation bridging (Kleber, Sollins and Sutton, 2007; Curti *et al.*, 2021; Kleber *et al.*, 2021). This resulted in greater quantity of water extractable OC in carboxyl-poor organo-minerals (Chapter 2) with greater bioavailability to be utilised by the soil microbial community (Chapter 3).

The composition of more complex heterogenous OC also effected the stability of organo-organic interactions in Chapter 4. The fungal necromass had more stable organo-organic interactions compared to Gr^+ and Gr^- bacteria necromass. There were no significant difference in the organo-organic interactions between the Gr^+ and Gr^- bacteria necromass where there was little difference in the CN composition of these two necromass types. This highlights that the OC composition has an effect on the stability of organo-organic interactions even for more heterogenous complex OC.

5.3. OC composition plays less of an important role in the stability of direct organo-mineral interactions

Direct organo-mineral interactions include the most stable interactions such as inner-sphere complexation of the OC with the mineral surface (Kleber, Sollins and Sutton, 2007; Newcomb *et al.*, 2017; Possinger, Zachman, *et al.*, 2020; Kleber *et al.*, 2021). This most stable organo-mineral OC fraction was more stable to chemical washes such as 0.5M NaOH (Chapter 2) and NaOCl (Chapter 4) in experiments within the thesis, as well as to microbial destabilisation (Chapter 3).

The amount of direct organo-mineral interactions was affected by the mineral composition rather than the OC composition. Unlike organo-organic interactions (see section 5.2), there was little difference in the 0.5M NaOH (Chapter 2) and NaOCl (Chapter 4) stable fraction between different organo-mineral OC compositions. However, in Chapter 4, the only experiment in this thesis that compared between different mineral types, there is a greater amount of NaOCl stable fraction in ferrihydrite compared to montmorillonite.

The mineral surface limits the amount of stable direct organo-mineral interactions through inner-sphere complexation, due to the surface area of the mineral and the density of reactive functional groups such as hydroxyls on the mineral surface (Kleber *et al.*, 2021). The composition of the OC does not affect the capacity of these stable direct organo-mineral interactions further than requiring a functional group that enables ligand exchange ferrihydrite (section 4.4.4). Although, the

insoluble fungal necromass having greater NaOCl stable OC in Chapter 4, suggests that OC composition can have some affect on the amount of the most stable fraction of organo-mineral OC.

5.4. Conclusions

This thesis has shown that OC composition was an important control on the stability of organo-minerals, particularly by affecting the stability of organo-organic interactions. The carboxyl-richness of simple OC molecules were able to control organo-mineral stability where a greater amount of carboxyl groups were able to interact in more stable organo-organic interactions or be able to hinder reductive dissolution of Fe-oxide minerals. The composition of more heterogenous necromass OC also impacted organo-mineral stability, where fungal necromass produced more stable organo-minerals. However, the mineral composition had a much greater affect than the OC composition on the most stable fraction of organo-mineral OC by controlling the amount of OC involved in direct organo-mineral interactions.

5.5. Wider implications

The importance of OC carboxyl-richness on enhancing organo-mineral stability and increasing the persistence of MAOM has been highlighted within this thesis. Slower turnover of MAOM driven by more stable carboxyl-rich organo-minerals enhances carbon retention within soils (see chapter 3)(Cotrufo and Lavallee, 2022; Sokol *et al.*, 2022; Angst *et al.*, 2023). This leads to an increase in SOC stocks (Cotrufo *et al.*, 2019), consequently, by contributing to SOC sequestration, organo-mineral carboxyl-richness plays a critical role in addressing broader soil-related anthropogenic challenges such as climate change mitigation and food security (Lal, Negassa and Lorenz, 2015; Cotrufo and Lavallee, 2022).

This includes enabling the recovery of degraded and over-farmed land (Lal, Negassa and Lorenz, 2015; Minasny *et al.*, 2017). Here, increasing the SOC stocks of a soil can improve key soil properties such as structure, water retention and nutrient availability, enhancing the soil fertility and support more resilient and sustainable agricultural systems (Oldfield, Wood and Bradford, 2020).

Therefore, the potential for increased SOC deriving from more stable carboxyl-rich MAOM, has wider implications for global food security (Lal, Negassa and Lorenz, 2015; Oldfield, Wood and Bradford, 2020).

Furthermore, if carboxyl-richness of MAOM can be increased, the reliability and permanence of using carbon sequestration as a nature-based CDR technology is enhanced (Schmidt *et al.*, 2011). Here, a carboxyl-rich MAOM can improve the confidence in the stability of MAOM pool, supporting the credibility of carbon markets reliant on verifiable, long-term sequestration (Fuss *et al.*, 2018), aiding the 4 per mille soil carbon sequestration target (Minasny *et al.*, 2017).

However, applicable soil management practices for increasing the stability of SOC specific to increasing the carboxyl-richness of MAOM have not been explored (Angst *et al.*, 2023; Just *et al.*, 2023). One approach could be through greater application of compost to soils as a soil amendment. Compost, derived from decomposed plant material, is not only nutrient-rich for crops but also contains a high abundance of carboxylic acid functional groups (Spaccini and Piccolo, 2007; Yu *et al.*, 2019). This makes compost a potentially effective source of carboxyl-rich SOC that could directly facilitate more stable MAOM formation. However, the addition of SOC amendments can stimulate the decomposition of existing SOC and MAOM through priming (Jilling *et al.*, 2021; Bernard *et al.*, 2022; Brown *et al.*, 2024). Therefore, further research is needed to understand the net impact of compost addition on long term MAOM stability.

Another management strategy to investigate is the practice of no tillage. No-till systems maintain soil structure and preserve soil aggregates, therefore helping to protect MAOM from physical disruption, increasing the MAOM pool (Blanco-Canqui and Lal, 2008; dos Reis Ferreira *et al.*, 2020; Jilling *et al.*, 2020). Furthermore, these practices tend to promote fungal dominance within soil microbial communities (Gao, Li and Li, 2022; Domnariu *et al.*, 2025), leading to a greater accumulation of fungal necromass. This could enhance MAOM stability further as fungal necromass has been shown to form more stable associations with soil minerals (see chapter 4). However, the role of different

microbial communities to destabilise organo-mineral complexes remains relatively unexplored (Buckeridge, Creamer and Whitaker, 2022).

Without these potential soil management practices being investigated, the impact of carboxyl-richness on enhancing organo-mineral stability will remain a mechanistic control, rather than being a process that can be affected by anthropogenic means.

5.6. Future Outlook

The stability of SOC such as MAOM is poorly resolved in earth system models (Wieder *et al.*, 2014; Bradford *et al.*, 2016; Luo *et al.*, 2016; Zhang *et al.*, 2020). This has led to uncertainty in predicted future climate brought about by anthropogenic climate change, as well as in the viability and long-term impact of using soil as a nature-based CDR technology (Bradford *et al.*, 2016). The results of this thesis progresses the understanding of the mechanisms that control organo-mineral stability and so enhancing the resolution of the earth systems models (Bailey, Pries and Lajtha, 2019). However, destabilisation of organo-minerals depends upon many factors more than just OC chemistry, such as the environmental factors of redox conditions and temperature (Giardina and Ryan, 2000; Luo *et al.*, 2017; Haddix *et al.*, 2020; Inagaki *et al.*, 2020; Possinger, Bailey, *et al.*, 2020). This highlights that with the onset of a changing climate, there is still so much uncertainty within the climate feedback that can impact organo-mineral destabilisation. Therefore, climate resilience of organo-mineral OC could be investigated further, which will in turn feed into more accurate climate models (Bradford *et al.*, 2016).

Although the mechanisms controlling organo-mineral stability are still not fully resolved (Bailey, Pries and Lajtha, 2019; Buckeridge, Creamer and Whitaker, 2022), future research should focus upon developing land management strategies that apply the knowledge of organo-mineral stability into real world solutions. This could include field experiments investigating the long term success of compost soil amendments and no-till farming practices on increasing organo-mineral stability, MAOM persistence and overall SOC stocks, as previously suggested (see section 5.5). This could lead to

tangible efforts in utilising soil as a nature based CDR technology to aid the 4 per mille soil carbon sequestration target (Minasny *et al.*, 2017), with greater confidence in its long-term sequestration.

References

Afsar, M.Z. *et al.* (2023) 'Redox oscillations destabilize and mobilize colloidal soil organic carbon', *Science of The Total Environment*, 864, p. 161153. Available at: https://doi.org/10.1016/j.scitotenv.2022.161153.

Aggarwal, V. *et al.* (2006) 'Enhanced Sorption of Trichloroethene by Smectite Clay Exchanged with Cs+', *Environmental Science & Technology*, 40(3), pp. 894–899. Available at: https://doi.org/10.1021/es0500411.

Angst, G. *et al.* (2023) 'Unlocking complex soil systems as carbon sinks: multi-pool management as the key', *Nature Communications*, 14(1), p. 2967. Available at: https://doi.org/10.1038/s41467-023-38700-5.

Bailey, V.L., Pries, C.H. and Lajtha, K. (2019) 'What do we know about soil carbon destabilization?', *Environmental Research Letters*, 14(8), p. 083004. Available at: https://doi.org/10.1088/1748-9326/ab2c11.

Barnard, R.L., Blazewicz, S.J. and Firestone, M.K. (2020) 'Rewetting of soil: Revisiting the origin of soil CO2 emissions', *Soil Biology and Biochemistry*, 147, p. 107819. Available at: https://doi.org/10.1016/j.soilbio.2020.107819.

Bergaya, F., Theng, B.K.G. and Lagaly, G. (2006) *Handbook of Clay Science*. Elsevier.

Bernard, L. *et al.* (2022) 'Advancing the mechanistic understanding of the priming effect on soil organic matter mineralisation', *Functional Ecology*, 36(6), pp. 1355–1377. Available at: https://doi.org/10.1111/1365-2435.14038.

Bhattacharyya, A. *et al.* (2018) 'Redox Fluctuations Control the Coupled Cycling of Iron and Carbon in Tropical Forest Soils', *Environmental Science & Technology*, 52(24), pp. 14129–14139. Available at: https://doi.org/10.1021/acs.est.8b03408.

Blanco-Canqui, H. and Lal, R. (2008) 'No-Tillage and Soil-Profile Carbon Sequestration: An On-Farm Assessment', *Soil Science Society of America Journal*, 72(3), pp. 693–701. Available at: https://doi.org/10.2136/sssaj2007.0233.

Bosatta, E. and Ågren, G.I. (1999) 'Soil organic matter quality interpreted thermodynamically', *Soil Biology and Biochemistry*, 31(13), pp. 1889–1891. Available at: https://doi.org/10.1016/S0038-0717(99)00105-4.

Bradbury, M.H. and Baeyens, B. (1999) 'Modelling the sorption of Zn and Ni on Ca-montmorillonite', *Geochimica et Cosmochimica Acta*, 63(3), pp. 325–336. Available at: https://doi.org/10.1016/S0016-7037(98)00281-6.

Bradford, M.A. *et al.* (2016) 'Managing uncertainty in soil carbon feedbacks to climate change', *Nature Climate Change*, 6(8), pp. 751–758. Available at: https://doi.org/10.1038/nclimate3071.

Brown, R.W. *et al.* (2024) 'Agronomic amendments drive a diversity of real and apparent priming responses within a grassland soil', *Soil Biology and Biochemistry*, 189, p. 109265. Available at: https://doi.org/10.1016/j.soilbio.2023.109265.

Buckeridge, K.M., Mason, K.E., *et al.* (2020) 'Environmental and microbial controls on microbial necromass recycling, an important precursor for soil carbon stabilization', *Communications Earth & Environment*, 1(1), pp. 1–9. Available at: https://doi.org/10.1038/s43247-020-00031-4.

Buckeridge, K.M., La Rosa, A.F., *et al.* (2020) 'Sticky dead microbes: Rapid abiotic retention of microbial necromass in soil', *Soil Biology and Biochemistry*, 149, p. 107929. Available at: https://doi.org/10.1016/j.soilbio.2020.107929.

Buckeridge, K.M., Creamer, C. and Whitaker, J. (2022) 'Deconstructing the microbial necromass continuum to inform soil carbon sequestration', *Functional Ecology*, n/a(n/a). Available at: https://doi.org/10.1111/1365-2435.14014.

Camenzind, T. *et al.* (2023) 'Formation of necromass-derived soil organic carbon determined by microbial death pathways', *Nature Geoscience*, 16(2), pp. 115–122. Available at: https://doi.org/10.1038/s41561-022-01100-3.

Catrouillet, C. *et al.* (2014) 'Geochemical modeling of Fe(II) binding to humic and fulvic acids', *Chemical Geology*, 372, pp. 109–118. Available at: https://doi.org/10.1016/j.chemgeo.2014.02.019.

Chan, C.S. *et al.* (2009) 'Iron oxyhydroxide mineralization on microbial extracellular polysaccharides', *Geochimica et Cosmochimica Acta*, 73(13), pp. 3807–3818. Available at: https://doi.org/10.1016/j.gca.2009.02.036.

Chen, C. *et al.* (2014) 'Properties of Fe-Organic Matter Associations via Coprecipitation versus Adsorption', *Environmental Science & Technology*, 48(23), pp. 13751–13759. Available at: https://doi.org/10.1021/es503669u.

Chen, C. *et al.* (2020) 'Iron-mediated organic matter decomposition in humid soils can counteract protection', *Nature Communications*, 11(1), p. 2255. Available at: https://doi.org/10.1038/s41467-020-16071-5.

Chen, C., Dong, Y. and Thompson, A. (2023) 'Electron Transfer, Atom Exchange, and Transformation of Iron Minerals in Soils: The Influence of Soil Organic Matter', *Environmental Science & Technology*, 57(29), pp. 10696–10707. Available at: https://doi.org/10.1021/acs.est.3c01876.

Chen, C., Kukkadapu, R. and Sparks, D.L. (2015) 'Influence of Coprecipitated Organic Matter on Fe2+(aq)-Catalyzed Transformation of Ferrihydrite: Implications for Carbon Dynamics', *Environmental Science & Technology*, 49(18), pp. 10927–10936. Available at: https://doi.org/10.1021/acs.est.5b02448.

Chen, C.-L., Chang ,Hou-Min and and Kirk, T.K. (1983) 'Carboxylic Acids Produced Through Oxidative Cleavage of Aromatic Rings During Degradation of Lignin in Spruce Wood by Phanerochaete

Chrysosporium', *Journal of Wood Chemistry and Technology*, 3(1), pp. 35–57. Available at: https://doi.org/10.1080/02773818308085150.

Chenu, C. *et al.* (2019) 'Increasing organic stocks in agricultural soils: Knowledge gaps and potential innovations', *Soil and Tillage Research*, 188, pp. 41–52. Available at: https://doi.org/10.1016/j.still.2018.04.011.

Colombo, C. *et al.* (2014) 'Review on iron availability in soil: interaction of Fe minerals, plants, and microbes', *Journal of Soils and Sediments*, 14(3), pp. 538–548. Available at: https://doi.org/10.1007/s11368-013-0814-z.

Cornell, R.M. and Schwertmann, U. (2003) 'Formation', in *The Iron Oxides: Structure, Properties, Reactions, Occurences and Uses*. Wiley, pp. 345–364.

Cotrufo, M.F. *et al.* (2013) 'The Microbial Efficiency-Matrix Stabilization (MEMS) framework integrates plant litter decomposition with soil organic matter stabilization: do labile plant inputs form stable soil organic matter?', *Global Change Biology*, 19(4), pp. 988–995. Available at: https://doi.org/10.1111/gcb.12113.

Cotrufo, M.F. *et al.* (2019) 'Soil carbon storage informed by particulate and mineral-associated organic matter', *Nature Geoscience*, (12), pp. 989–994.

Cotrufo, M.F. and Lavallee, J.M. (2022) 'Chapter One - Soil organic matter formation, persistence, and functioning: A synthesis of current understanding to inform its conservation and regeneration', in D.L. Sparks (ed.) *Advances in Agronomy*. Academic Press, pp. 1–66. Available at: https://doi.org/10.1016/bs.agron.2021.11.002.

Cotrufo, M.F. and Pressler, Y. (2023) *A Primer on Stable Isotopes in Ecology*. Oxford University Press.

Coward, E.K., Ohno, T. and Sparks, D.L. (2019) 'Direct Evidence for Temporal Molecular Fractionation of Dissolved Organic Matter at the Iron Oxyhydroxide Interface', *Environmental Science & Technology*, 53(2), pp. 642–650. Available at: https://doi.org/10.1021/acs.est.8b04687.

Crow, S.E. *et al.* (2007) 'Density fractionation of forest soils: methodological questions and interpretation of incubation results and turnover time in an ecosystem context', *Biogeochemistry*, 85(1), pp. 69–90. Available at: https://doi.org/10.1007/s10533-007-9100-8.

Curti, L. *et al.* (2021) 'Carboxyl-richness controls organic carbon preservation during coprecipitation with iron (oxyhydr)oxides in the natural environment', *Communications Earth & Environment*, 2(1), p. 229. Available at: https://doi.org/10.1038/s43247-021-00301-9.

Das, S., Hendry, M.J. and Essilfie-Dughan, J. (2011) 'Transformation of Two-Line Ferrihydrite to Goethite and Hematite as a Function of pH and Temperature', *Environmental Science & Technology*, 45(1), pp. 268–275. Available at: https://doi.org/10.1021/es101903y.

DeAngelis, K.M. *et al.* (2010) 'Microbial communities acclimate to recurring changes in soil redox potential status', *Environmental Microbiology*, 12(12), pp. 3137–3149. Available at: https://doi.org/10.1111/j.1462-2920.2010.02286.x.

Deng, F. and Liang, C. (2022) 'Revisiting the quantitative contribution of microbial necromass to soil carbon pool: Stoichiometric control by microbes and soil', *Soil Biology and Biochemistry*, 165, p. 108486. Available at: https://doi.org/10.1016/j.soilbio.2021.108486.

Di Lonardo, D.P. *et al.* (2020) 'Effect of nitrogen on fungal growth efficiency', *Plant Biosystems - An International Journal Dealing with all Aspects of Plant Biology*, 154(4), pp. 433–437. Available at: https://doi.org/10.1080/11263504.2020.1779849.

Domnariu, H. *et al.* (2025) 'Long-term impact of tillage on microbial communities of an Eastern European Chernozem', *Scientific Reports*, 15(1), p. 642. Available at: https://doi.org/10.1038/s41598-024-84590-y.

Duarte-Guardia, S. *et al.* (2020) 'Biophysical and socioeconomic factors influencing soil carbon stocks: a global assessment', *Mitigation and Adaptation Strategies for Global Change*, 25(6), pp. 1129–1148. Available at: https://doi.org/10.1007/s11027-020-09926-1.

Dynarski, K.A., Bossio, D.A. and Scow, K.M. (2020) 'Dynamic Stability of Soil Carbon: Reassessing the "Permanence" of Soil Carbon Sequestration', *Frontiers in Environmental Science*, 8. Available at: https://doi.org/10.3389/fenvs.2020.514701.

Elias, D.M.O. *et al.* (2024) 'Microbial and mineral interactions decouple litter quality from soil organic matter formation', *Nature Communications*, 15(1), p. 10063. Available at: https://doi.org/10.1038/s41467-024-54446-0.

Evans, S.E. and Wallenstein, M.D. (2012) 'Soil microbial community response to drying and rewetting stress: does historical precipitation regime matter?', *Biogeochemistry*, 109(1), pp. 101–116. Available at: https://doi.org/10.1007/s10533-011-9638-3.

Fawzy, S. *et al.* (2020) 'Strategies for mitigation of climate change: a review', *Environmental Chemistry Letters*, 18(6), pp. 2069–2094. Available at: https://doi.org/10.1007/s10311-020-01059-w.

Feng, W. *et al.* (2014) 'Soil organic matter stability in organo-mineral complexes as a function of increasing C loading', *Soil Biology and Biochemistry*, 69, pp. 398–405. Available at: https://doi.org/10.1016/j.soilbio.2013.11.024.

Fuss, S. *et al.* (2018) 'Negative emissions—Part 2: Costs, potentials and side effects', *Environmental Research Letters*, 13(6), p. 063002. Available at: https://doi.org/10.1088/1748-9326/aabf9f.

Gao, J. *et al.* (2018) 'Organic matter coatings of soil minerals affect adsorptive interactions with phenolic and amino acids', *European Journal of Soil Science*, 69(4), pp. 613–624. Available at: https://doi.org/10.1111/ejss.12562.

Gao, J. *et al.* (2020) 'The multilayer model of soil mineral–organic interfaces—a review', *Journal of Plant Nutrition and Soil Science*, 183(1), pp. 27–41. Available at: https://doi.org/10.1002/jpln.201900530.

Gao, M., Li, H. and Li, M. (2022) 'Effect of No Tillage System on Soil Fungal Community Structure of Cropland in Mollisol: A Case Study', *Frontiers in Microbiology*, 13, p. 847691. Available at: https://doi.org/10.3389/fmicb.2022.847691.

Garcia-Rubio, R. *et al.* (2020) 'The Fungal Cell Wall: Candida, Cryptococcus, and Aspergillus Species', *Frontiers in Microbiology*, 10. Available at: https://www.frontiersin.org/article/10.3389/fmicb.2019.02993 (Accessed: 23 March 2022).

Georgiou, K. *et al.* (2022) 'Global stocks and capacity of mineral-associated soil organic carbon', *Nature Communications*, 13(1), p. 3797. Available at: https://doi.org/10.1038/s41467-022-31540-9.

Giardina, C.P. and Ryan, M.G. (2000) 'Evidence that decomposition rates of organic carbon in mineral soil do not vary with temperature', *Nature*, 404(6780), pp. 858–861. Available at: https://doi.org/10.1038/35009076.

Goodall, T. and Griffiths, R. (In progress) 'Biotic destabilisation of organo-mineral OC in home and away soil pH conditions'.

Gooday, G.W. (1990) 'The Ecology of Chitin Degradation', in K.C. Marshall (ed.) *Advances in Microbial Ecology*. Boston, MA: Springer US, pp. 387–430. Available at: https://doi.org/10.1007/978-1-4684-7612-5_10.

Grandy, A.S. and Neff, J.C. (2008) 'Molecular C dynamics downstream: The biochemical decomposition sequence and its impact on soil organic matter structure and function', *Science of The Total Environment*, 404(2), pp. 297–307. Available at: https://doi.org/10.1016/j.scitotenv.2007.11.013.

Griffiths, P.R. (1983) 'Fourier Transform Infrared Spectrometry', *Science*, 222(4621), pp. 297–302. Available at: https://doi.org/10.1126/science.6623077.

Gunina, A. and Kuzyakov, Y. (2022) 'From energy to (soil organic) matter', *Global Change Biology*, 28(7), pp. 2169–2182. Available at: https://doi.org/10.1111/gcb.16071.

Guo, Y.X. *et al.* (2020) 'ORGANO-MODIFICATION OF MONTMORILLONITE', *Clays and Clay Minerals*, 68(6), pp. 601–622. Available at: https://doi.org/10.1007/s42860-020-00098-2.

Haddix, M.L. *et al.* (2020) 'Climate, carbon content, and soil texture control the independent formation and persistence of particulate and mineral-associated organic matter in soil', *Geoderma*, 363, p. 114160. Available at: https://doi.org/10.1016/j.geoderma.2019.114160.

Han, L. *et al.* (2019) 'Mobilization of ferrihydrite-associated organic carbon during Fe reduction: Adsorption versus coprecipitation', *Chemical Geology*, 503, pp. 61–68. Available at: https://doi.org/10.1016/j.chemgeo.2018.10.028.

Hannula, S.E. *et al.* (2017) 'Shifts in rhizosphere fungal community during secondary succession following abandonment from agriculture', *The ISME Journal*, 11(10), pp. 2294–2304. Available at: https://doi.org/10.1038/ismej.2017.90.

Hart, M.M. *et al.* (2018) 'Fungal inoculants in the field: Is the reward greater than the risk?', *Functional Ecology*, 32(1), pp. 126–135.

Hassink, J. (1997) 'The capacity of soils to preserve organic C and N by their association with clay and silt particles', *Plant and Soil*, 191(1), pp. 77–87. Available at: https://doi.org/10.1023/A:1004213929699.

Hay, M.B. and Myneni, S.C.B. (2007) 'Structural environments of carboxyl groups in natural organic molecules from terrestrial systems. Part 1: Infrared spectroscopy', *Geochimica et Cosmochimica Acta*, 71(14), pp. 3518–3532. Available at: https://doi.org/10.1016/j.gca.2007.03.038.

Heckman, K. *et al.* (2011) 'Changes in water extractable organic matter during incubation of forest floor material in the presence of quartz, goethite and gibbsite surfaces', *Geochimica et Cosmochimica Acta*, 75(15), pp. 4295–4309. Available at: https://doi.org/10.1016/j.gca.2011.05.009.

Heckman, K., Lawrence, C.R. and Harden, J.W. (2018) 'A sequential selective dissolution method to quantify storage and stability of organic carbon associated with Al and Fe hydroxide phases', *Geoderma*, 312, pp. 24–35. Available at: https://doi.org/10.1016/j.geoderma.2017.09.043.

Henneberry, Y.K. *et al.* (2012) 'Structural stability of coprecipitated natural organic matter and ferric iron under reducing conditions', *Organic Geochemistry*, 48, pp. 81–89. Available at: https://doi.org/10.1016/j.orggeochem.2012.04.005.

Hiemstra, T. (2013) 'Surface and mineral structure of ferrihydrite', *Geochimica et Cosmochimica Acta*, 105, pp. 316–325. Available at: https://doi.org/10.1016/j.gca.2012.12.002.

Hu, Y. *et al.* (2018) 'Significant release and microbial utilization of amino sugars and d-amino acid enantiomers from microbial cell wall decomposition in soils', *Soil Biology and Biochemistry*, 123, pp. 115–125. Available at: https://doi.org/10.1016/j.soilbio.2018.04.024.

Huang, P.M. and Schnitzer, M. (1986) *Interactions of Soil Minerals with Natural Organics and Microbes*. Soil Science Society of America.

Huang, W. and Hall, S.J. (2017) 'Optimized high-throughput methods for quantifying iron biogeochemical dynamics in soil', *Geoderma*, 306, pp. 67–72. Available at: https://doi.org/10.1016/j.geoderma.2017.07.013.

Inagaki, T.M. *et al.* (2020) 'Subsoil organo-mineral associations under contrasting climate conditions', *Geochimica et Cosmochimica Acta*, 270, pp. 244–263. Available at: https://doi.org/10.1016/j.gca.2019.11.030.

IPCC (2018) 'Global warming of 1.5°C. An IPCC Special Report on the impacts of global warming of 1.5°C above pre-industrial levels and related global greenhouse gas emission pathways, in the context of strengthening the global response to the threat of climate change, sustainable development, and efforts to eradicate poverty', [V. Masson-Delmotte, P. Zhai, H. O. Pörtner, D. Roberts, J. Skea, P.R. Shukla, A. Pirani, W. Moufouma-Okia, C. Péan, R. Pidcock, S. Connors, J. B. R. Matthews, Y. Chen, X. Zhou, M. I. Gomis, E. Lonnoy, T. Maycock, M. Tignor, T. Waterfield (eds.)] IPCC, Geneva, Switzerland.

IPCC (2023) 'Climate Change 2023: Synthesis Report', Contribution of Working Groups I, II and III to the Sixth Assessment Report of the Intergovernmental Panel on Climate Change [Core Writing Team, H. Lee and J. Romero (eds.)]. IPCC, Geneva, Switzerland, pp. 35–115. Available at: https://doi.org/10.59327/IPCC/AR6-9789291691647.

Ito, A. and Wagai, R. (2017) 'Global distribution of clay-size minerals on land surface for biogeochemical and climatological studies', *Scientific Data*, 4(1), p. 170103. Available at: https://doi.org/10.1038/sdata.2017.103.

Jackson, R.B. *et al.* (2017) 'The Ecology of Soil Carbon: Pools, Vulnerabilities, and Biotic and Abiotic Controls', *Annual Review of Ecology, Evolution, and Systematics*, 48(Volume 48, 2017), pp. 419–445. Available at: https://doi.org/10.1146/annurev-ecolsys-112414-054234.

Janusz, G. *et al.* (2017) 'Lignin degradation: microorganisms, enzymes involved, genomes analysis and evolution', *FEMS Microbiology Reviews*, 41(6), pp. 941–962. Available at: https://doi.org/10.1093/femsre/fux049.

Jastrow, J.D., Amonette, J.E. and Bailey, V.L. (2007) 'Mechanisms controlling soil carbon turnover and their potential application for enhancing carbon sequestration', *Climatic Change*, 80(1), pp. 5–23. Available at: https://doi.org/10.1007/s10584-006-9178-3.

Jia, N. *et al.* (2024) 'Important role of Fe oxides in global soil carbon stabilization and stocks', *Nature Communications*, 15(1), p. 10318. Available at: https://doi.org/10.1038/s41467-024-54832-8.

Jiang, W.-X. *et al.* (2022) 'A pathway for chitin oxidation in marine bacteria', *Nature Communications*, 13(1), p. 5899. Available at: https://doi.org/10.1038/s41467-022-33566-5.

Jilling, A. *et al.* (2018) 'Minerals in the rhizosphere: overlooked mediators of soil nitrogen availability to plants and microbes', *Biogeochemistry*, 139(2), pp. 103–122. Available at: https://doi.org/10.1007/s10533-018-0459-5.

Jilling, A. *et al.* (2020) 'Rapid and distinct responses of particulate and mineral-associated organic nitrogen to conservation tillage and cover crops', *Geoderma*, 359, p. 114001.

Jilling, A. *et al.* (2021) 'Priming mechanisms providing plants and microbes access to mineral-associated organic matter', *Soil Biology and Biochemistry*, 158, p. 108265. Available at: https://doi.org/10.1016/j.soilbio.2021.108265.

Jones, A.M. *et al.* (2009) 'The effect of silica and natural organic matter on the Fe(II)-catalysed transformation and reactivity of Fe(III) minerals', *Geochimica et Cosmochimica Acta*, 73(15), pp. 4409–4422. Available at: https://doi.org/10.1016/j.gca.2009.04.025.

Just, C. *et al.* (2023) 'Soil organic carbon sequestration in agricultural long-term field experiments as derived from particulate and mineral-associated organic matter', *Geoderma*, 434, p. 116472. Available at: https://doi.org/10.1016/j.geoderma.2023.116472.

Kaiser, K. and Guggenberger, G. (2000) 'The role of DOM sorption to mineral surfaces in the preservation of organic matter in soils', *Organic Geochemistry*, 31(7), pp. 711–725. Available at: https://doi.org/10.1016/S0146-6380(00)00046-2.

Kaiser, K. and Guggenberger, G. (2003) 'Mineral surfaces and soil organic matter', *European Journal of Soil Science*, 54(2), pp. 219–236. Available at: https://doi.org/10.1046/j.1365-2389.2003.00544.x.

Kaiser, K. and Guggenberger, G. (2007) 'Sorptive stabilization of organic matter by microporous goethite: sorption into small pores vs. surface complexation', *European Journal of Soil Science*, 58(1), pp. 45–59. Available at: https://doi.org/10.1111/j.1365-2389.2006.00799.x.

Kato, S., Hashimoto, K. and Watanabe, K. (2013) 'Iron-Oxide Minerals Affect Extracellular Electron-Transfer Paths of Geobacter spp.', *Microbes and Environments*, 28(1), pp. 141–148. Available at: https://doi.org/10.1264/jsme2.ME12161.

Keiluweit, M. *et al.* (2015) 'Mineral protection of soil carbon counteracted by root exudates', *Nature Climate Change*, 5(6), pp. 588–595. Available at: https://doi.org/10.1038/nclimate2580.

Keiluweit, M. *et al.* (2017) 'Anaerobic microsites have an unaccounted role in soil carbon stabilization', *Nature Communications*, 8(1), p. 1771. Available at: https://doi.org/10.1038/s41467-017-01406-6.

Keiluweit, M. *et al.* (2022) *Multi-Scale Biogeochemical Processes in Soil Ecosystems: Critical Reactions and Resilience to Climate Changes*. Newark, UNITED STATES: John Wiley & Sons, Incorporated. Available at: http://ebookcentral.proquest.com/lib/lancaster/detail.action?docID=6939770 (Accessed: 6 January 2023).

Kirsten, M. *et al.* (2021) 'Iron oxides and aluminous clays selectively control soil carbon storage and stability in the humid tropics', *Scientific Reports*, 11(5076). Available at: https://www.nature.com/articles/s41598-021-84777-7 (Accessed: 24 November 2024).

Kleber, M. *et al.* (2015) 'Chapter One - Mineral–Organic Associations: Formation, Properties, and Relevance in Soil Environments', in D.L. Sparks (ed.) *Advances in Agronomy*. Academic Press, pp. 1–140. Available at: https://doi.org/10.1016/bs.agron.2014.10.005.

Kleber, M. *et al.* (2021) 'Dynamic interactions at the mineral–organic matter interface', *Nature Reviews Earth & Environment*, 2(6), pp. 402–421. Available at: https://doi.org/10.1038/s43017-021-00162-y.

Kleber, M., Sollins, P. and Sutton, R. (2007) 'A conceptual model of organo-mineral interactions in soils: self-assembly of organic molecular fragments into zonal structures on mineral surfaces', *Biogeochemistry*, 85(1), pp. 9–24. Available at: https://doi.org/10.1007/s10533-007-9103-5.

Klein, D.R. (2020) *Organic chemistry*. John Wiley & Sons.

Klink, S. *et al.* (2022) 'Stable isotopes reveal that fungal residues contribute more to mineral-associated organic matter pools than plant residues', *Soil Biology and Biochemistry*, 168, p. 108634. Available at: https://doi.org/10.1016/j.soilbio.2022.108634.

Klotzbücher, T. *et al.* (2011) 'A new conceptual model for the fate of lignin in decomposing plant litter', *Ecology*, 92(5), pp. 1052–1062. Available at: https://doi.org/10.1890/10-1307.1.

Kögel-Knabner, I. (2002) 'The macromolecular organic composition of plant and microbial residues as inputs to soil organic matter', *Soil Biology and Biochemistry*, 34(2), pp. 139–162. Available at: https://doi.org/10.1016/S0038-0717(01)00158-4.

Kögel-Knabner, I. *et al.* (2008) 'Organo-mineral associations in temperate soils: Integrating biology, mineralogy, and organic matter chemistry', *Journal of Plant Nutrition and Soil Science*, 171(1), pp. 61–82. Available at: https://doi.org/10.1002/jpln.200700048.

Kopittke, P.M. *et al.* (2018) 'Nitrogen-rich microbial products provide new organo-mineral associations for the stabilization of soil organic matter', *Global Change Biology*, 24(4), pp. 1762–1770. Available at: https://doi.org/10.1111/gcb.14009.

Kopittke, P.M. *et al.* (2020) 'Soil organic matter is stabilized by organo-mineral associations through two key processes: The role of the carbon to nitrogen ratio', *Geoderma*, 357, p. 113974. Available at: https://doi.org/10.1016/j.geoderma.2019.113974.

Kramer, M.G. and Chadwick, O.A. (2018) 'Climate-driven thresholds in reactive mineral retention of soil carbon at the global scale', *Nature Climate Change*, 8(12), pp. 1104–1108. Available at: https://doi.org/10.1038/s41558-018-0341-4.

Lal, R., Negassa, W. and Lorenz, K. (2015) 'Carbon sequestration in soil', *Current Opinion in Environmental Sustainability*, 15, pp. 79–86. Available at: https://doi.org/10.1016/j.cosust.2015.09.002.

LaRowe, D.E. and Van Cappellen, P. (2011) 'Degradation of natural organic matter: A thermodynamic analysis', *Geochimica et Cosmochimica Acta*, 75(8), pp. 2030–2042. Available at: https://doi.org/10.1016/j.gca.2011.01.020.

Larsen, O. and Postma, D. (2001) 'Kinetics of reductive bulk dissolution of lepidocrocite, ferrihydrite, and goethite', *Geochimica et Cosmochimica Acta*, 65(9), pp. 1367–1379. Available at: https://doi.org/10.1016/S0016-7037(00)00623-2.

Lavallee, J.M., Soong, J.L. and Cotrufo, M.F. (2020) 'Conceptualizing soil organic matter into particulate and mineral-associated forms to address global change in the 21st century', *Global Change Biology*, 26(1), pp. 261–273. Available at: https://doi.org/10.1111/gcb.14859.

Lecomte, S.M. *et al.* (2018) 'Diversifying Anaerobic Respiration Strategies to Compete in the Rhizosphere', *Frontiers in Environmental Science*, 6. Available at: https://doi.org/10.3389/fenvs.2018.00139.

Lehmann, J. *et al.* (2008) 'Spatial complexity of soil organic matter forms at nanometre scales', *Nature Geoscience*, 1(4), pp. 238–242. Available at: https://doi.org/10.1038/ngeo155.

Lehmann, J. *et al.* (2020) 'Persistence of soil organic carbon caused by functional complexity', *Nature Geoscience*, 13(8), pp. 529–534. Available at: https://doi.org/10.1038/s41561-020-0612-3.

Lehmann, J., Kinyangi, J. and Solomon, D. (2007) 'Organic matter stabilization in soil microaggregates: implications from spatial heterogeneity of organic carbon contents and carbon forms', *Biogeochemistry*, 85(1), pp. 45–57. Available at: https://doi.org/10.1007/s10533-007-9105-3.

Lehmann, J. and Kleber, M. (2015) 'The contentious nature of soil organic matter', *Nature*, 528(7580), pp. 60–68. Available at: https://doi.org/10.1038/nature16069.

Li, H. *et al.* (2021) 'Simple Plant and Microbial Exudates Destabilize Mineral-Associated Organic Matter via Multiple Pathways', *Environmental Science & Technology*, 55(5), pp. 3389–3398. Available at: https://doi.org/10.1021/acs.est.0c04592.

Liang, C. *et al.* (2019) 'Quantitative assessment of microbial necromass contribution to soil organic matter', *Global Change Biology*, 25(11), pp. 3578–3590. Available at: https://doi.org/10.1111/gcb.14781.

Liang, C. (2020) ‘Soil microbial carbon pump: Mechanism and appraisal’, *Soil Ecology Letters*, 2(4), pp. 241–254. Available at: https://doi.org/10.1007/s42832-020-0052-4.

Liang, C., Schimel, J.P. and Jastrow, J.D. (2017) ‘The importance of anabolism in microbial control over soil carbon storage’, *Nature Microbiology*, 2(8), pp. 1–6. Available at: https://doi.org/10.1038/nmicrobiol.2017.105.

Lipson, D.A. *et al.* (2010) ‘Reduction of iron (III) and humic substances plays a major role in anaerobic respiration in an Arctic peat soil’, *Journal of Geophysical Research: Biogeosciences*, 115(G4). Available at: https://doi.org/10.1029/2009JG001147.

Lopez-Sangil, L. and Rovira, P. (2013) ‘Sequential chemical extractions of the mineral-associated soil organic matter: An integrated approach for the fractionation of organo-mineral complexes’, *Soil Biology and Biochemistry*, 62, pp. 57–67. Available at: https://doi.org/10.1016/j.soilbio.2013.03.004.

Luo, Y. *et al.* (2016) ‘Toward more realistic projections of soil carbon dynamics by Earth system models’, *Global Biogeochemical Cycles*, 30(1), pp. 40–56. Available at: https://doi.org/10.1002/2015GB005239.

Luo, Z. *et al.* (2017) ‘Soil organic carbon dynamics jointly controlled by climate, carbon inputs, soil properties and soil carbon fractions’, *Global Change Biology*, 23(10), pp. 4430–4439. Available at: https://doi.org/10.1111/gcb.13767.

Maddison, A.L. *et al.* (2017) ‘Predicting future biomass yield in Miscanthus using the carbohydrate metabolic profile as a biomarker’, *GCB Bioenergy*, 9(7), pp. 1264–1278. Available at: https://doi.org/10.1111/gcbb.12418.

Mander, Ü. *et al.* (2024) ‘Peatland restoration pathways to mitigate greenhouse gas emissions and retain peat carbon’, *Biogeochemistry*, 167(4), pp. 523–543. Available at: https://doi.org/10.1007/s10533-023-01103-1.

Manzoni, S. *et al.* (2012) 'Environmental and stoichiometric controls on microbial carbon-use efficiency in soils', *New Phytologist*, 196(1), pp. 79–91. Available at: https://doi.org/10.1111/j.1469-8137.2012.04225.x.

Marschner, B. *et al.* (2008) 'How relevant is recalcitrance for the stabilization of organic matter in soils?', *Journal of Plant Nutrition and Soil Science*, 171(1), pp. 91–110. Available at: https://doi.org/10.1002/jpln.200700049.

McFarland, J.W. *et al.* (2019) 'Biological and mineralogical controls over cycling of low molecular weight organic compounds along a soil chronosequence', *Soil Biology and Biochemistry*, 133, pp. 16–27. Available at: https://doi.org/10.1016/j.soilbio.2019.01.013.

McFarlane, K.J. *et al.* (2013) 'Comparison of soil organic matter dynamics at five temperate deciduous forests with physical fractionation and radiocarbon measurements', *Biogeochemistry*, 112(1), pp. 457–476. Available at: https://doi.org/10.1007/s10533-012-9740-1.

McNamara, N.P., Mason, K.E. and Oakley, S. (Manuscript in preparation) 'Flooded Fungi'.

Merino, C. *et al.* (2021) 'Iron-reducing bacteria decompose lignin by electron transfer from soil organic matter', *Science of The Total Environment*, 761, p. 143194. Available at: https://doi.org/10.1016/j.scitotenv.2020.143194.

Mikutta, R. *et al.* (2005) 'Review', *Soil Science Society of America Journal*, 69(1), pp. 120–135. Available at: https://doi.org/10.2136/sssaj2005.0120.

Mikutta, R. *et al.* (2006) 'Stabilization of Soil Organic Matter: Association with Minerals or Chemical Recalcitrance?', *Biogeochemistry*, 77(1), pp. 25–56. Available at: https://doi.org/10.1007/s10533-005-0712-6.

Mikutta, R. *et al.* (2007) 'Biodegradation of forest floor organic matter bound to minerals via different binding mechanisms', *Geochimica et Cosmochimica Acta*, 71(10), pp. 2569–2590. Available at: https://doi.org/10.1016/j.gca.2007.03.002.

Mikutta, R. *et al.* (2019) 'Microbial and abiotic controls on mineral-associated organic matter in soil profiles along an ecosystem gradient', *Scientific Reports*, 9(1), p. 10294. Available at: https://doi.org/10.1038/s41598-019-46501-4.

Mikutta, R. and Kaiser, K. (2011) 'Organic matter bound to mineral surfaces: Resistance to chemical and biological oxidation', *Soil Biology and Biochemistry*, 43(8), pp. 1738–1741. Available at: https://doi.org/10.1016/j.soilbio.2011.04.012.

Minasny, B. *et al.* (2017) 'Soil carbon 4 per mille', *Geoderma*, 292, pp. 59–86. Available at: https://doi.org/10.1016/j.geoderma.2017.01.002.

Minx, J.C. *et al.* (2018) 'Negative emissions—Part 1: Research landscape and synthesis', *Environmental Research Letters*, 13(6), p. 063001. Available at: https://doi.org/10.1088/1748-9326/aabf9b.

Mobaraki, N. and Hemmateenejad, B. (2011) 'Structural characterization of carbonyl compounds by IR spectroscopy and chemometrics data analysis', *Chemometrics and Intelligent Laboratory Systems*, 109(2), pp. 171–177. Available at: https://doi.org/10.1016/j.chemolab.2011.08.011.

Morel, F.M. and Herring, J.G. (1993) *Principles and applications of aquatic chemistry*. John Wiley & Sons, Incorporated.

Murray, H.H. (2006) 'Structure and Composition of the Clay Minerals and their Physical and Chemical Properties', in *Applied Clay Mineralogy: Occurrences, Processing and Applications of Kaolins, Bentonites, Palygorskitesepiolite, and Common Clays*. Elsevier, pp. 7–32.

Nemet, G.F. *et al.* (2018) 'Negative emissions—Part 3: Innovation and upscaling', *Environmental Research Letters*, 13(6), p. 063003. Available at: https://doi.org/10.1088/1748-9326/aabff4.

Newcomb, C.J. *et al.* (2017) 'Developing a molecular picture of soil organic matter–mineral interactions by quantifying organo–mineral binding', *Nature Communications*, 8(1), p. 396. Available at: https://doi.org/10.1038/s41467-017-00407-9.

NOAA (2024) *Trends in CO2 - NOAA Global Monitoring Laboratory*. Available at: https://gml.noaa.gov/ccgg/trends/index.html (Accessed: 28 December 2024).

Oldfield, E.E., Wood, S.A. and Bradford, M.A. (2020) 'Direct evidence using a controlled greenhouse study for threshold effects of soil organic matter on crop growth', *Ecological Applications*, 30(4), p. e02073. Available at: https://doi.org/10.1002/eap.2073.

Parada, J. *et al.* (2024) 'Management and liming-induced changes in organo-Al/Fe complexes and amorphous mineral-associated organic carbon: Implications for carbon sequestration in volcanic soils', *Soil and Tillage Research*, 242, p. 106133. Available at: https://doi.org/10.1016/j.still.2024.106133.

Pedersen, H.D. *et al.* (2005) 'Fast transformation of iron oxyhydroxides by the catalytic action of aqueous Fe(II)', *Geochimica et Cosmochimica Acta*, 69(16), pp. 3967–3977. Available at: https://doi.org/10.1016/j.gca.2005.03.016.

Possinger, A.R., Bailey, S.W., *et al.* (2020) 'Organo-mineral interactions and soil carbon mineralizability with variable saturation cycle frequency', *Geoderma*, 375, p. 114483. Available at: https://doi.org/10.1016/j.geoderma.2020.114483.

Possinger, A.R., Zachman, M.J., *et al.* (2020) 'Organo–organic and organo–mineral interfaces in soil at the nanometer scale', *Nature Communications*, 11(1), p. 6103. Available at: https://doi.org/10.1038/s41467-020-19792-9.

Puissant, J. *et al.* (2017) 'Climate change effects on the stability and chemistry of soil organic carbon pools in a subalpine grassland', *Biogeochemistry*, 132(1), pp. 123–139. Available at: https://doi.org/10.1007/s10533-016-0291-8.

Rasmussen, C. *et al.* (2018) 'Beyond clay: towards an improved set of variables for predicting soil organic matter content', *Biogeochemistry*, 137(3), pp. 297–306. Available at: https://doi.org/10.1007/s10533-018-0424-3.

Reddy, T.R. *et al.* (2015) 'The effect of pH on stable iron isotope exchange and fractionation between aqueous Fe(II) and goethite', *Chemical Geology*, 397, pp. 118–127. Available at: https://doi.org/10.1016/j.chemgeo.2015.01.018.

dos Reis Ferreira, C. *et al.* (2020) 'Dynamics of soil aggregation and organic carbon fractions over 23 years of no-till management', *Soil and Tillage Research*, 198, p. 104533.

Rinnan, Å., Berg, F. van den and Engelsen, S.B. (2009) 'Review of the most common pre-processing techniques for near-infrared spectra', *TrAC Trends in Analytical Chemistry*, 28(10), pp. 1201–1222. Available at: https://doi.org/10.1016/j.trac.2009.07.007.

Roth, V.-N. *et al.* (2019) 'Persistence of dissolved organic matter explained by molecular changes during its passage through soil', *Nature Geoscience*, 12(9), pp. 755–761. Available at: https://doi.org/10.1038/s41561-019-0417-4.

Saidy, A.R. *et al.* (2013) 'The sorption of organic carbon onto differing clay minerals in the presence and absence of hydrous iron oxide', *Geoderma*, 209–210, pp. 15–21. Available at: https://doi.org/10.1016/j.geoderma.2013.05.026.

Schimel, J. and Schaeffer, S.M. (2012) 'Microbial control over carbon cycling in soil', *Frontiers in Microbiology*, 3. Available at: https://doi.org/10.3389/fmicb.2012.00348.

Schmidt, M.W.I. *et al.* (2011) 'Persistence of soil organic matter as an ecosystem property', *Nature*, 478(7367), pp. 49–56. Available at: https://doi.org/10.1038/nature10386.

Schweizer, S.A. (2022) 'Perspectives from the Fritz-Scheffer Awardee 2021: Soil organic matter storage and functions determined by patchy and piled-up arrangements at the microscale', *Journal of Plant Nutrition and Soil Science*, 185(6), pp. 694–706. Available at: https://doi.org/10.1002/jpln.202200217.

Schwertmann, U. and Cornell, R.M. (2008) *Iron Oxides in the Laboratory: Preparation and Characterization*. John Wiley & Sons.

Shi, S. *et al.* (2011) 'Effects of selected root exudate components on soil bacterial communities', *FEMS Microbiology Ecology*, 77(3), pp. 600–610. Available at: https://doi.org/10.1111/j.1574-6941.2011.01150.x.

Simpson, A.J. *et al.* (2007) 'Microbially Derived Inputs to Soil Organic Matter: Are Current Estimates Too Low?', *Environmental Science & Technology*, 41(23), pp. 8070–8076. Available at: https://doi.org/10.1021/es071217x.

Singh, M. *et al.* (2018) 'Chapter Two - Stabilization of Soil Organic Carbon as Influenced by Clay Mineralogy', in D.L. Sparks (ed.) *Advances in Agronomy*. Academic Press, pp. 33–84. Available at: https://doi.org/10.1016/bs.agron.2017.11.001.

Siregar, A. *et al.* (2005) 'Sodium hypochlorite oxidation reduces soil organic matter concentrations without affecting inorganic soil constituents', *European Journal of Soil Science*, 56(4), pp. 481–490. Available at: https://doi.org/10.1111/j.1365-2389.2004.00680.x.

Six, J., Elliott, E.T. and Paustian, K. (2000) 'Soil macroaggregate turnover and microaggregate formation: a mechanism for C sequestration under no-tillage agriculture', *Soil Biology and Biochemistry*, 32(14), pp. 2099–2103. Available at: https://doi.org/10.1016/S0038-0717(00)00179-6.

Smith, B. (2011) *Fundamentals of Fourier Transform Infrared Spectroscopy*. CRC press.

Sokol, N.W. *et al.* (2022) 'Global distribution, formation and fate of mineral-associated soil organic matter under a changing climate: A trait-based perspective', *Functional Ecology*, 36(6), pp. 1411–1429. Available at: https://doi.org/10.1111/1365-2435.14040.

Sollins, P. *et al.* (2006) 'Organic C and N stabilization in a forest soil: Evidence from sequential density fractionation', *Soil Biology and Biochemistry*, 38(11), pp. 3313–3324. Available at: https://doi.org/10.1016/j.soilbio.2006.04.014.

Sollins, P. *et al.* (2009) 'Sequential density fractionation across soils of contrasting mineralogy: evidence for both microbial- and mineral-controlled soil organic matter stabilization', *Biogeochemistry*, 96(1), pp. 209–231. Available at: https://doi.org/10.1007/s10533-009-9359-z.

Song, X. *et al.* (2022) 'Towards a better understanding of the role of Fe cycling in soil for carbon stabilization and degradation', *Carbon Research*, 1(1), p. 5. Available at: https://doi.org/10.1007/s44246-022-00008-2.

Spaccini, R. and Piccolo, A. (2007) 'Molecular Characterization of Compost at Increasing Stages of Maturity. 1. Chemical Fractionation and Infrared Spectroscopy', *Journal of Agricultural and Food Chemistry*, 55(6), pp. 2293–2302. Available at: https://doi.org/10.1021/jf0625398.

Stefánsson, A. (2007) 'Iron(III) Hydrolysis and Solubility at 25 °C', *Environmental Science & Technology*, 41(17), pp. 6117–6123. Available at: https://doi.org/10.1021/es070174h.

Stuart, B.H. (2004) *Infrared spectroscopy: fundamentals and applications*. John Wiley & Sons.

Stumm, W. and Morgan, J.J. (1995) *Aquatic Chemistry: Chemical Equilibria and Rates in Natural Water*. Wiley.

Sykes, A.J. *et al.* (2020) 'Characterising the biophysical, economic and social impacts of soil carbon sequestration as a greenhouse gas removal technology', *Global Change Biology*, 26(3), pp. 1085–1108. Available at: https://doi.org/10.1111/gcb.14844.

ThomasArrigo, L.K. *et al.* (2017) 'Iron(II)-Catalyzed Iron Atom Exchange and Mineralogical Changes in Iron-rich Organic Freshwater Flocs: An Iron Isotope Tracer Study', *Environmental Science & Technology*, 51(12), pp. 6897–6907. Available at: https://doi.org/10.1021/acs.est.7b01495.

ThomasArrigo, L.K. *et al.* (2018) 'Impact of Organic Matter on Iron(II)-Catalyzed Mineral Transformations in Ferrihydrite–Organic Matter Coprecipitates', *Environmental Science & Technology*, 52(21), pp. 12316–12326. Available at: https://doi.org/10.1021/acs.est.8b03206.

ThomasArrigo, L.K., Kaegi, R. and Kretzschmar, R. (2019) 'Ferrihydrite Growth and Transformation in the Presence of Ferrous Iron and Model Organic Ligands', *Environmental Science & Technology*, 53(23), pp. 13636–13647. Available at: https://doi.org/10.1021/acs.est.9b03952.

Totsche, K.U. *et al.* (2010) 'Biogeochemical interfaces in soil: The interdisciplinary challenge for soil science', *Journal of Plant Nutrition and Soil Science*, 173(1), pp. 88–99. Available at: https://doi.org/10.1002/jpln.200900105.

Tülp, H.C. *et al.* (2009) 'pH-Dependent Sorption of Acidic Organic Chemicals to Soil Organic Matter', *Environmental Science & Technology*, 43(24), pp. 9189–9195. Available at: https://doi.org/10.1021/es902272j.

Vollmer, W., Blanot, D. and De Pedro, M.A. (2008) 'Peptidoglycan structure and architecture', *FEMS Microbiology Reviews*, 32(2), pp. 149–167. Available at: https://doi.org/10.1111/j.1574-6976.2007.00094.x.

de Vries, F.T. *et al.* (2006) 'Fungal/bacterial ratios in grasslands with contrasting nitrogen management', *Soil Biology and Biochemistry*, 38(8), pp. 2092–2103. Available at: https://doi.org/10.1016/j.soilbio.2006.01.008.

Wagai, R. and Mayer, L.M. (2007) 'Sorptive stabilization of organic matter in soils by hydrous iron oxides', *Geochimica et Cosmochimica Acta*, 71(1), pp. 25–35. Available at: https://doi.org/10.1016/j.gca.2006.08.047.

Wang, K. and Xing, B. (2005) 'Structural and Sorption Characteristics of Adsorbed Humic Acid on Clay Minerals', *Journal of Environmental Quality*, 34(1), pp. 342–349. Available at: https://doi.org/10.2134/jeq2005.0342.

Wang, S. *et al.* (2020) 'Stabilization and transformation of selenium during the Fe(II)-induced transformation of Se(IV)-adsorbed ferrihydrite under anaerobic conditions', *Journal of Hazardous Materials*, 384, p. 121365. Available at: https://doi.org/10.1016/j.jhazmat.2019.121365.

Wang, T. *et al.* (2020) 'Nitrogen acquisition from mineral-associated proteins by an ectomycorrhizal fungus', *New Phytologist*, 228(2), pp. 697–711. Available at: https://doi.org/10.1111/nph.16596.

Waring, B.G. *et al.* (2020) 'From pools to flow: The PROMISE framework for new insights on soil carbon cycling in a changing world', *Global Change Biology*, 26(12), pp. 6631–6643. Available at: https://doi.org/10.1111/gcb.15365.

Whalen, E.D. *et al.* (2022) 'Clarifying the evidence for microbial- and plant-derived soil organic matter, and the path toward a more quantitative understanding', *Global Change Biology*, 28(24), pp. 7167–7185. Available at: https://doi.org/10.1111/gcb.16413.

Wieder, W.R. *et al.* (2014) 'Integrating microbial physiology and physio-chemical principles in soils with the MIcrobial-MIneral Carbon Stabilization (MIMICS) model', *Biogeosciences*, 11(14), pp. 3899–3917. Available at: https://doi.org/10.5194/bg-11-3899-2014.

Wiesmeier, M. *et al.* (2019) 'Soil organic carbon storage as a key function of soils - A review of drivers and indicators at various scales', *Geoderma*, 333, pp. 149–162. Available at: https://doi.org/10.1016/j.geoderma.2018.07.026.

Winkler, P. *et al.* (2018) 'Contrasting evolution of iron phase composition in soils exposed to redox fluctuations', *Geochimica et Cosmochimica Acta*, 235, pp. 89–102. Available at: https://doi.org/10.1016/j.gca.2018.05.019.

Xuan, M. *et al.* (2024) 'Biomarkers evidence shows a preferential occlusion of microbial necromass in mineral-associated and not particle organic matter', *Geoderma*, 450, p. 117030. Available at: https://doi.org/10.1016/j.geoderma.2024.117030.

Yan, F., Schubert, S. and Mengel, K. (1996) 'Soil pH increase due to biological decarboxylation of organic anions', *Soil Biology and Biochemistry*, 28(4), pp. 617–624. Available at: https://doi.org/10.1016/0038-0717(95)00180-8.

Yan, W., Hu, S. and Jing, C. (2012) 'Enrofloxacin sorption on smectite clays: Effects of pH, cations, and humic acid', *Journal of Colloid and Interface Science*, 372(1), pp. 141–147. Available at: https://doi.org/10.1016/j.jcis.2012.01.016.

Yang, J. *et al.* (2012) 'Preparation, characterization and anticoagulant activity in vitro of heparin-like 6-carboxylchitin derivative', *International Journal of Biological Macromolecules*, 50(4), pp. 1158–1164. Available at: https://doi.org/10.1016/j.ijbiomac.2012.01.007.

Yoo, S.-H. *et al.* (2005) 'Effects of selective oxidation of chitosan on physical and biological properties', *International Journal of Biological Macromolecules*, 35(1), pp. 27–31. Available at: https://doi.org/10.1016/j.ijbiomac.2004.11.004.

Yu, J.-Y. *et al.* (2004) 'Adsorption of phenol and chlorophenols on hexadecyltrimethylammonium-and tetramethylammonium-montmorillonite from aqueous solutions', *Geosciences Journal*, 8(2), pp. 191–198. Available at: https://doi.org/10.1007/BF02910195.

Yu, Z. *et al.* (2019) 'Molecular insights into the transformation of dissolved organic matter during hyperthermophilic composting using ESI FT-ICR MS', *Bioresource Technology*, 292, p. 122007. Available at: https://doi.org/10.1016/j.biortech.2019.122007.

Zhang, H. *et al.* (2020) 'Microbial dynamics and soil physicochemical properties explain large-scale variations in soil organic carbon', *Global Change Biology*, 26(4), pp. 2668–2685. Available at: https://doi.org/10.1111/gcb.14994.

Zhao, Q. *et al.* (2020) 'Oxidation of soil organic carbon during an anoxic-oxic transition', *Geoderma*, 377, p. 114584. Available at: https://doi.org/10.1016/j.geoderma.2020.114584.

Zhao, Y. *et al.* (2022) 'The role and fate of organic carbon during aging of ferrihydrite', *Geochimica et Cosmochimica Acta*, 335, pp. 339–355. Available at: https://doi.org/10.1016/j.gca.2022.07.003.

Zhou, Z. *et al.* (2018) 'Fe(II)-Catalyzed Transformation of Organic Matter–Ferrihydrite Coprecipitates: A Closer Look Using Fe Isotopes', *Environmental Science & Technology*, 52(19), pp. 11142–11150. Available at: https://doi.org/10.1021/acs.est.8b03407.

Zhou, Z. *et al.* (2024) 'Global turnover of soil mineral-associated and particulate organic carbon', *Nature Communications*, 15(1), p. 5329. Available at: https://doi.org/10.1038/s41467-024-49743-7.

Zhu, X. *et al.* (2020) 'The soil microbial carbon pump: From conceptual insights to empirical assessments', *Global Change Biology*, p. gcb.15319. Available at: https://doi.org/10.1111/gcb.15319.